2013

Control Method for the Wind Turbine Driven by Doubly Fed Induction Generator Under the Unbalanced Operating Conditions

Xiangpeng Zheng
Cleveland State University

CONTROL METHOD FOR THE WIND TURBINE DRIVEN BY DOUBLY FED INDUCTION GENERATOR UNDER THE UNBALANCED OPERATING CONDITIONS

XIANGPENG ZHENG

Bachelor of Electrical Engineering

Nankai University

June, 2008

submitted in partial fulfillment of requirements for the degree

MASTER OF SCIENCE IN ELECTRICAL ENGINEERING

at

CLEVELAND STATE UNIVERSITY

May, 2013

This thesis has been approved
for the Department of Electrical and Computer Engineering
and the College of Graduate Studies by

_____

Dissertation Committee Chairperson, Dr. Ana V Stankovic

_____

Department/Date

_____

Committee Member, Dr. Lili Dong

_____

Department/Date

_____

Committee Member, D. Hanz Richter

_____

Department/Date

ACKNOWLEDGEMENTS

I would like to thank my academic advisor Dr. Stankovic, for her persistent guidance on my thesis and financial support throughout my graduate program. Without her criticisms and suggestions, I could not complete the thesis. I would also like to thank Shuang Wu, for her outstanding research results on the control of permanent magnet generator and induction generator under the unbalanced operating conditions. Special thanks to Ms. Adrienne Fox for taking care of countless things so well during my study in the EEC department. And last but not the least, I would like to thank my family for their encouragement, supports and love these years.

CONTROL METHOD FOR THE WIND TURBINE DRIVEN BY DOUBLY FED INDUCTION GENERATOR UNDER THE UNBALANCED OPERATING CONDITIONS

XIANGPENG ZHENG

ABSTRACT

This thesis illustrates the principle and the behavior for doubly fed electric machines used in variable speed wind power systems under the balanced and unbalanced operating conditions. A generalized control method for complete stator pulsating power elimination and harmonic elimination in grid currents with adjustable power factor of a doubly fed induction generator under the unbalanced operating conditions is proposed. The theoretical analysis of this proposed control method is presented and then demonstrated by the simulation in Powersim®. The grid ride-through-fault ability by using the proposed method is also tested.

TABLE OF CONTENTS

Page

LIST OF TABLES

Table **Page**

LIST OF FIGURES

Figure **Page**

NOMENCLATURE

AC: alternating current

DC: direct current

DFEM: doulbly fed electric machine

DFIG: doubly fed induction generator

DFIM: doubly fed induction machine

d-q: direct and quadrature axes

FFT: fast Fourier transform

GSC: grid side converter

IGBT: insulated-gate bipolar transistor

RSC: rotor side converter

PWM: pulse width modulation

rms: root mean square

SCIG: Squirrel Cage Induction Generator

SFOC: stator flux oriented control

SVOC: stator voltage oriented control

CHAPTER I

INTRODUCTION AND LITERATURE SEARCH

1.1 Introduction

Wind generation is a fast growing form of electrical energy generation[1]. The $787 billion economic stimulus bill passed in the Senate on February 2009 contains various provisions to benefit the wind and other renewable energy projects. By the end of 2010, the installed cumulative capacity of wind power in United States was over 40,000 Megawatts[2, 3], which is the second place in the world right after China. The installed wind power has grown exponentially over the past decade in the United States, which is shown in Figure 1.1[4]. There are currently 5,600 MW of projects under construction in 2011[2]. In Department of Energy's 2008 report, it stated that "the U.S. possesses sufficient and affordable wind resources to obtain at least 20% of its electricity from the wind by 2030" [5].

In the past decade, many types of generator concepts have been developed and applied to generate electric power to the three phase utility grid[6]. The utility grid

with a specific frequency always requests the wind turbine to run at a given rotating speed if it is directly connected to the grid. With the pitch control strategy, wind turbine can still run and maintain at a constant speed during the inscrutable wind profile. However, the gear box coupled with the generator also brings in the significant aerodynamically generated noise. Moreover, the nonlinear aerodynamic characteristics make this application more complex to deal with the increased sensitivity by the pitch control strategy. This leads to the increasing interests of variable speed wind energy conversion systems, which can effectively deliver twenty to thirty percents more energy to the grid.

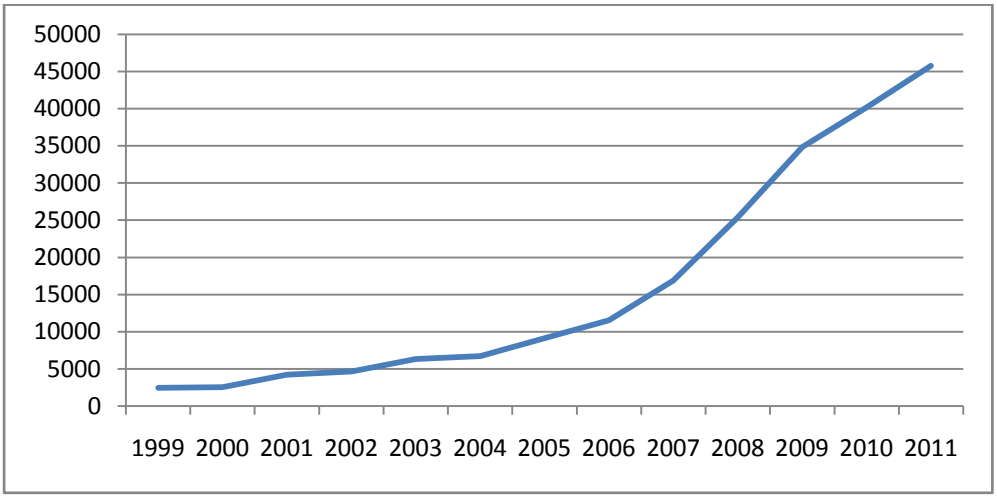

Figure 1.1: Annual installed wind power in United States over the past decade[4]

Recent work shows that the a typical wind energy conversion system has some major components as following, a wind turbine, generator, interconnection apparatus and control systems. Basically, the frequency conversion can be achieved by using two power electronics converters connected between the grid and the generator. These power electronics converters are also called as back-to-back (BTB) PWM converters. The machine side converter keeps track of the torque demand based on the wind speed to obtain the optimal wind power and then delivers to the DC link. The grid side inverter, delivers the DC link power to the grid with desired magnitude and

frequency. Meanwhile, the desired DC link voltage is maintained as constant by controlling the grid side converter [7-10]. It has been shown in [11, 12] that unbalanced grid voltages can create a significant second-order harmonic in DC link voltage and then lead to the third-order harmonics in line currents.

In this thesis, a generalized control method with complete stator pulsating power elimination and adjustable power factor is proposed for the wind turbine driven by doubly fed induction generator (DFIG) under the balanced and unbalanced operating conditions. This research method is on the basic of the harmonic elimination control, which was proposed and implemented for a PWM rectifier [13-17]. The method proposed in a wind turbine inverter [18-22] has been adjusted and applied to a wind turbine driven DFIG application.

1.2 Literature search

In this section, the previous related research and topic were reviewed and then presented. The following five general categories are shown as below.

1. Wind turbine's characteristics and typical types of variable-speed wind energy system;

2. Comparison of DFIG and the other basic variable-speed wind energy conversion application;

3. Rotor side converter control of DFIG;

4. Grid side converter control of DFIG;

5. The recent studies on the control strategy of DFIG under the balanced and unbalanced grid voltage conditions.

1.2.1 Wind turbine's characteristics and typical types of variable-speed wind energy system

Variable speed wind energy system allows the turbine to operate most efficiently and generate the optimal power over a wide range wind speed profile. In mechanical aspect, the output power obtained by a wind turbine is expressed as below.

$$P_m = \frac{1}{2}\rho_A A_{blade}\, C_p(\beta,\lambda) v_w^3 \quad (1.1)$$

, where ρ_A is the density of air [kg/m^3]; A is the area swept the rotor blades [m^2]; C_p is the power performance coefficient; and v_w is the wind speed [m/s]. The power performance coefficient is a function of the pitch angle of the rotor blades β and the tip-speed-ratio λ, which also can be represented as below.

$$\lambda = R\frac{\omega_w}{v_w} \quad (1.2)$$

In the above equation, R is the radius of the wind turbine's rotor blades [m], and ω_w is the wind turbine angular speed [rad/s]. As seen in Equation (1.1), wind energy can be extracted most efficiently when the highest power performance coefficient C_{p_max} is obtained. The optimal tip-speed-ratio λ_{opt} is inherent characteristic and determined by the turbine itself. Since the rotor speed of the generator changes as the wind speed changes, the electromagnetic torque has to be controlled so that the optimum wind power can be exploited most efficiently, which can be expressed as following:

$$T_{opt} = K_{opt}\,\omega_{opt}^2 \quad (1.3)$$

$$P_{opt} = K_{opt}\,\omega_{opt}^{3} \quad (1.4)$$

, where K_{opt} is the optimum power performance coefficient.

In order to transfer the output mechanical power as mentioned above into electrical power, the electromagnetic torque of the generator has to be controlled by the stator currents or rotor currents depends on the control strategy. The machine side converter , which normally as a PWM voltage source rectifier (VSR), keeps track of the torque demand based on the wind speed, obtains and delivers the optimal wind power to the DC link.

Due to the different wind potential capability and different level of wind power penetration in the world, wind turbine generator (WTG) designs nowadays vary considerably from OEM to OEM. Regardless of the fix-speed wind energy system and variable-speed wind energy system with pitch control strategy as discussed previously, variable-speed wind energy conversion systems can be sort out into three basic types generally, which are displayed in Figure 1.2 to 1.4[19]. However, it should be known that these three types cover majority of the variable-speed wind generation. But not all wind generation falls into these three categories.

1.2.2 Comparison of DFIG and the other basic variable-speed wind energy conversion applications

As shown in Figure 1.2, Type 1 WTG is as same as an induction generator which is directly connected to the grid, except that the generator includes a wound rotor and a circuit to quickly adjust the rotor current by manipulating the resistance value of the rotor side circuit. The main benefit of this type is the current control strategy at the

rotor side circuit. It enables relatively fast torque control, and shortens the response time of such dynamic events as the wind gust. It also decreases the torque fluctuation and power pulsation within the drive train. Variable slip in a narrow range is achieved with absence of slip rings, which led to an improved operating speed range with respect to the Squirrel Cage Induction Generator(SCIG).

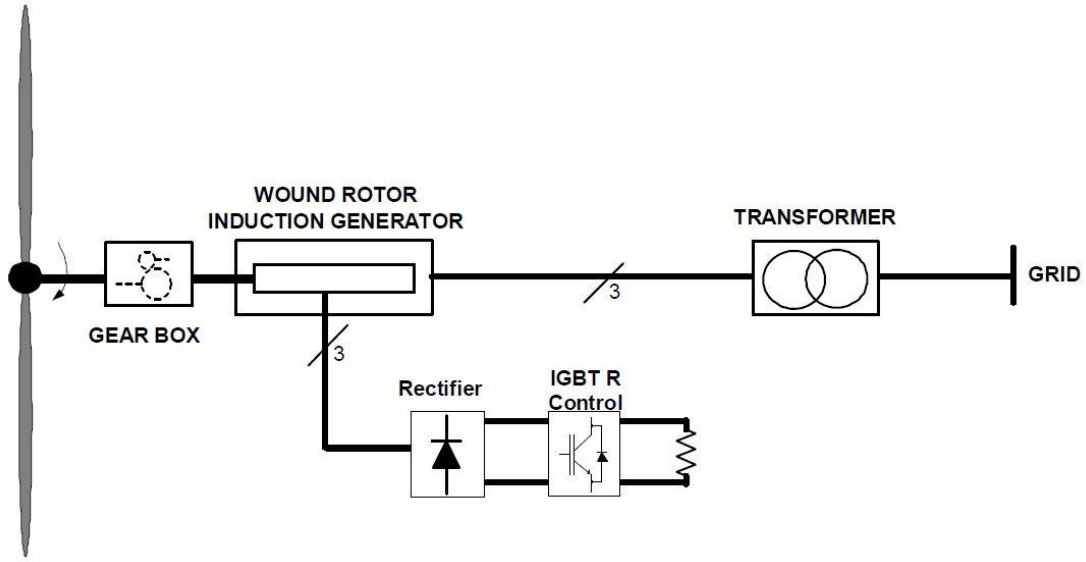

Figure 1.2: Type 1 WTG: Wound Rotor Induction Generator with variable slip[19]

However, this type of WTG highly depends on the wind turbine active power production at the shaft. A reactive power compensation system is still requisite. The speed range is typically restricted between zero percent to ten percents, more than its synchronous speed, as it is count on the range of the variable rotor resistance. The slip power dissipated on the rotor is considered to be a losses based on variable resistance.

As shown in Figure 1.3, Type 2 WTG passes all wind turbine power to the grid through a BTB power electronic converter. The main preponderance of this type is its omnibearing control of the reactive power and speed. At the same time, the BTB converter enables the voltage control, output power control during the grid disturbance or fault. The gearbox is designed so that maximum rotor speed can be

achieved with the rated speed of the generator. Or the gearbox is not necessary if a multi-pole synchronous generator is applied. Type 2 WTG is compatible with the recent grid code requirements.

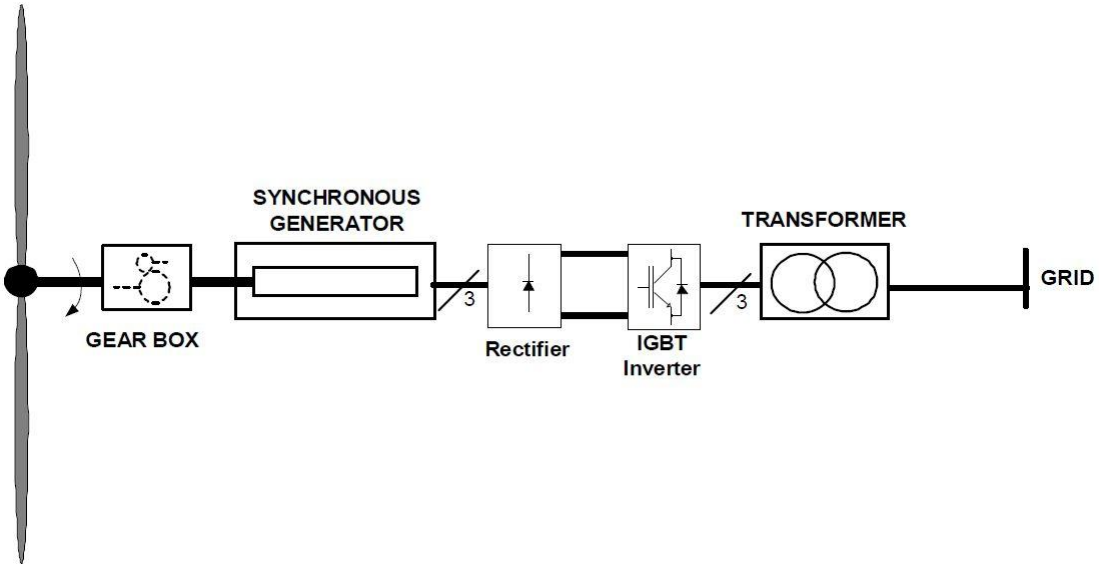

Figure 1.3: Type 2 WTG: Synchronous Generator with a BTB converter[19]

However, this type of WTG highly depends on the power converter, which ought to be rated and limited as the total system power. All the components in the BTB converter should be rated at one per unit output power also, making the filter design costly. Converter efficiency will affect the system efficiency over the entire operating range significantly.

As displayed in Figure 1.4, DFIG, which is used extensively for high level wind power applications, has the rotor connected to a BTB converter and the stator is connected to the grid directly. Compared with Type 1, DFIG operates at a wide range of variable speeds, which improves the power efficiency and controllability of the WTG. Rotor side converter enables reactive power control and variable speed operation. The wind turbine can operate ±33% around the synchronous speed with maximum efficiency. Compared with Type 2 WTG, the power converters of DFIG

just need to be rated as proportional as the total output power, around twenty to thirty percents typically. This design is attractive from an economic perspective and more suitable for high power wind turbines. It makes the ratings of all the components in the BTB converter small, and in return, lower cost, lower power dissipation and lower power losses would be achieved.

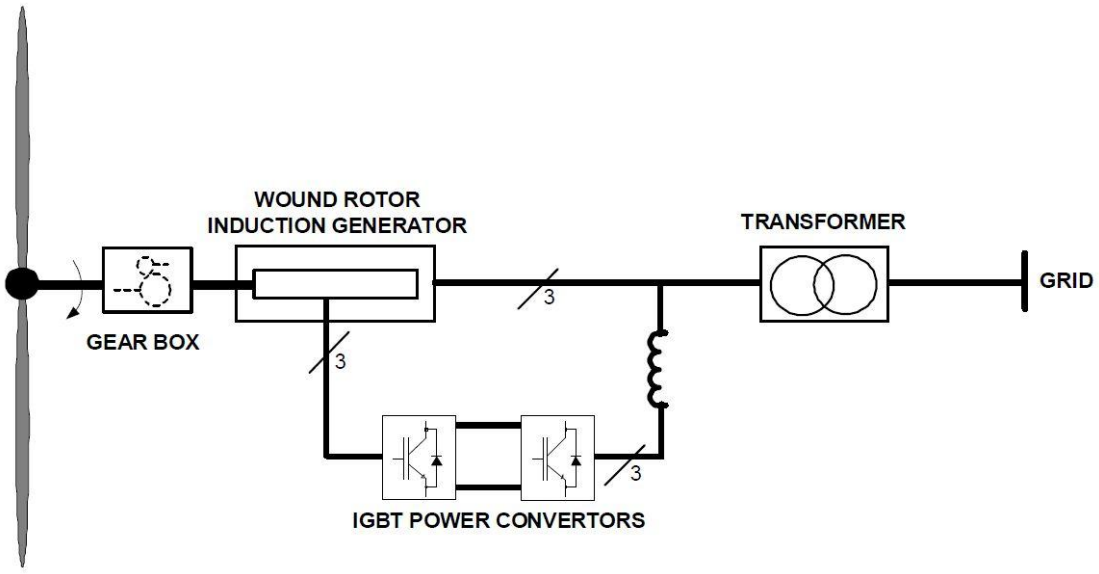

Figure 1.4: Type 3 WTG: Doubly Fed Induction Generator[19]

Although the features of DFIG are competitive and attractive, it has its own drawbacks. As we known, the BTB converter is connected to the power grid through the transformer. In such a case, the grid side converter is very sensitive to the unbalanced grid voltage which lead to the low order harmonics in line currents as well as the huge pulsation in a DC link voltage. This can present difficulties to deal with the torque pulsations, active power pulsations and unbalanced currents with lots of harmonics. These problems make the entire wind turbine system instable and noneffective.

Recently, many different control algorithms have been proposed and applied to control the DFIG under the balanced and unbalanced grid voltage conditions.

1.2.3 Rotor side converter control of DFIG

The rotor side converter is displayed in Figure 1.5. Stator voltage oriented control (SVOC) [23] and stator flux oriented control (SFOC) [24] are discussed.

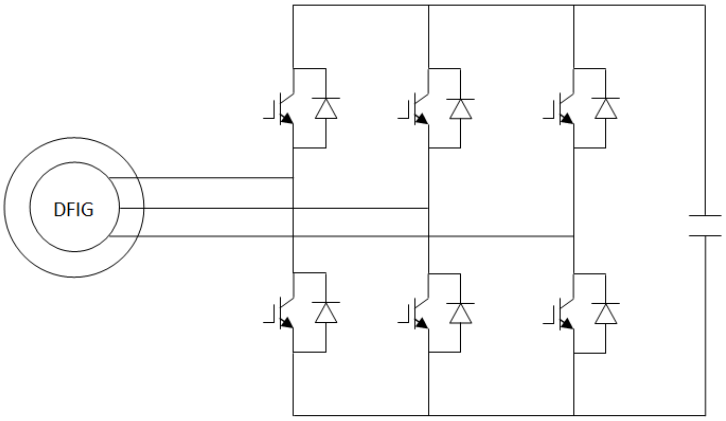

Figure 1.5: Rotor side converter of DFIG

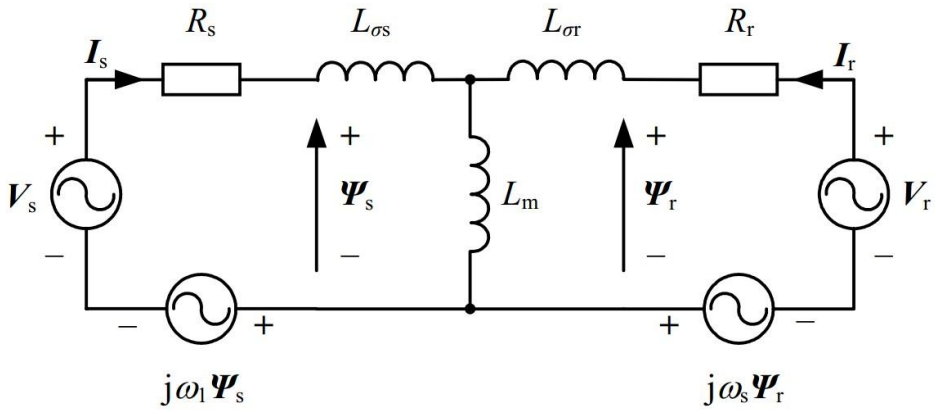

Figure 1.6: DFIG equivalent circuit in dq synchronous rotating frame[25]

In dq synchronous rotating frame as displayed in Figure 1.6, the stator voltage vector and the rotor voltage vector can be obtained as following:

$$V_s = R_s I_s + \frac{d\Psi_s}{dt} + j\omega_1 \Psi_s \tag{1.5}$$

$$V_r = R_r I_r + \frac{d\Psi_r}{dt} + j\omega_s \Psi_r \tag{1.6}$$

, where V_s, V_r are the stator and rotor voltage vector which can be represented as

$V_s = V_{sd} + jV_{sq}$ and $V_r = V_{rd} + jV_{rq}$; R_s, R_r are the stator and rotor resistance; I_s, I_r are the stator and rotor current vector which can be represented as $I_s = I_{sd} + jI_{sq}$ and $I_r = I_{rd} + jI_{rq}$;Ψ_s, Ψ_r are the stator and rotor flux vector which can be represented as $\Psi_s = \Psi_{sd} + j\Psi_{sq}$ and $\Psi_r = \Psi_{rd} + j\Psi_{rq}$. ω_1, ω_s are the synchronous angular speed and slip angular speed; $L_{\sigma s}$, $L_{\sigma r}$ and L_m are the stator leakage inductance, rotor leakage inductance and the magnetizing inductance respectively.

Stator and rotor flux can be obtained as following.

$$\Psi_s = L_s I_s + L_m I_r \tag{1.7}$$

$$\Psi_r = L_r I_r + L_m I_s \tag{1.8}$$

, where $L_s = L_{\sigma s} + L_m$ and $L_r = L_{\sigma r} + L_m$.

From Equation (1.7), the stator current vector can be represented as,

$$I_s = \frac{\Psi_s - L_m I_r}{L_s}$$

By substituting the above equation into Equation (1.8), the following equation is obtained and given by,

$$\Psi_r = \frac{L_m}{L_s}\Psi_s + L_r I_r \left(1 - \frac{L_m^2}{L_s L_r}\right) = \frac{L_m}{L_s}\Psi_s + \sigma L_r I_r \tag{1.9}$$

, where $\sigma = 1 - \frac{L_m^2}{L_s L_r}$.

The magnetizing current vector can be represented as:

$$I_m = \frac{\Psi_s}{L_m} = \frac{L_s}{L_m} I_s + I_r = I_{md} + jI_{mq} \tag{1.10}$$

By substituting (1.9) and (1.10) into (1.5) and (1.6), the following equation is obtained,

$$V_s = R_s I_s + L_m \frac{dI_m}{dt} + j\omega_1 \Psi_s \tag{1.11}$$

$$V_r = R_r I_r + \sigma L_r \frac{dI_r}{dt} + j\omega_s \Psi_r + \frac{L_m^2}{L_s}\frac{dI_m}{dt} \tag{1.12}$$

For both traditional stator voltage oriented control and stator flux oriented control, stator voltage vector V_s and stator flux vector Ψ_s in Equation (1.11) are usually assumed to be constant[25]. So it yields that,

$$\frac{d\mathrm{I}_m}{dt} = 0$$

Then the rotor voltage vector can be simplified as below,

$$V_r = R_r I_r + \sigma L_r \frac{d\mathrm{I}_r}{dt} + j\omega_s \Psi_r \tag{1.13}$$

From Equation (1.13), dq components of rotor voltage can be represented as below.

$$V_{rd} = \sigma L_r \frac{d\mathrm{I}_{rd}}{dt} + R_r \mathrm{I}_{rd} - \omega_s \Psi_{rd} \tag{1.14}$$

$$V_{rq} = \sigma L_r \frac{d\mathrm{I}_{rq}}{dt} + R_r \mathrm{I}_{rq} + \omega_s \Psi_{rq} \tag{1.15}$$

As shown on the right hand sides of the equations above, the first two terms are used for designing a PI current controller as an inner loop in the RSC. The third term is used for elimination of the cross coupling.

The stator active power and reactive power can be expressed as following:

$$P_s = \frac{3}{2}\left(\mathrm{V}_{sd}\mathrm{I}_{sd} + \mathrm{V}_{sq}\mathrm{I}_{sq}\right) \tag{1.16}$$

$$Q_s = \frac{3}{2}\left(\mathrm{V}_{sq}\mathrm{I}_{sd} - \mathrm{V}_{sd}\mathrm{I}_{sq}\right) \tag{1.17}$$

The electromagnetic torque can be obtained as below:

$$T_e = \frac{3}{2}p\left(\Psi_{sd}\mathrm{I}_{sq} - \Psi_{sq}\mathrm{I}_{sd}\right)$$

, where p is the number of the poles.

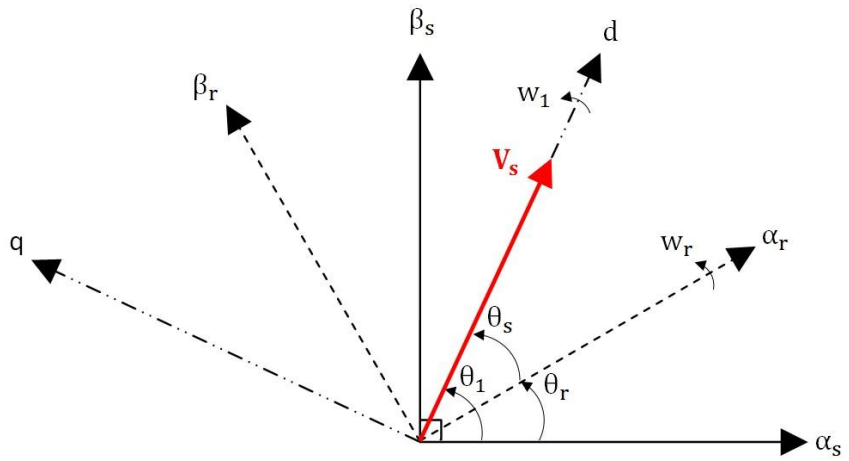

Figure 1.7: Vector diagram of stator voltage oriented control method (SVOC)[23]

As shown in Figure 1.7, stator voltage vector position is along with the d-axis of the dq synchronous rotating frame if SVOC is implemented.

Then we can obtain the dq components of the stator voltage vector as following:

$$V_{sd} = V_s \tag{1.18}$$

$$V_{sq} = 0 \tag{1.19}$$

Neglecting the stator resistance value, then Equation (1.11) can be adjusted as below:

$$V_{sd} = -\omega_1 \Psi_{sq} = -\omega_1 \left(\mathrm{L_s I_{sq}} + \mathrm{L_m I_{rq}}\right) = V_s \tag{1.20}$$

$$V_{sq} = \omega_1 \Psi_{sd} = \omega_1 (\mathrm{L_s I_{sd}} + \mathrm{L_m I_{rd}}) = 0 \tag{1.21}$$

By substituting Equations (1.18-21) into Equations (1.16) and (1.17), the stator active power and the stator reactive power can be approximately controlled by I_{rd} and I_{rq} respectively as following:

$$P_s = -\frac{3}{2}\frac{L_m}{L_s}\mathrm{V_s I}_{rd} \tag{1.22}$$

$$Q_s = \frac{3}{2}\frac{\mathrm{V_s}}{L_s}\left(\frac{\mathrm{V_s}}{\omega_e} - L_m \mathrm{I}_{rq}\right) \tag{1.23}$$

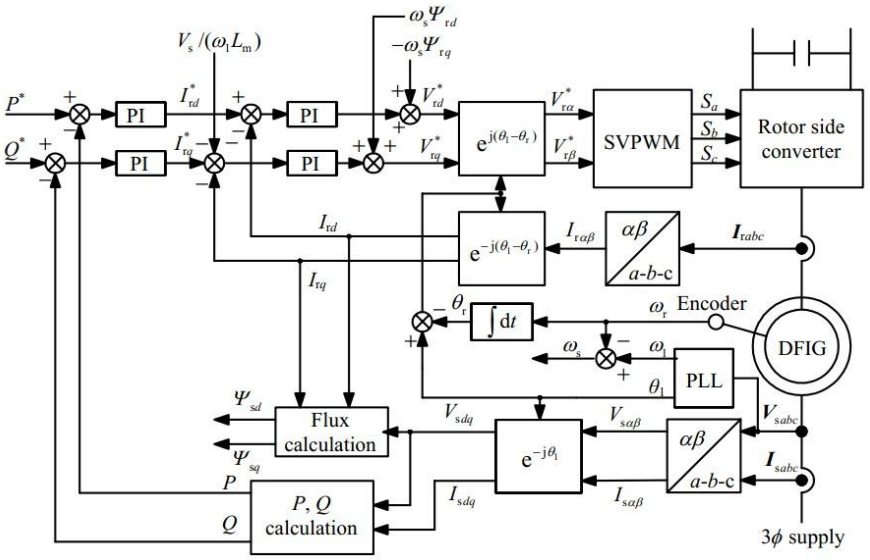

Figure 1.8: Diagram of the traditional SVOC[25]

As shown in Figure 1.8, the traditional SVOC method is implemented[25]. The stator active power and the stator reactive power are controlled by using Equations (1.22-23). And the PI controllers are implemented to regulate the rotor voltage reference by using Equations (1.14-15). Space vector PWM control is then used to generate the switch sequence for the IGBTs of the rotor side converter.

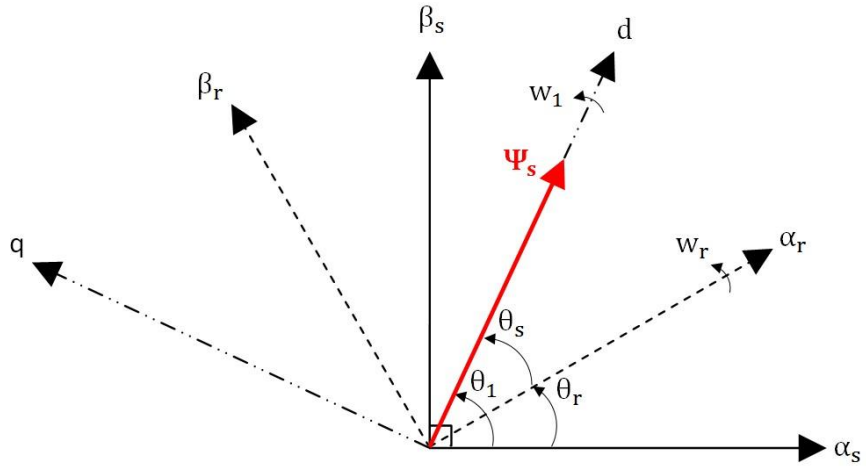

Figure 1.9: Vector diagram of stator flux oriented control method (SFOC)[24]

As shown in Figure 1.9, stator flux vector position is along with the d-axis of the dq synchronous rotating frame. The dq components of the stator flux vector are obtained as following:

$$\Psi_{sd} = \Psi_s \tag{1.24}$$

$$\Psi_{sq} = 0 \tag{1.25}$$

Neglecting the stator resistance value, then Equation (1.11) can be adjusted as below:

$$V_{sd} = -\omega_1 \Psi_{sq} = -\omega_1 \left(\mathrm{L_s I_{sq}} + \mathrm{L_m I_{rq}}\right) = 0 \tag{1.26}$$

$$V_{sq} = \omega_1 \Psi_{sd} = \omega_1 (\mathrm{L_s I_{sd}} + \mathrm{L_m I_{rd}}) = \omega_1 \Psi_s \tag{1.27}$$

By substituting Equations (1.24-27) into Equations (1.16) and (1.17), the stator active power and the stator reactive power can be approximately controlled by I_{rq} and I_{rd} as following:

$$P_s = -\frac{3}{2}\omega_1 \frac{L_m}{L_s} \Psi_s \mathrm{I}_{rq} \tag{1.28}$$

$$Q_s = \frac{3}{2}\omega_1 \Psi_s \left(\frac{\Psi_s - L_m \mathrm{I}_{rd}}{L_s}\right) \tag{1.29}$$

As shown in Figure 1.10, the traditional SFOC method is implemented[25]. The stator active power and the stator reactive power are controlled by using Equations (1.28-29). And the rotor voltage reference are regulated by using the PI controllers as indicated in Equations (1.14-15). Space vector PWM control is implemented to generate the switch sequence for the rotor side converter.

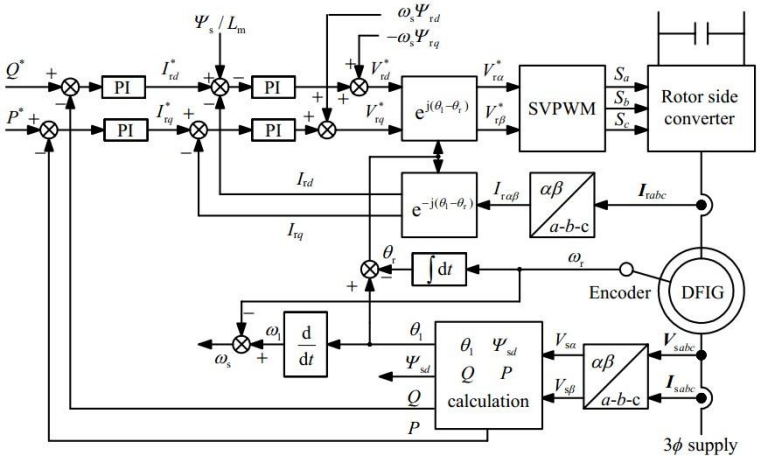

Figure 1.10: Diagram of the traditional SFOC [25]

1.2.4 Grid side converter control of DFIG

The grid side converter is displayed in Figure 1.11.

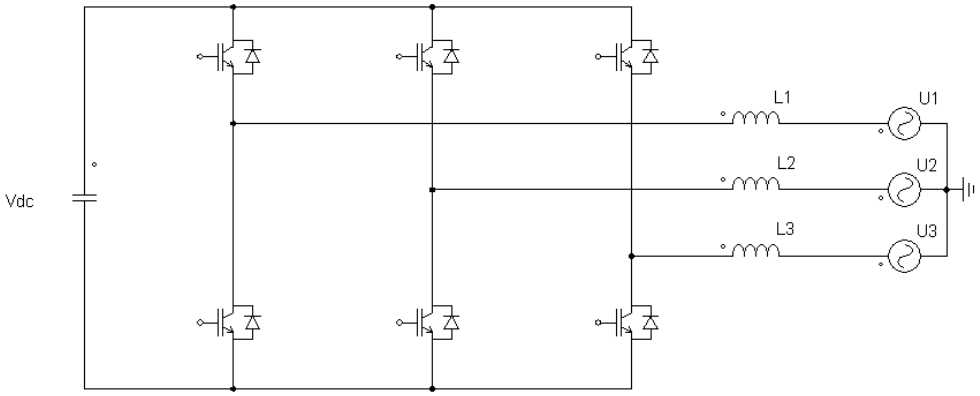

Figure 1.11: Grid side converter of DFIG

Based on Kirchhoff's current laws and Kirchhoff's voltage laws, the following equation in matrix form can be defined as in the GSC of DFIG.

$$\begin{bmatrix} u_a \\ u_b \\ u_c \end{bmatrix} = \begin{bmatrix} u_{sa} \\ u_{sb} \\ u_{sc} \end{bmatrix} - R \begin{bmatrix} i_a \\ i_b \\ i_c \end{bmatrix} - L \frac{d}{dt} \begin{bmatrix} i_a \\ i_b \\ i_c \end{bmatrix} \tag{1.30}$$

, where L and R are the line inductance and resistance in the GSC; u_a, u_b and u_c are the output voltages of the GSC; u_{sa}, u_{sb} and u_{sc} are the IGBT bridge's output voltages; i_a, i_b and i_c are the line currents in the GSC.

The grid side converter balances and delivers the power between the three phase grid and the DC link capacitor. Also the DC link voltage needs to be controlled and maintain as a constant value under the balanced and unbalanced operating conditions. The direct power control method for the grid side converter is one of the major control strategies and has been proposed in references [24, 26, 27].

The dynamic model of the grid side converter can be represented by the following equations using the synchronous rotating frame:

$$u_d = u_{sd} - Ri_d - L\frac{di_d}{dt} + \omega_e L i_q \tag{1.31}$$

$$u_q = u_{sq} - Ri_q - L\frac{di_q}{dt} - \omega_e L i_d \tag{1.32}$$

Under the balanced operating condition, the three phase output voltages of GSC are with identical magnitude and frequency. In such a case, the dq components after the transformation u_d and u_q are consider as the constant values. The q-axis component u_q is then set as zero when the d-axis oriented along the output voltage position. It follows that the GSC's active power and reactive power can be simplified as following.

$$P = \frac{3}{2}\left(u_d i_d + u_q i_q\right) = \frac{3}{2} u_d i_d \tag{1.33}$$

$$Q = \frac{3}{2}\left(u_d i_q + u_q i_d\right) = \frac{3}{2} u_d i_q \tag{1.34}$$

Since the grid side converter balances and delivers the power between the three phase grid and the DC link capacitor. The DC link power should be equal to the grid side converter's output power. It follows that the grid side converter's active power can be manipulated by the d-axis component of line current i_d which can be expressed as below.

$$V_{dc} I_{dc} = \frac{3}{2} u_d i_d \tag{1.35}$$

Also the reactive power in GSC in Equation (1.34) can be set as a injecting reference based on the demand of the BTB converter and the grid operating conditions. In such a case, the q-axis component of the line current i_q will be controlled.

One of the other major control strategies is the indirect current control[28]. It can be applied to the grid side converter control of DFIG.

The voltage error between the actual DC link voltage and the reference DC link voltage is multiplied by a constant so that it can be derived as the sinusoidal line current reference of GSC. Consequently, a phase shift is applied to this sinusoidal line current reference which is proportional to output voltage of the GSC. Since the power factor is determined by the phase angle difference between the line current and output voltage of the GSC, variable power factor can be achieved by manipulating the phase shift angle. By using the hysteresis controller, the line current of the GSC is then controlled with a varying switching frequency to keep tracks of the current reference.

1.3 The recent research on the control strategy of DFIG under the balanced and unbalanced grid voltage conditions

In [29], Ali et al proposed an effective control method for maximum power point tracking (MPPT) from the wind energy system. Rotor side converter's active power is controlled by the d-axis component of the rotor current in outer control layer. Rotor side converter's reactive power is controlled by q-axis component of the rotor current. The control method of the rotor side converter is based on SFOC. For the grid side converter, it is a vector control strategy with the grid voltage orientation[29]. The d-axis voltage component is along with the position of grid voltage space vector, and the q-axis voltage component is regarded as zero. So the grid side converter's active power and reactive power can be manipulated by using d-axis and q-axis components of grid side converter's line current respectively. The control diagram is shown in

Figure 1.12. However, DFIG under the unbalanced conditions is not discussed in this paper.

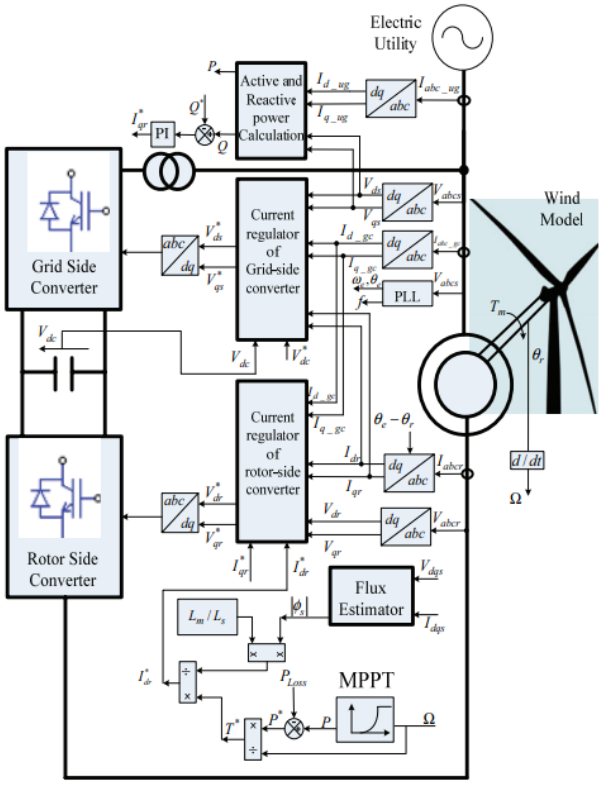

Figure 1.12: Control scheme in ref. [29]

In [30], Vijay et al proposed a control method for unity power factor operation with the loss minimization strategy. By keeping track of the maximize power point of the wind turbine, the active and reactive power are under control so that maximum power can be extracted from the shaft. For the rotor side converter, stator flux-oriented reference frame is chosen to control the rotor currents in such a way to maintain the active and reactive power flow. For the grid side converter, the active power control is implemented to regulate the DC link voltage. The DC link reference voltage is proportional to the reference of the GSC's active power. Unity power factor of the GSC is achieved when the reference of the GSC's reactive power is set to be zero. The control schemes for both of the RSC and GSC are shown in Figure 1.13.

The performance of DFIG under sub-synchronous speed and super-synchronous speed are also discussed in this paper. However, DFIG under the unbalanced grid voltage conditions is not analyzed in this paper at all.

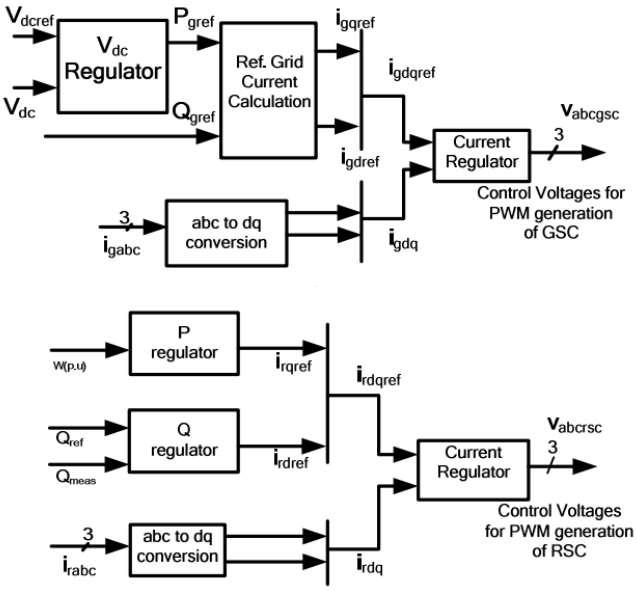

Figure 1.13: Control scheme in ref. [30]

In [31], Vishal proposed an indirect current control method to regulate the power flow in the RSC of DFIG. Also, unity power factor of the GSC is achieved when the reference of the GSC's reactive power is set to be zero. The power is balanced between the GSC and DC link capacitor so that the DC link voltage is maintained as a constant value. The control scheme in this paper is displayed in Figure 1.14. The rotor side converter's active and reactive power are decoupled and controlled independently. The actual active power and the reactive power are measured and compared with the reference power separately. These differences errors are then are fed to PI controller to determine the dq reference values of the rotor current. The d-q components of the rotor current can be transformed and expressed in the abc reference frame. The hysteresis current control is implemented to generate the switching table for the IGBTs in the RSC. The GSC's active power and reactive power are controlled in the

similar way using the PI control and hysteresis current control strategies. The unity power factor is also achieved when the q-axis component of the reference rotor current is kept at zero ion. Instead of using the constant switching frequency of the space vector PWM controller in ref. [29, 30], the hysteresis controller in ref. [31] has a variable switching frequency.

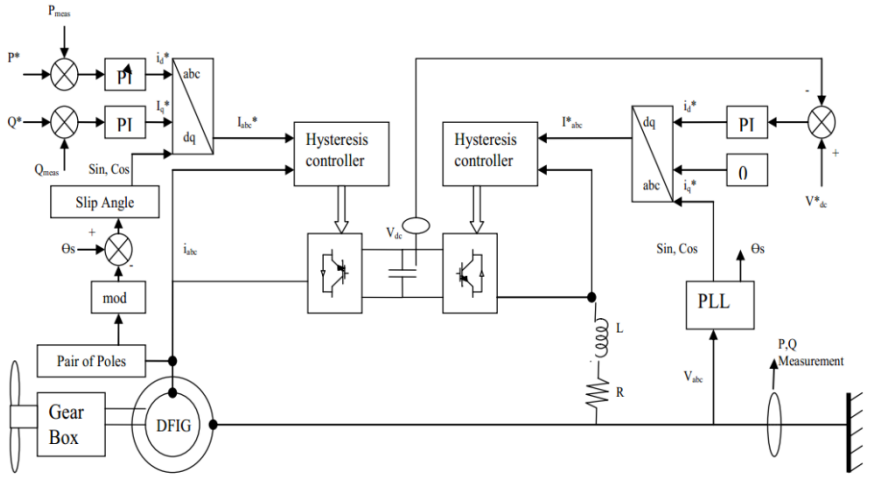

Figure 1.14: Control scheme in ref. [31]

As discussed above, the reported research focuses on the DFIG control under the balanced operating condition. However, under the unbalanced operating condition, the three phase stator voltages supplied by the grid may have different magnitudes and phase shift angles. In such cases, the grid voltage and current will contain the negative sequence components and cause the low order harmonics to flow between the grid and the GSC, also between the rotor and RSC. The torque generated by the induction generator will have periodic pulsating terms at twice the grid frequency. The grid voltage disturbance may lead to the appearance of low order harmonics in GSC's line currents as well as a huge pulsation the DC link voltage. Stator currents and rotor currents in DFIG will bump up if no further control efforts are adopted for the RSC. Even more, during the asymmetrical grid disturbance, two slip frequency sf_s and

$|2 - s|f_s$ can be seen in the rotor windings. Details about the effect and behavior of DFIG under unbalance grid voltage will be discussed in Chapter II. In sum, unbalanced operating condition requires additional control efforts in order to avoid pulsating electromagnetic torque, pulsating stator and rotor power, distorted grid currents and huge ripple on the DC link capacitor.

Until recently, the issues and the corresponding control strategies of DFIG under the unbalanced operating conditions have not been a main research topic. To enhance the grid's fault ride through capability by a DFIG, the first solution is to protect the rotor side converter by shorting the rotor windings circuit with so-called crowbar as shown in Figure 1.15[32]. The crowbar is a bypass resistor as to limit the inrush current when the voltage disturbance occurs. The configuration is connected to the rotor windings directly with the switches. With this scheme, the wind turbine should be disconnected from the grid which may conflict with the grid codes. The other approach is introduced by Patrick[33] using a series-connected GSC. In such configuration, DFIG low voltage ride through capability is significantly improved. However, the required additional converters configuration is costly and complicated.

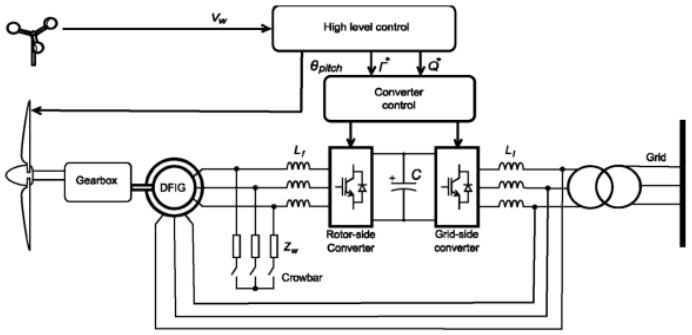

Figure 1.15: Traditional crowbar configuration in ref. [32]

In absence of the crowbar or additional GSC configuration, Miguel [34] et al proposed and implemented a direct rotor current mode control for the RSC of DFIG,

which improve both of the transient and dynamic performance. However, during the generalized unsymmetrical unbalanced grid voltage conditions, the positive sequence components and negative sequence components are employed into the rotor side controller which makes the control variables complicated and hard to implement. The proposed control method is shown in Figure 1.16. Even more, this control strategy lacks the investigation of GSC.

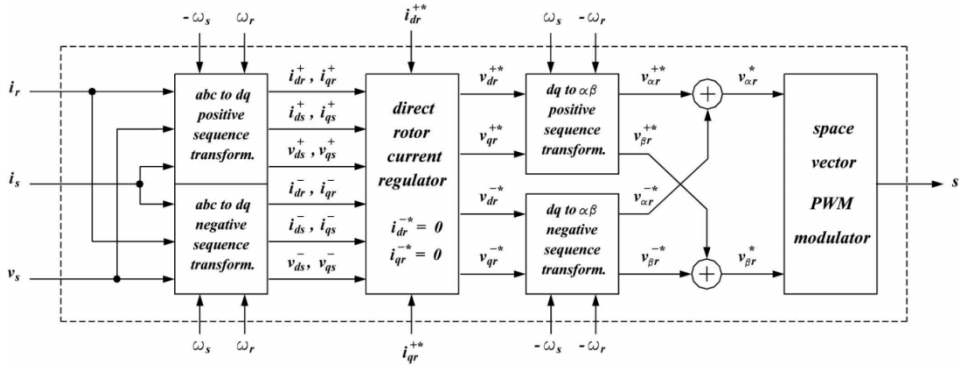

Figure 1.16: Rotor side converter control scheme in ref. [34]

Unlike the control method based on the synchronous dq reference frame, Alvaro Luna et al[35] proposed and developed a control strategy so called voltage oriented control in the rotor reference frame. It employed such a method to control the generator under the unbalanced operating conditions without introducing the torque ripples. As shown in Figure 1.17, the control loops are simplified as the adaptive frequency resonant controllers are implemented to extract the positive and the negative sequences. Moreover, a fed-forward concept is proposed to finalize the injecting rotor currents. However, this control strategy still lacks the investigation of GSC.

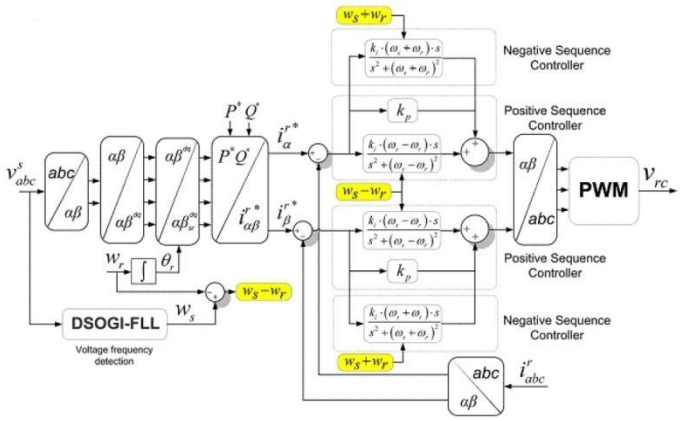

Figure 1.17: Rotor side converter control scheme in ref. [35]

As a generalized unbalanced operating condition stated in[36], the stator active power and reactive power can be controlled as constant, while electromagnetic torque oscillations and rotor current distortions will occur as a trade-off. In this paper, Gonzalo et al developed a direct power control to eliminate the electromagnetic torque oscillation, where active power reference of the RSC are generated without any sequence component extraction compared with ref [34]. However, the GSC must handle the disturbances caused by the unbalanced grid voltages and the rotor active pulsating power. Thus, this will increase the stress on the RSC and the DC link capacitor, leading to the nonsinusoidal rotor side currents unstable DC link voltage.

Jun Yao et al [37] proposed an instantaneous power feedback control method on RSC to minimize the DC link ripple voltage of DFIG. However, in this paper, only the symmetrical grid disturbance is discussed to demonstrate grid ride-through-fault ability.

Dawei Xiang et el [38] proposed a new control method at RSC to compensate the distorted components in the stator flux linkage. The control objective in this paper is to constrain the instantaneous rotor current below 2.0 per unit, while the converter DC link voltage is also maintained below the device's voltage rating.

David et al[39, 40] analyzed and presented the effect of the grid voltage disturbance of DFIG and proposed a novel control strategy so called dynamic programming power control plus, by adjusting the dynamic programming control strategy based on their previous research. As analyzed in this paper, the stator power injected to grid can be maintained as constant by implementing the proposed method into the RSC under the balanced operating conditions. Under the unbalanced operating conditions, this accomplishment is inconspicuous if the stator current is nonsinusoidal as a result. Therefore, different control targets can be defined and chosen depending on the severity of the perturbation as following[39, 40]: 1) maintain constant stator active power and reactive power; 2) maintain sinusoidal stator currents; 3) maintain constant electromagnetic torque; and 4) inject stator currents while the stator active power and reactive power have as little pulsations as possible. It can be seen that not all the control targets as above could be adopted simultaneously.

In summary, unbalanced operation conditions of wind turbine include unbalanced grid voltage (symmetrical and asymmetrical voltage dips), unbalanced line impedance and both unbalanced grid voltage and line impedance[18]. The corresponding problems include undesirable distortions in line currents and huge ripple voltage on the DC link capacitor[18,19]. Moreover, the disturbance occurs at the grid side voltage will increase the control difficulty regarding of lots of variable control targets.

A generalized control method for DFIG under extreme network disturbances is proposed in this thesis. The proposed grid side converter control method is based on the abc reference frame which make it unnecessary to extract and transform the sequence components. Also, this generalized control method can be applied to all kinds of the unbalance operating conditions, including unbalanced grid voltages and

unbalanced line impedances. The power factor can be adjusted and set as unity as well. The main control target is to eliminate the stator power pulsations, maintain the DC link voltage constant, and inject the sinusoidal stator currents while inevitably sacrificing the pulsating torque. Simulation results of a variable speed wind turbine system driven by DFIG under the balanced and unbalanced operating conditions are presented. The proposed control is implemented into the BTB converter of DFIG when the event of severe voltage disturbances occur.

In Chapter II, the principle and behavior for the doubly fed electric machine (DFEM) used in variable speed wind power systems under the balanced and unbalanced operating conditions is presented in details. Simulation results of DFEM operating in a four-quadrant plain is also presented in this chapter. Under the unbalanced grid voltages, the stator power, rotor power and electromagnetic torque contain undesirable pulsations.

In Chapter III, a general scheme for stator pulsating power elimination under the unbalanced operating conditions is analyzed and presented in details. Complete harmonic elimination for line currents is achieved and adjustable power factor of the GSC is also obtained by implementing the proposed method.

In Chapter IV, the model of a wind turbine driven DFIG is developed and simulated by using the software Powersim. The simulation results for a wind turbine driven DFIG with proposed method under the balanced and unbalanced voltages are presented.

In Chapter V, the conclusion as well as future work is presented.

CHAPTER II

DFIG AND DFIM - PRINCIPLE OF OPERATION

2.1 Operating mode of DFEM

Doubly fed electric machine is generally an electric motor or electric generator, where it depends on the torque and rotating speed. It has its stator windings and rotor windings connected to some electric parts, where both windings absorb or deliver the power between shaft and the entire electrical system. When a motoring torque is produced, which means the torque is positive, the DFEM operates as a doubly fed induction motor. When a generating torque is produced, which means the torque is negative, the DFEM operates as a doubly fed induction generator.

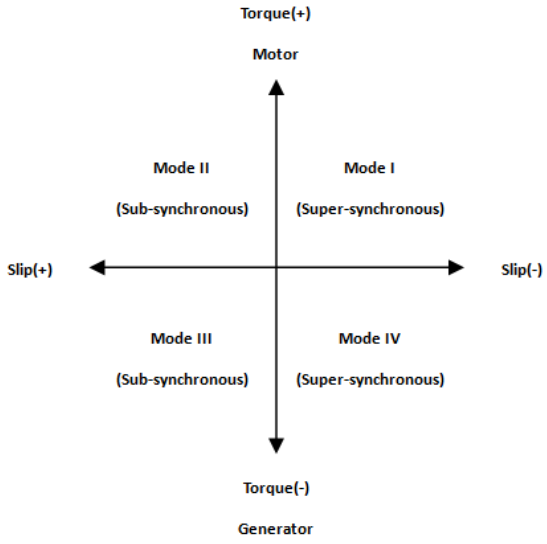

Figure 2.1: Operation modes of DFEM

Also DFEM can be operated in two different modes as following, depending on the rotating speed. Sub-synchronous speed represents a speed below the synchronous speed while super-synchronous mode represents a speed above the synchronous speed. Therefore, the rotor power can flow in both directions correspondingly, for example, from the grid to the RSC or from RSC to the grid. The four operating modes of the DFEM are displayed in Figure 2.1.

In this chapter, characteristics of DFEM in four operating modes under the balanced operating conditions are discussed in details. The simulation results demonstrate the characteristics of these four operating modes. Then DFIG under the unbalanced operating conditions is then discussed and analyzed.

2.2 DFEM Principle of Operation

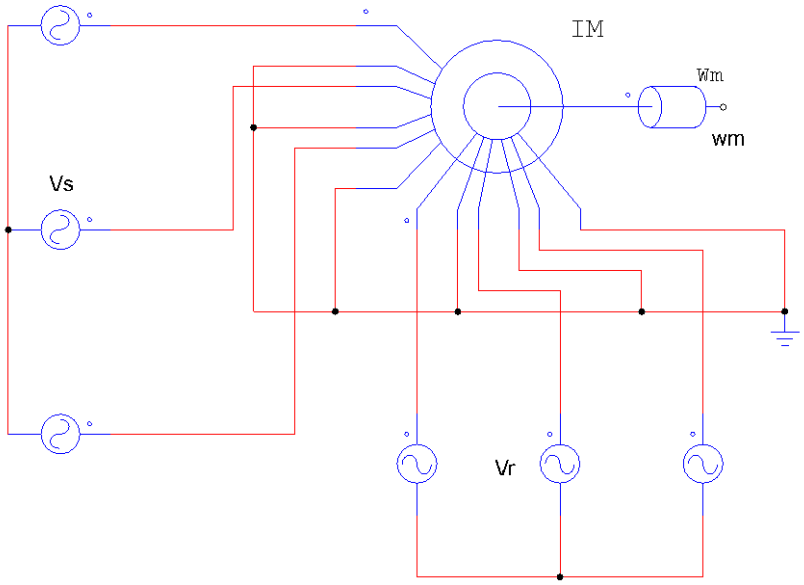

Figure 2.2: Configuration of a DFEM supplied by two AC sources

As shown in Figure 2.2, DFEM can be emulated by injecting two three phase sinusoidal voltages at both stator windings and rotor windings based on a wound rotor induction machine. The shaft speed, n, can be set above or below the synchronous speed to emulate the super-synchronous and sub-synchronous operating modes. It is known that the synchronous speed of the wound rotor induction machine, n_e is given by,

$$n_e = \frac{120 * f_s}{P} \tag{2.1}$$

, where f_s is the frequency of the stator voltage[Hz], P is the number of the poles of the wound rotor induction machine.

One of the important characteristics of DFEM is the slip, which is given by,

$$s = \frac{f_r}{f_s} = \frac{n_e - n}{n_e}$$

, where f_s and f_r are the frequency of the stator and rotor voltage.

The balanced positive phase sequence stator voltages (ABC) are given,

$$V_{sa} = V_s \sin(2\pi f_s t) \quad (2.2)$$

$$V_{sb} = V_s \sin(2\pi f_s t - 120°) \quad (2.3)$$

$$V_{sc} = V_s \sin(2\pi f_s t + -120°) \quad (2.4)$$

By changing the shaft speed n_r, rotor voltage V_r, rotor frequency f_r and phase sequence of the rotor voltages (ABC or ACB), the DFEM can operate in four modes as analyzed in Figure 2.1. The parameters of the wound rotor induction machine are displayed in Table 2.1. The simulation results demonstrate the power flow characteristics of DFEM.

Table 2.1: Parameters of the wound rotor induction machine used in the simulation

stator winding resistance (Ohms)	1.115
stator inductance (H)	0.005974
rotor winding resistance (Ohms)	1.083
rotor inductance (H)	0.005974
number of poles	4
mutual inductance (H)	0.2037
rated voltage (V)	460
rated speed (Rpm)	1800

2.2.1 DFIM at sub-synchronous speed

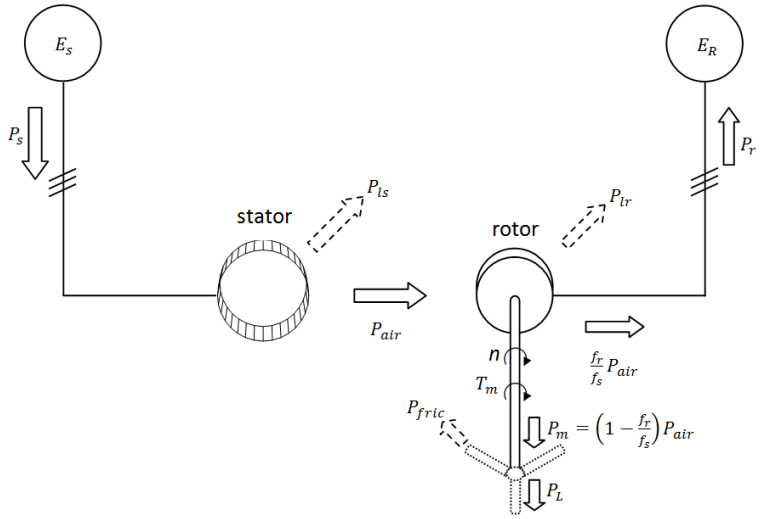

Figure 2.3: Power flow of DFIM at sub-synchronous speed

As displayed in Figure 2.3, DFEM operates as a motor at a sub-synchronous speed. In this mode, a motoring torque which is positive is produced on the shaft. The slip is positive as seen from Equation (2.2). Both the rotor circuit and the shaft are consuming power from the stator circuit. By neglecting the power losses both of the stator windings and rotor windings and the friction losses, the following equations are obtained:

$$P_r \approx \frac{f_r}{f_s}|P_s| > 0;\ P_s < 0 \tag{2.5}$$

$$P_m \approx |P_s| - |P_r| = -P_s - P_r \approx T_e * n * \frac{2*\pi}{60} \tag{2.6}$$

DFIM in the sub-synchronous speed mode is simulated and shown in Figure 2.4. In such a case, the magnitude of the stator voltage V_s is chosen as 311.1V. Shaft speed is chosen as 1500 rpm which is smaller than the synchronous speed (1800 rpm). The stator voltages and stator currents of DFIM are measured and shown in Figure 2.5. The rotor voltages and rotor currents of DFIM are measured and shown in Figure 2.6. Stator power, rotor power and electromagnetic torque of DFIM are measured and

shown in Figure 2.7. The simulation results with all the measurements are summarized in Table 2.2.

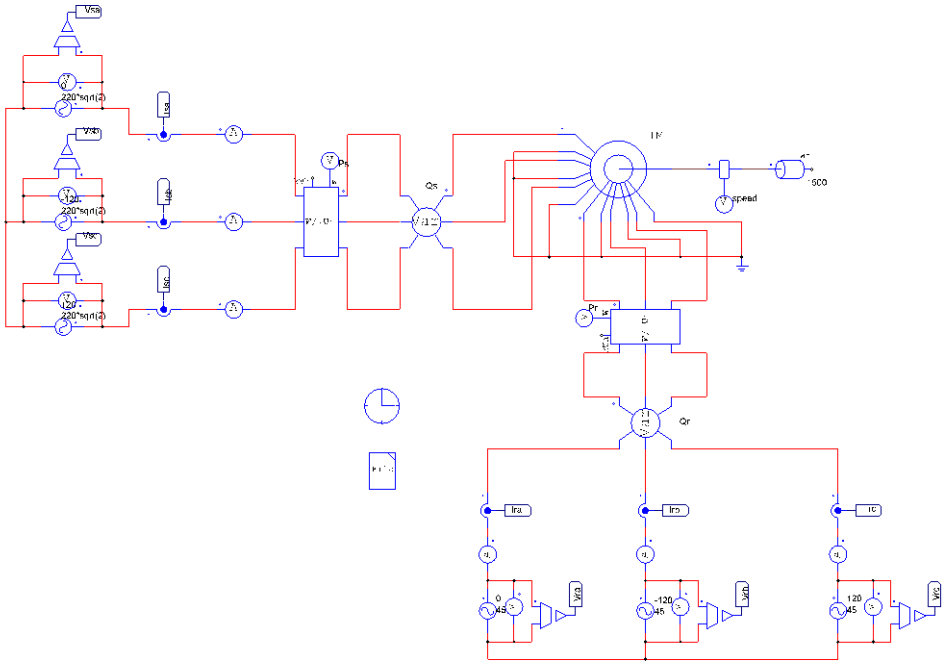

Figure 2.4: Simulation configuration of DFIM in the sub-synchronous mode

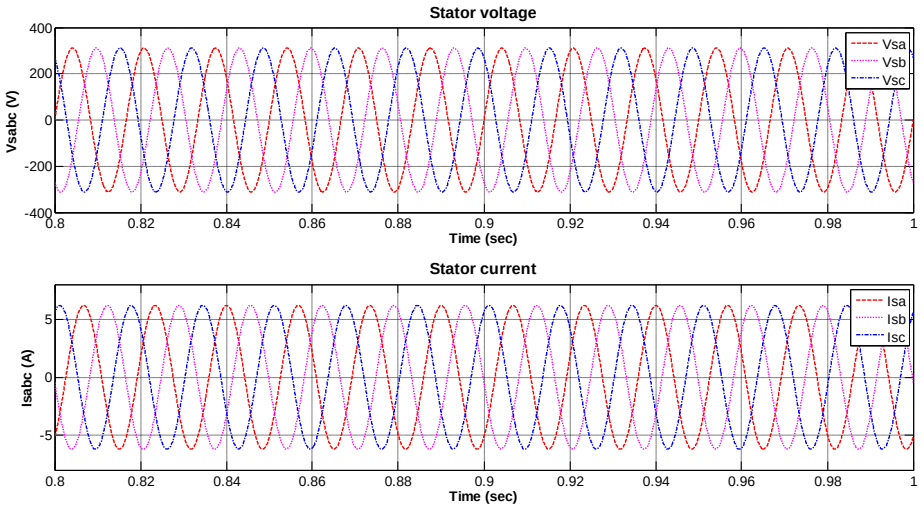

Figure 2.5: Stator voltage and stator current of DFIM at sub-synchronous speed

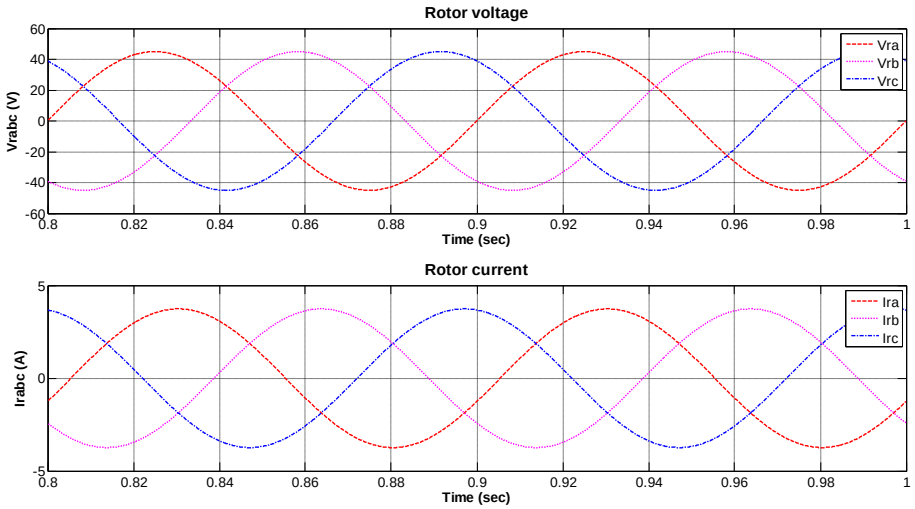

Figure 2.6: Rotor voltage and rotor current of DFIM at sub-synchronous speed mode

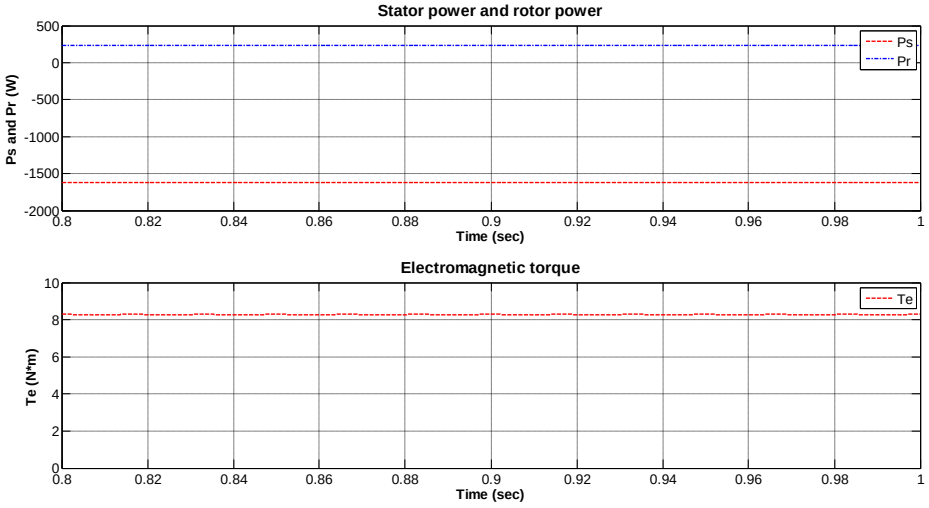

Figure 2.7: Stator power, rotor power and electromagnetic torque of DFIM at sub-synchronous speed mode

As depicted in Table 2.2, the stator active power P_s and the rotor active power P_r measured in the simulation demonstrate the power flow in Figure 2.3.

Table 2.2: Simulation results of DFIM at sub-synchronous speed

	stator	**rotor**
voltage magnitude (V)	311.10	45.00
frequency (Hz) (phase sequence)	60 (ABC)	10 (ABC)
current magnitude (A)	6.20	3.74
active power (W)	-1625.17	237.46
speed (Rpm)	1500	
slip	1/6	
torque (N*m)	8.28	

2.2.2 DFIM at super-synchronous speed

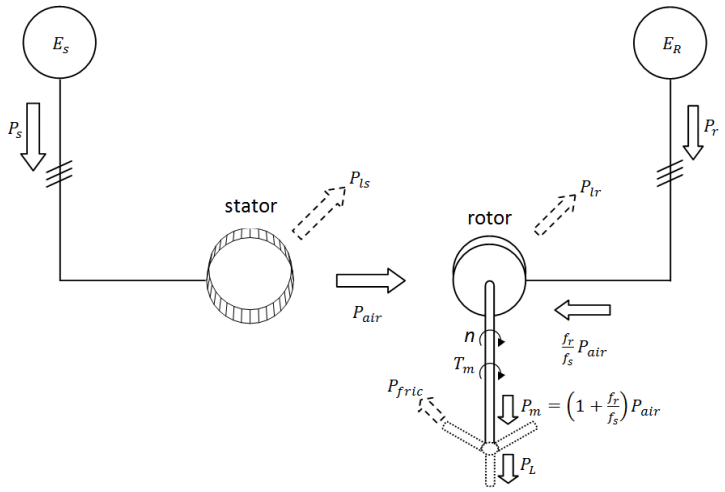

Figure 2.8: Power flow of DFIM at super-synchronous speed

As shown in Figure 2.8, DFEM operates as a motor at a super-synchronous speed. In this mode, a motoring torque which is positive is produced at the shaft. The slip is negative from Equation (2.2) and both the stator and rotor circuit are generating power. A negative slip also means the phase sequence of the injecting rotor voltage is

changed from ABC to ACB. By neglecting the power losses both of the stator windings and rotor windings and the friction losses, the following equations are obtained:

$$P_r \approx -\frac{f_r}{f_s}|P_s| < 0; P_s < 0 \tag{2.7}$$

$$P_m \approx |P_s| + |P_r| = -P_s - P_r \approx T_e * n * \frac{2*\pi}{60} \tag{2.8}$$

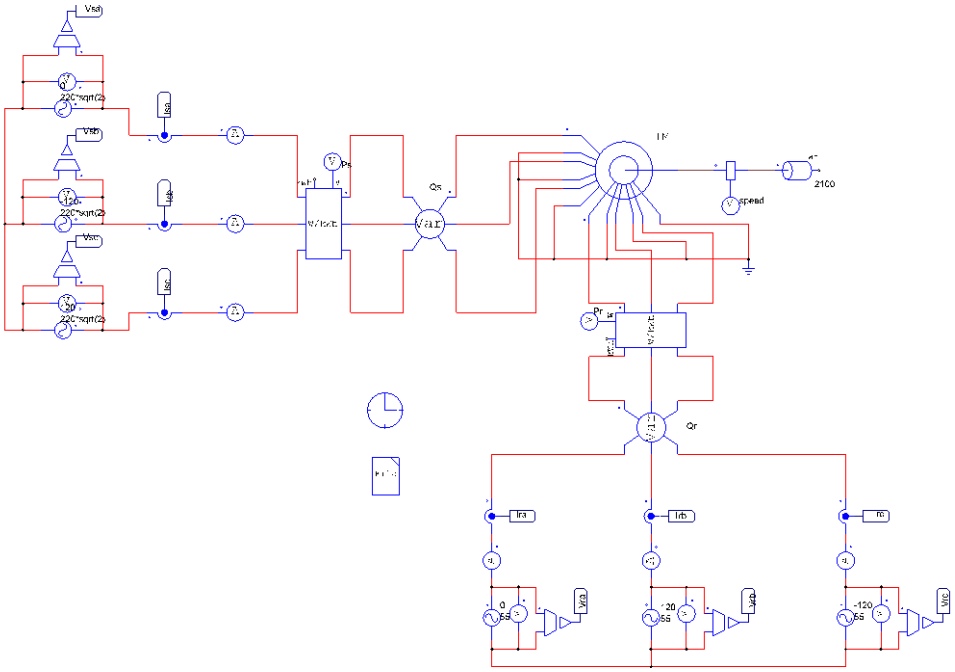

Figure 2.9: Simulation configuration of DFIM at super-synchronous speed

DFIM at super-synchronous speed is simulated as shown in Figure 2.9. In such a case, the magnitude of the stator voltage V_s is still chosen to be 311.1V. Shaft speed is chosen to be 2100 rpm which is larger than the synchronous speed (1800 rpm). The stator voltages and stator currents of DFIM are measured and shown in Figure 2.10. The rotor voltages and rotor currents of DFIM are measured and shown in Figure 2.11. Stator power, rotor power and electromagnetic torque of DFIM are measured and shown in Figure 2.12. The simulation results with all the measurements are summarized in Table 2.3.

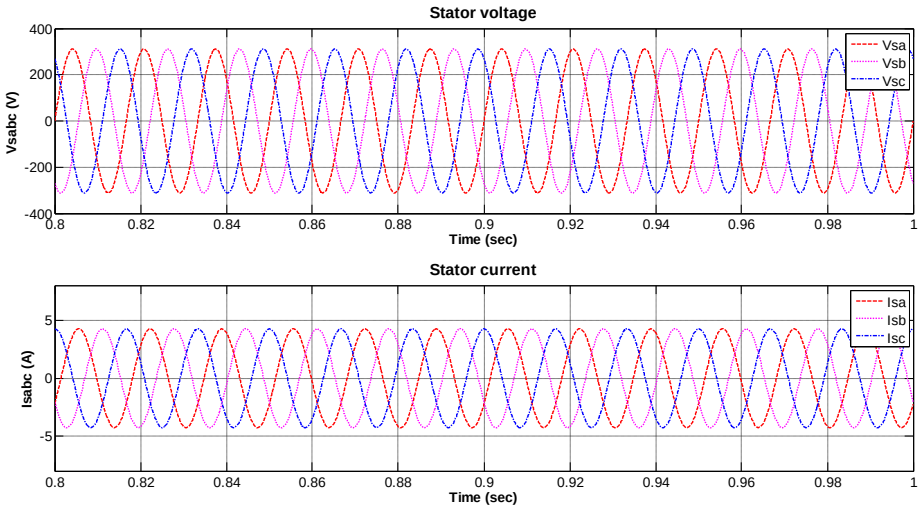

Figure 2.10: Stator voltage and stator current of DFIM at super-synchronous speed

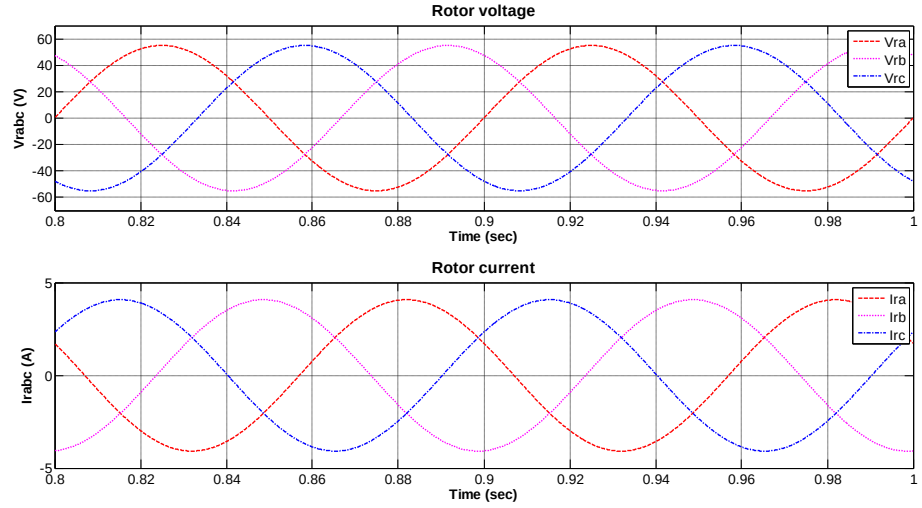

Figure 2.11: Rotor voltage and rotor current of DFIM at super-synchronous speed

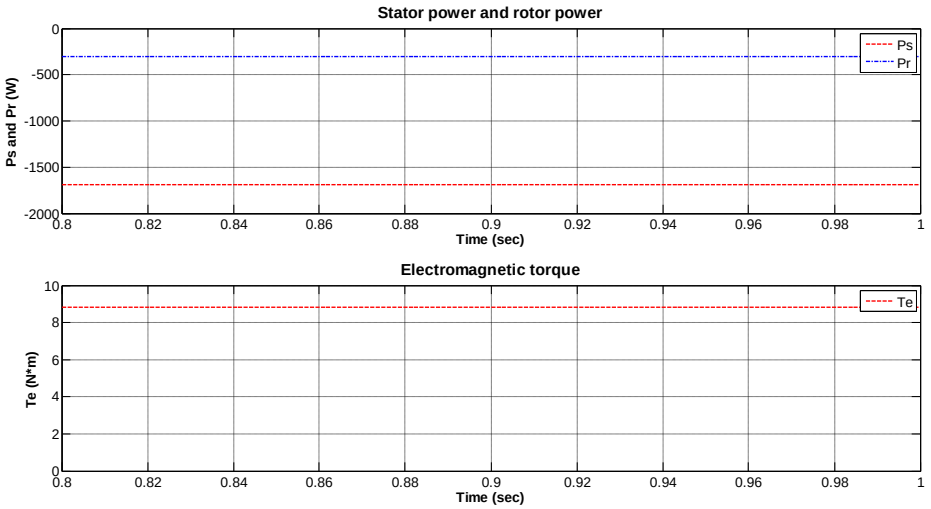

Figure 2.12: Stator power, rotor power and electromagnetic torque of DFIM at super-synchronous speed

As depicted in Table 2.3, the stator active power P_s and the rotor active power P_r measured in the simulation demonstrates the power flow in Figure 2.8.

Table 2.3: Simulation results of DFIM at super-synchronous speed

	stator	**rotor**
voltage magnitude (V)	311.10	55.00
frequency (Hz) (phase sequence)	60 (ABC)	10 (ACB)
current magnitude (A)	4.25	4.08
active power (W)	-1692.80	-304.11
speed (Rpm)	2100	
slip	-1/6	
torque (N*m)	8.82	

2.2.3 DFIG at sub-synchronous speed

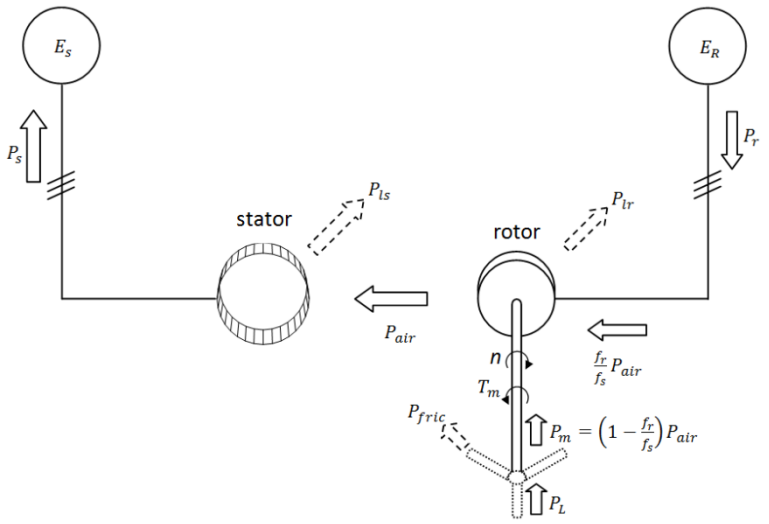

Figure 2.13: Power flow of DFIG at sub-synchronous speed

As shown in Figure 2.13, DFEM operates as a generator at a sub-synchronous speed. In this mode, a generating torque which is negative is produced at the shaft. The slip is positive as seen from Equation (2.2) and both of the rotor circuit and the shaft are generating power. By neglecting the power losses both of the stator windings and rotor windings and the friction losses, the following equations are obtained:

$$P_r \approx \frac{f_r}{f_s}(-P_s) < 0; P_s > 0 \tag{2.9}$$

$$P_m \approx -(|P_s| - |P_r|) = -P_s - P_r \approx T_e * n * \frac{2*\pi}{60} \tag{2.10}$$

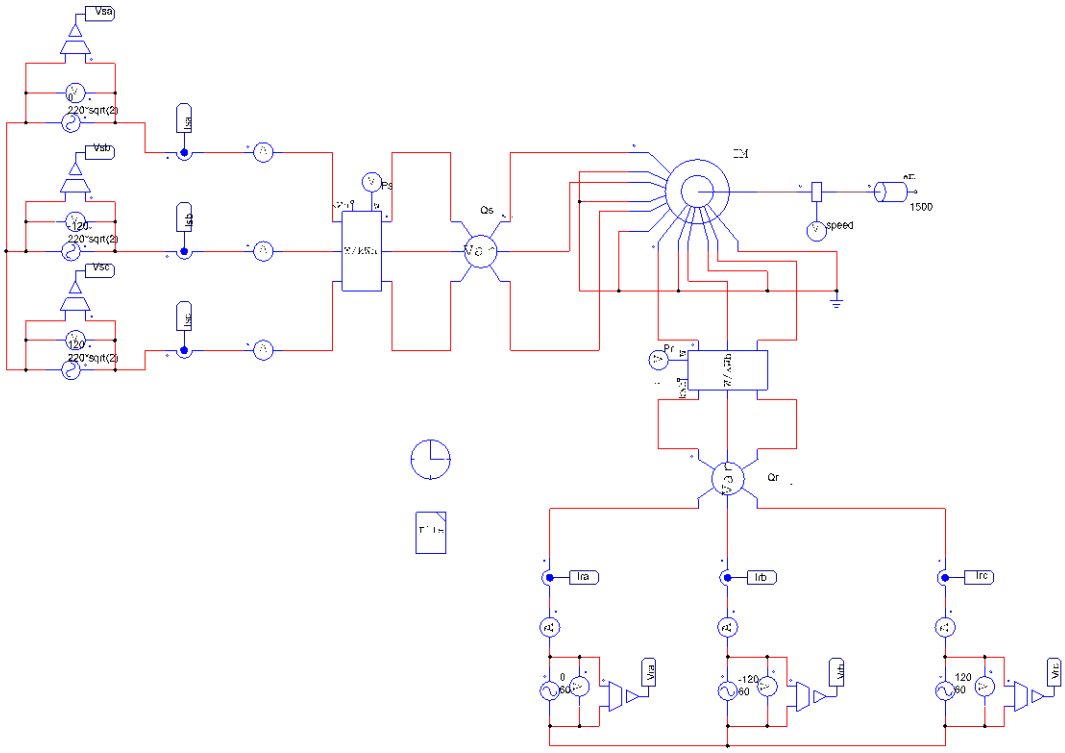

Figure 2.14: Simulation configuration of DFIG at sub-synchronous speed

DFIG at sub-synchronous speed is simulated as shown in Figure 2.14. In such a case, the magnitude of the stator voltage V_s is settled as 311.1V. Shaft speed is chosen to be 1500 rpm which is smaller than the synchronous speed (1800 rpm). The stator voltages and stator currents of DFIG are measured and shown in Figure 2.15. The rotor voltages and rotor currents of DFIG are measured and shown in Figure 2.16. Stator power, rotor power and electromagnetic torque of DFIG are measured and shown in Figure 2.17. The simulation results with all the measurements are tabulated in Table 2.4.

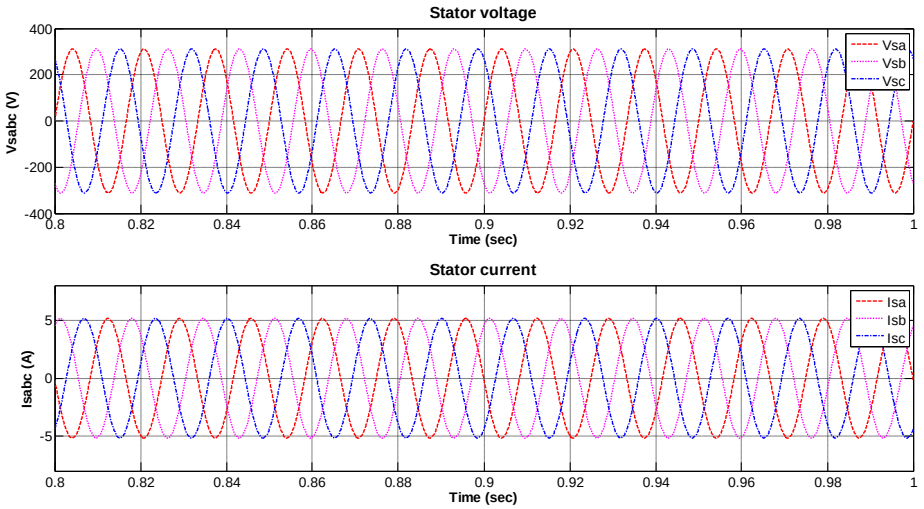

Figure 2.15: Stator voltage and stator current of DFIG at sub-synchronous speed mode

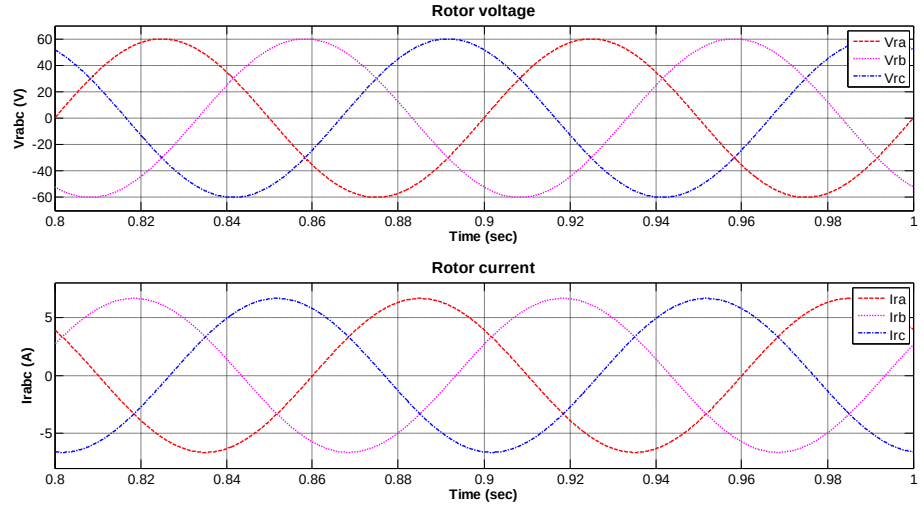

Figure 2.16: Rotor voltage and rotor current of DFIG at sub-synchronous speed

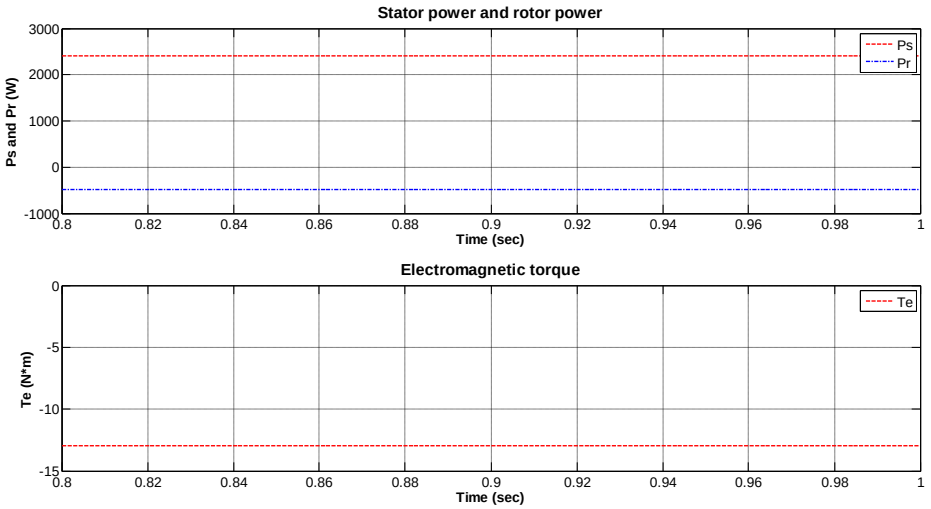

Figure 2.17: Stator power, rotor power and electromagnetic torque of DFIG at sub-synchronous speed

As shown in Table 2.4, the stator active power P_s and the rotor active power P_r measured in the simulation demonstrates the power flow in Figure 2.13.

Table 2.4: Simulation results of DFIG at sub-synchronous speed

	stator	**rotor**
voltage magnitude (V)	311.10	60.00
frequency (Hz) (phase sequence)	60 (ABC)	10 (ABC)
current magnitude (A)	5.15	6.63
active power (W)	2401.86	-479.20
speed (Rpm)	1500	
slip	1/6	
torque (N*m)	-12.98	

2.2.4 DFIG at super-synchronous speed

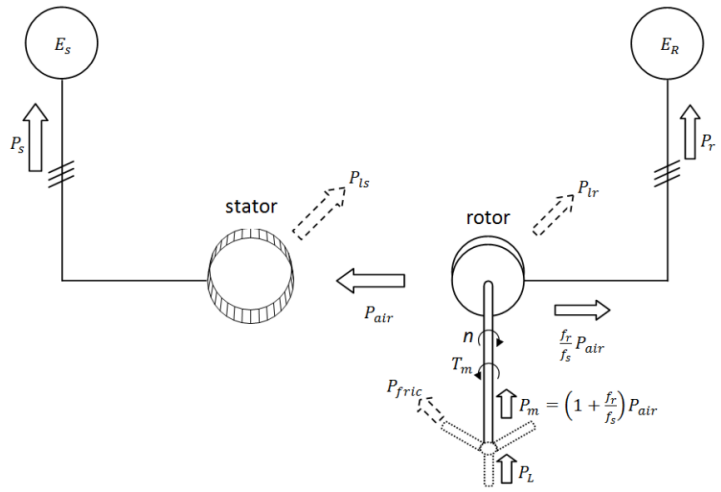

Figure 2.18: Power flow of DFIG at super-synchronous speed mode

As displayed in Figure 2.18, DFEM operates as a generator at a super-synchronous speed. In this mode, a generating torque which is negative is produced at the shaft. The slip is negative from Equation (2.2) and both the stator and rotor circuit are consuming power from the shaft. A negative slip also means the phase sequence of the injecting rotor voltage is changed from ABC to ACB. By neglecting the power losses both of the stator windings and rotor windings and the friction losses, the following equations are obtained:

$$P_r \approx -\frac{f_r}{f_s}(-P_s) > 0; P_s > 0 \tag{2.11}$$

$$P_m \approx -(|P_s| + |P_r|) = -P_s - P_r \approx T_e * n * \frac{2*\pi}{60} \tag{2.12}$$

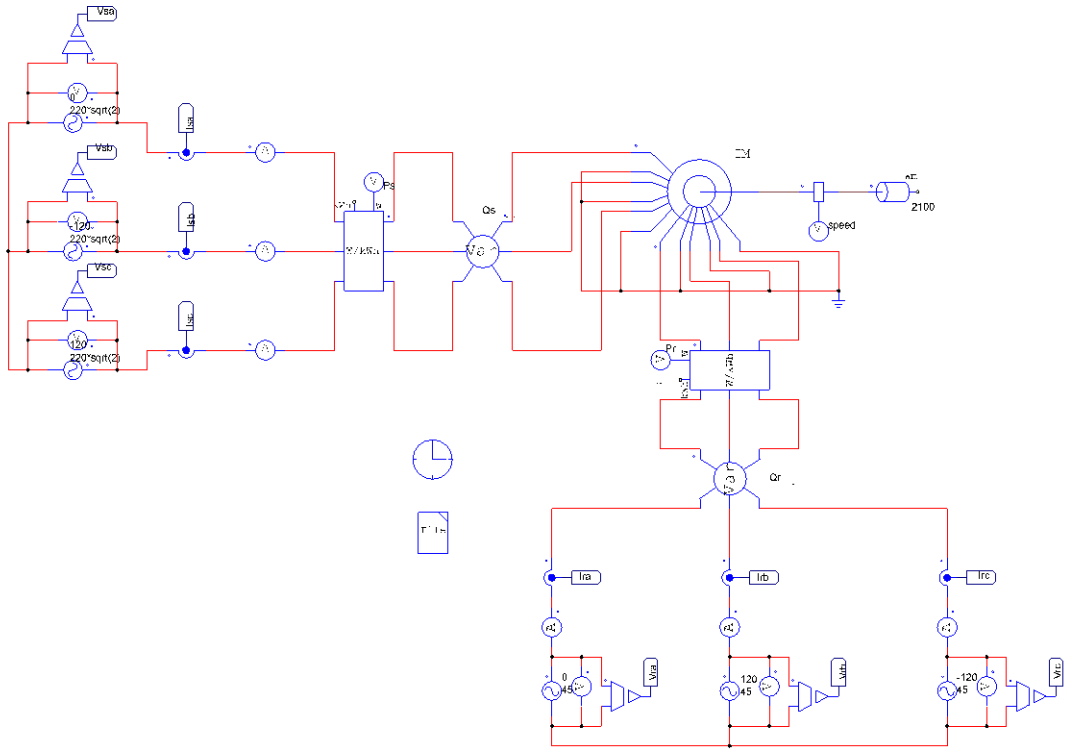

Figure 2.19: Simulation configuration of DFIG at super-synchronous speed mode

DFEM operates as a generator at super-synchronous speed mode is simulated and shown in Figure 2.19. In such a case, the magnitude of the stator voltage V_s is pick as 311.1V. Shaft speed is chosen to be 2100 rpm which is larger than the synchronous speed (1800 rpm). The stator voltages and stator currents of DFIG are measured and shown in Figure 2.20. The rotor voltages and rotor currents of DFIG are measured and shown in Figure 2.21. Stator power, rotor power and electromagnetic torque of DFIG are measured and shown in Figure 2.22. The simulation results with all the measurements are summarized in Table 2.5.

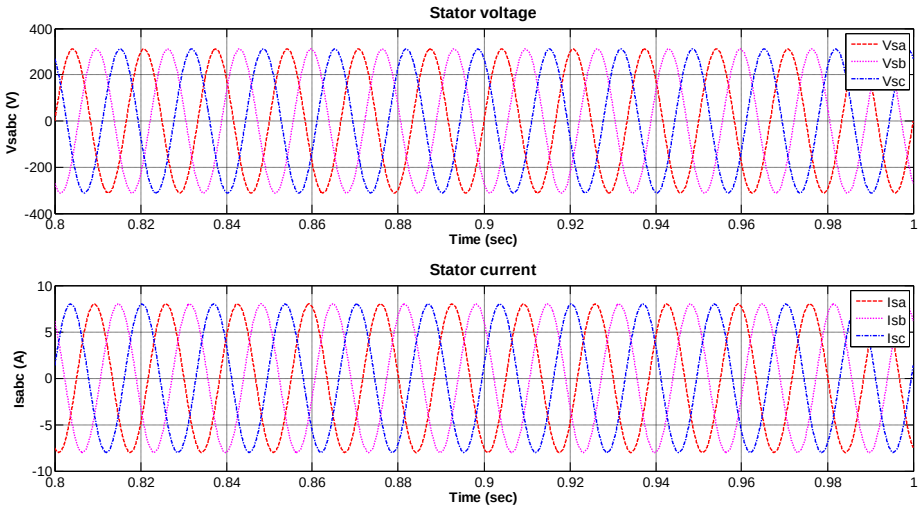

Figure 2.20: Stator voltage and stator current of DFIG at super-synchronous speed

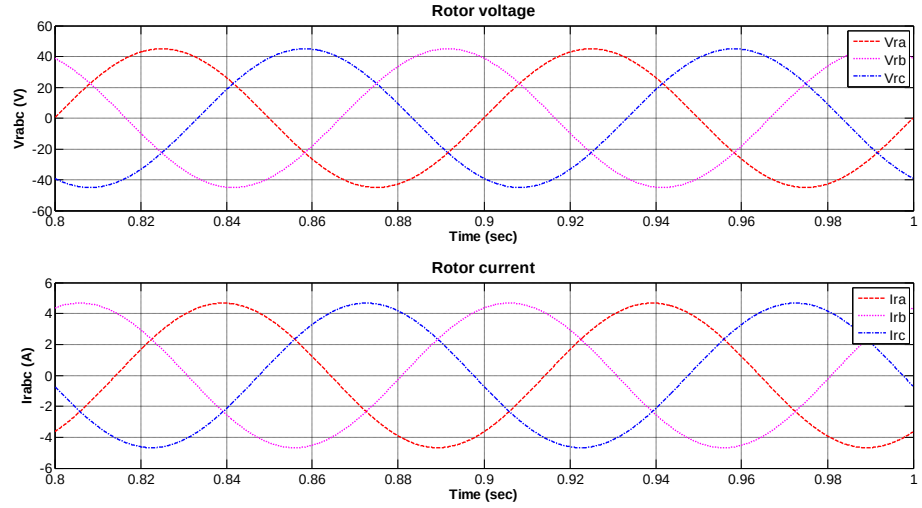

Figure 2.21: Rotor voltage and rotor current of DFIG at super-synchronous speed

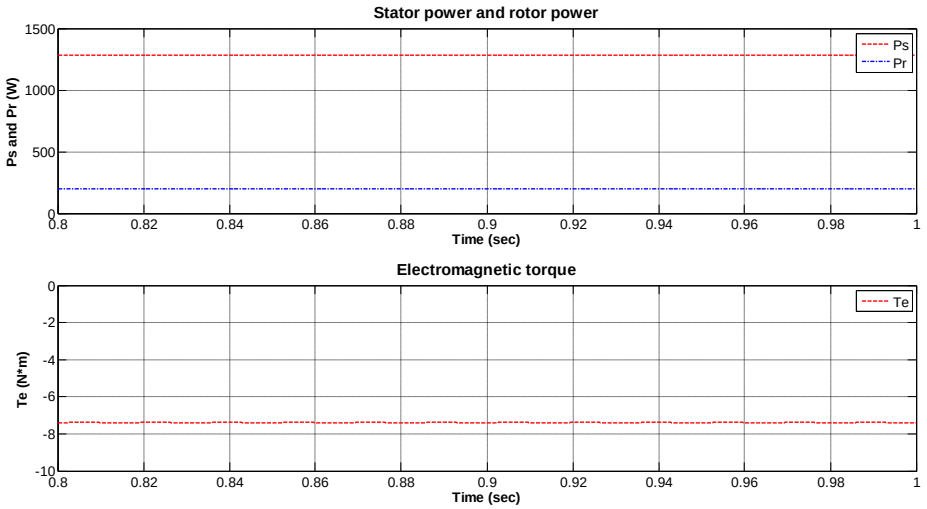

Figure 2.22: Stator power, rotor power and electromagnetic torque of DFIG at super-synchronous speed

As depicted in Table 2.5, the stator active power P_s and the rotor active power P_r measured in the simulation demonstrates the power flow in Figure 2.18.

Table 2.5: Simulation results of DFIG at super-synchronous speed

	stator	**rotor**
voltage magnitude (V)	311.10	45.00
frequency (Hz) (phase sequence)	60 (ABC)	10 (ACB)
current magnitude (A)	8.00	4.67
active power (W)	1286.15	196.67
speed (Rpm)	2100	
slip	-1/6	
torque (N*m)	-7.39	

2.3 DFIG under the unbalanced conditions

By using the symmetrical component theory, any given set of unbalanced voltages

V_{sa}, V_{sb} and V_{sc} can be expressed in terms of the positive, negative and zero sequence components as below:

1) Zero sequence components, which include of three phasors with an identical magnitude V_{s0} and a zero phase displacement, is depicted in Figure 2.23(a).

2) Positive sequence components, which include of three phasors with an identical magnitude V_{s1} and $\pm 120°$ phase displacement in order of a positive ABC sequence, is depicted in Figure 2.23(b).

3) Negative sequence components, which include of three phasors with an identical magnitude V_{s2} and $\pm 120°$ phase displacement in order of a negative ACB sequence, is depicted in Figure 2.23(c).

The stator voltages can be obtained in terms of symmetrical components as displayed below:

$$\begin{bmatrix} V_{sa} \\ V_{sb} \\ V_{sc} \end{bmatrix} = \begin{bmatrix} 1 & 1 & 1 \\ 1 & a^2 & a \\ 1 & a & a^2 \end{bmatrix} \begin{bmatrix} V_{s0} \\ V_{s1} \\ V_{s2} \end{bmatrix} \tag{2.13}$$

, where a=$1\underline{/120°} = -\frac{1}{2} + j\frac{\sqrt{3}}{2}$.

Similarly, the stator currents can be expressed in terms of symmetrical components as shown below:

$$\begin{bmatrix} I_{sa} \\ I_{sb} \\ I_{sc} \end{bmatrix} = \begin{bmatrix} 1 & 1 & 1 \\ 1 & a^2 & a \\ 1 & a & a^2 \end{bmatrix} \begin{bmatrix} I_{s0} \\ I_{s1} \\ I_{s2} \end{bmatrix} \tag{2.14}$$

As seen in Figure 2.2, in any three-wire Y-connected system with an ungrounded neutral, line currents have no zero sequence components according to KCL. $I_{s0} = 0$. In other words, zero sequence components of the stator voltage have no impact on the operation of the DFIG.

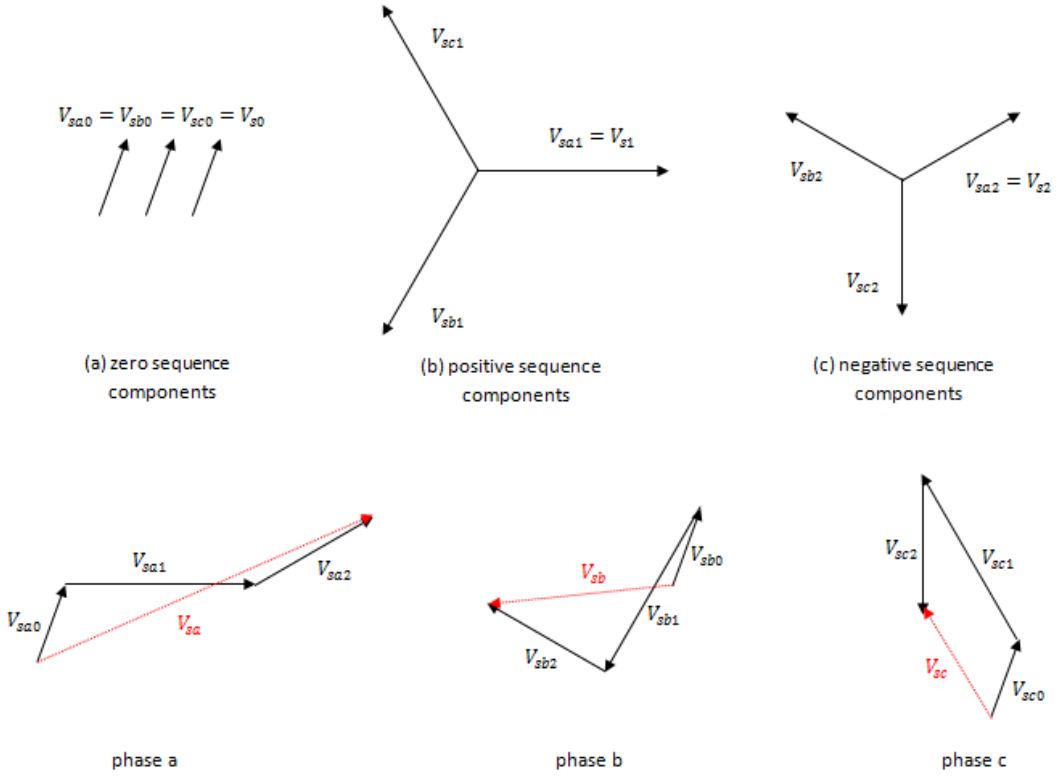

Figure 2.23: Diagram of resolving stator voltages into three sets of symmetrical components

Under the balanced operating conditions, the stator voltage has no zero sequence or negative sequence components. By adjusting Equation (2.2), the frequency of the rotor voltage can be simplified as,

$$f_{r1} = f_s * \frac{n_e - n}{n_e} = sf_s \tag{2.15}$$

As seen in this equation, a negative rotor frequency indicates that the phase sequence is ACB for super-synchronous speed. The rotor frequency is positive and with ABC sequence when operating in sub-synchronous speed. The steady state equivalent circuit of DFIG under the balanced operating conditions is displayed in Figure 2.24(a). It can be noticed that, the power flow direction is determined by the phase sequence of the rotor frequency under the balanced conditions. When DFIG operates under a sub-synchronous speed, the active power flows from the rotor side to the stator side, which means that the rotor circuit is generating power to the grid.

When DFIG operates in the super-synchronous speed mode, the active power flows from the shaft to the rotor circuit, which means that the rotor circuit is absorbing power from the shaft.

Under the unbalanced operating conditions, the stator voltage of DFIG can be represented with symmetrical components as following;

$$\begin{bmatrix} V_{s0} \\ V_{s1} \\ V_{s2} \end{bmatrix} = \frac{1}{3}\begin{bmatrix} 1 & 1 & 1 \\ 1 & a & a^2 \\ 1 & a^2 & a \end{bmatrix}\begin{bmatrix} V_{sa} \\ V_{sb} \\ V_{sc} \end{bmatrix} \tag{2.16}$$

Since the zero components of the stator voltage have no impact on the operation of DFIG, the steady state equivalent circuit of DFIG under the unbalanced operating conditions is displayed in Figure 2.24(b).

The frequency of the negative sequence rotor voltage can be represented as shown below:

$$f_{r2} = -f_s * \frac{-n_e - n}{-n_e} = -f_s \frac{2n_e - n_e + n}{n_e} = -f_s \left(2 - \frac{n_e - n}{n_e}\right) = (s-2)f_s \tag{2.17}$$

Since the slip, s, has a range between -1 and 1, the rotor frequency will always be negative regardless of the mode of operation (sub-synchronous speed or super-synchronous speed).

In summary, under the unbalanced operating conditions, the injected three phase rotor voltage may have two components V_{r1} with the frequency $|s|f_s$ (in ABC or ACB sequence) and V_{r2} with the frequency $|(s-2)|f_s$ (only in ACB sequence). The steady state model of the DFIG under the unbalanced voltages is shown in Fig.2.24

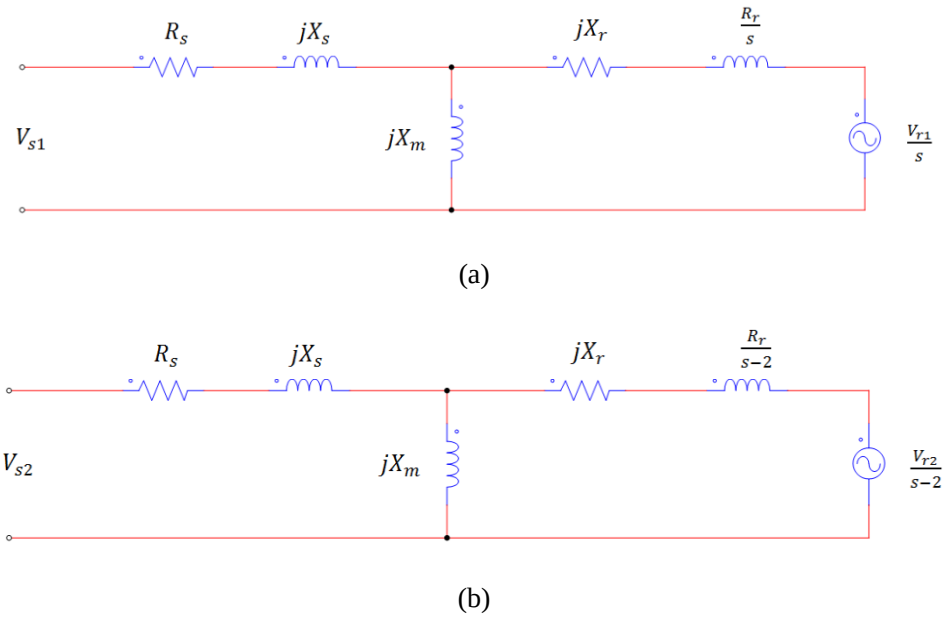

Figure 2.24: Equivalent circuit of a DFIG in the steady state steady: a) positive sequence; b) negative sequence

The open loop operation of DFIG under the unbalanced voltage supply at super-synchronous speed is simulated and displayed in Figure 2.25. The stator phase B voltage is then set to zero as a line fault condition. The stator voltages represented as phasors

are shown below,

$V_{sa} = 220\underline{/0°}; V_{sb} = 0\underline{/\text{-}120°}; V_{sc} = 220\underline{/120°}$.

The rotor circuit is replaced with a three-phase resistive load $R_L = 48$ Ohms. Shaft speed is chosen as 2100 rpm which is larger than the synchronous speed (1800 rpm). The stator voltages and stator currents of DFIG are displayed in Figure 2.26. The rotor voltages and rotor currents of DFIG are displayed in Figure 2.27. Stator power, rotor power and electromagnetic torque of DFIG are displayed in Figure 2.28.

As shown in Figure 2.30, the rotor frequency has two components:

$f_{r1} = sf_s = -\frac{1}{6} * 60 = -10\text{Hz}$ (in ACB sequence);

$f_{r2} = (s-2)f_s = -\frac{13}{6} * 60 = -130Hz$ (in ACB sequence).

The stator active power, rotor active power and electromagnetic torque have pulsations at $2f_s$=120Hz as depicted in Figure 2.28.

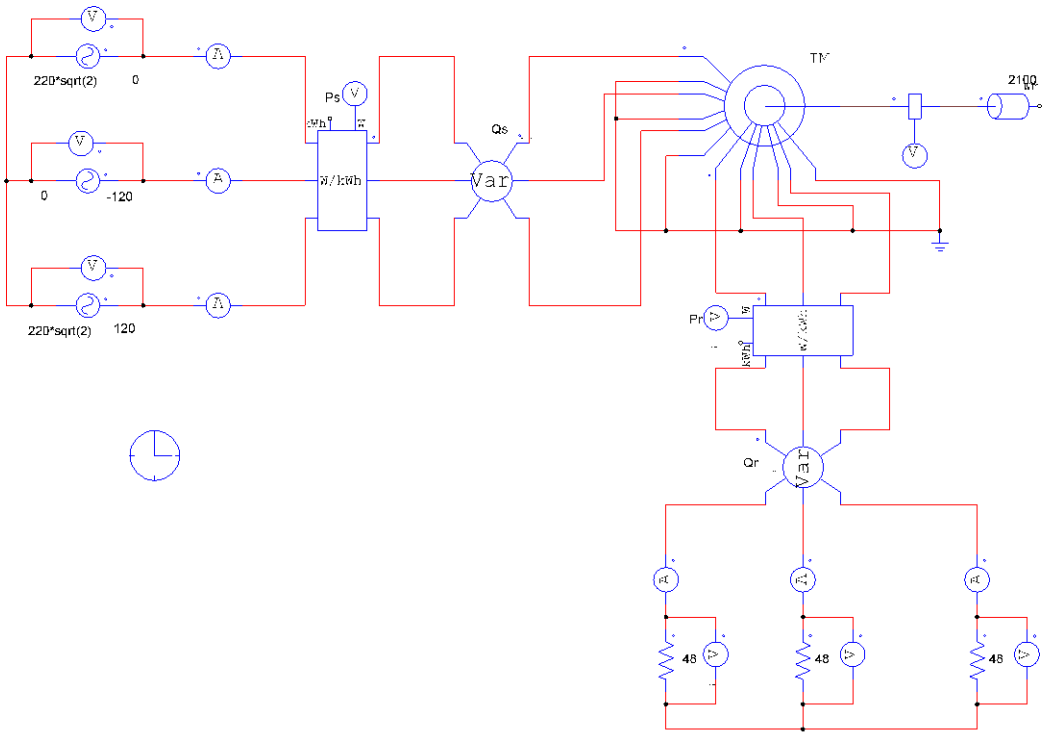

Figure 2.25: Simulation configuration of DFIG under the unbalanced condition ($V_{sb} = 0$)

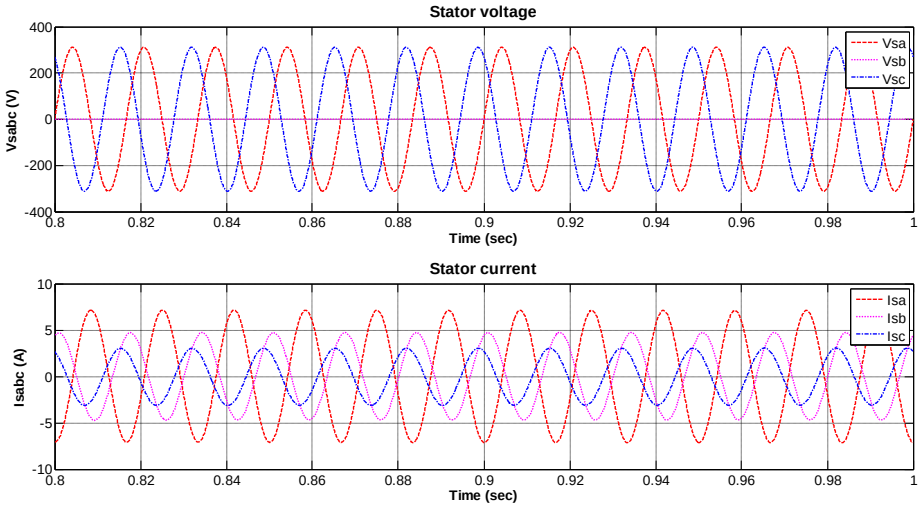

Figure 2.26: Stator voltage and stator current of DFIG under the unbalanced condition

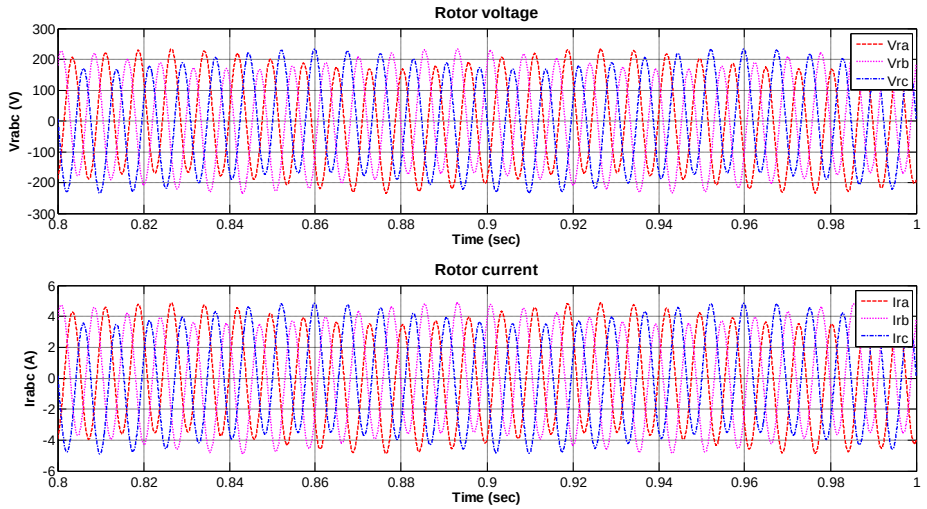

Figure 2.27: Rotor voltage and rotor current of DFIG under the unbalanced condition

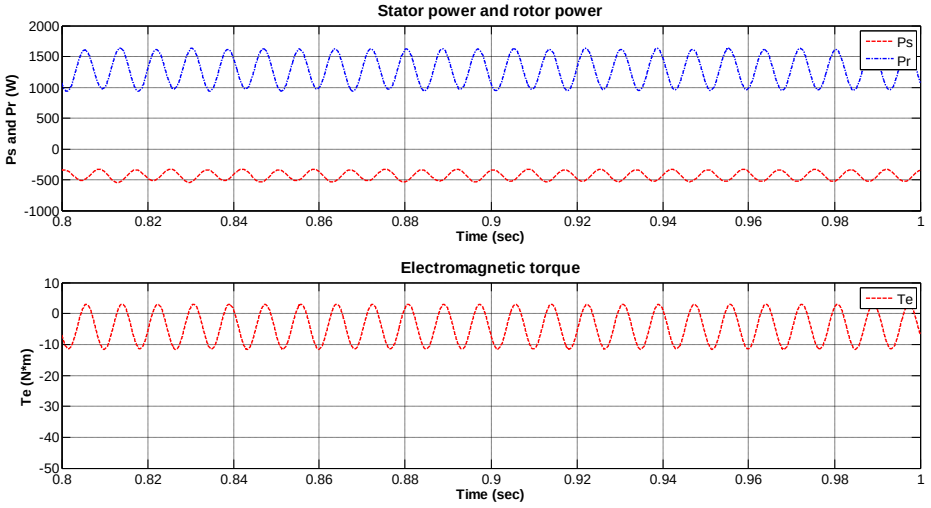

Figure 2.28: Stator power, rotor power and electromagnetic torque of DFIG under the unbalanced condition

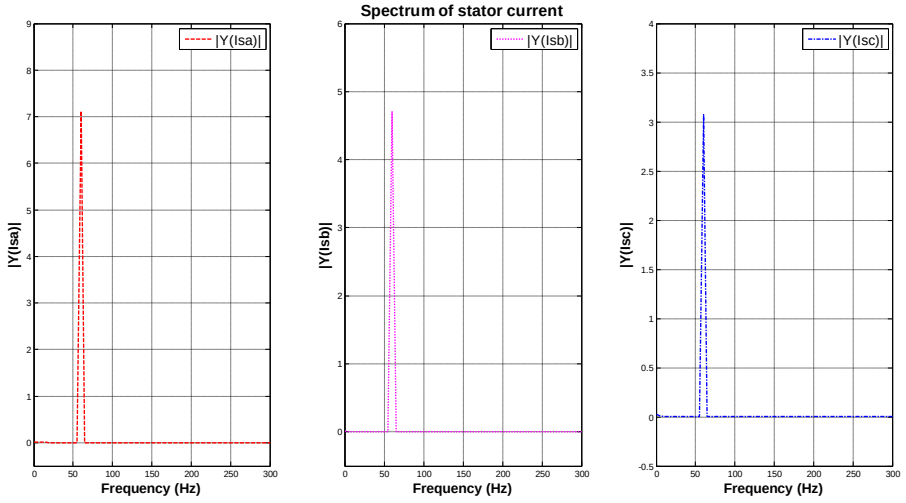

Figure 2.29: Spectrum of stator current of DFIG under the unbalanced condition

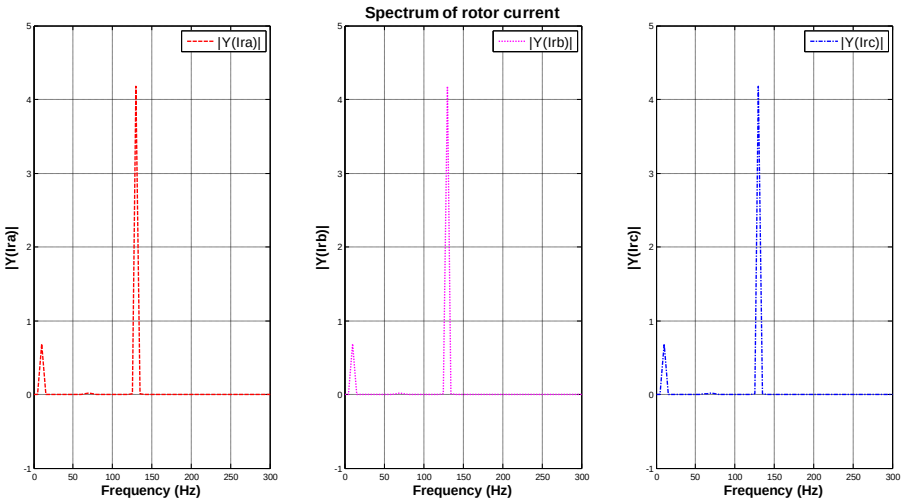

Figure 2.30: Spectrum of rotor current of DFIG under the unbalanced condition

CHAPTER III

THEORETICAL ANALYSIS

3.1 A wind turbine driven DFIG connected to an unbalanced grid

A wind turbine driven by DFIG is basically a standard wound rotor induction machine, which its stator windings is directly connected to the grid and its rotor windings is connected to the grid through a BTB PWM converter and a three phase transformer. The BTB converter includes of a RSC, a GSC and a DC link capacitor between them. The RSC is connecting between the rotor windings and DC link capacitor, while the GSC is connecting between the DC link capacitor and the three phase transformer. The other side of the transformer is connecting to the grid directly. Both PWM converters in the BTB circuits can work as a rectifier or an inverter depending on the rotating speed. Under the balanced condition, the active power flows from the rotor via the BTB converter and transformer to the grid at a super-synchronous speed, whereas it flows in the opposite direction in a sub-synchronous speed.

Under the unbalanced grid voltage operation, the stator voltage and the stator current will contain both of the positive and negative sequence components. These negative sequence components will force the stator power to create the periodic pulsating terms at twice the grid frequency. This leads to the appearance of the low order harmonics in the line current, as well as the huge pulsation in a DC link voltage pulsation.

3.2 Control strategy for the RSC of DFIG under the unbalanced operating conditions

The equivalent circuit of a DFIG in dq synchronous rotating frame is shown in Figure 3.1[25].

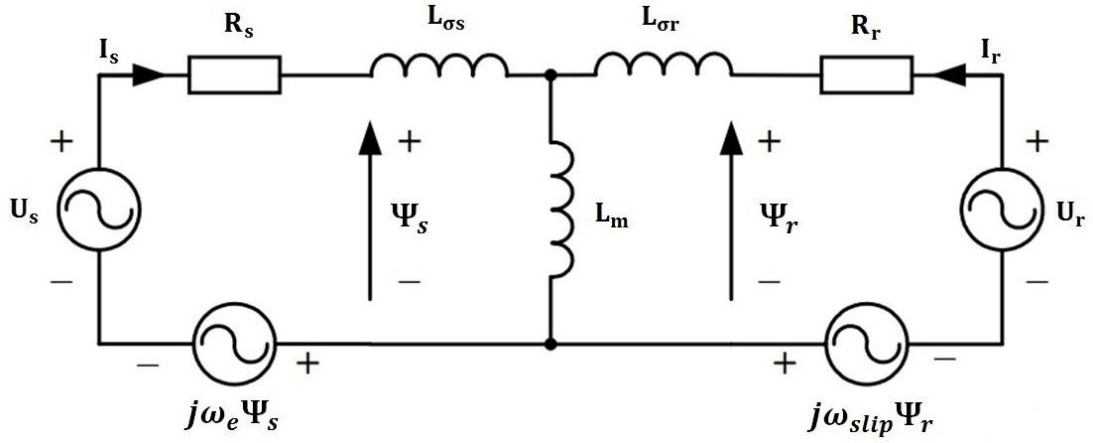

Figure 3.1: DFIG equivalent circuit in dq synchronous rotating frame[25]

As displayed in the above figure, the stator voltage vector and the rotor voltage vector can be obtained as following[25].

$$U_s = R_s I_s + \frac{d\Psi_s}{dt} + j\omega_e \Psi_s \tag{3.1}$$

$$U_r = R_r I_r + \frac{d\Psi_r}{dt} + j\omega_{slip} \Psi_r \tag{3.2}$$

, where U_s, U_r are the stator and rotor voltage vectors separately, which can be represented as $U_s = u_{sd} + ju_{sq}$ and $U_r = u_{rd} + ju_{rq}$; I_s, I_r are the stator and rotor current vectors respectively, which can be represented as $I_s = i_{sd} + ji_{sq}$ and $I_r = i_{rd} + ji_{rq}$; Ψ_s, Ψ_r are the stator flux vector and rotor flux vector separately, which can be represented as $\Psi_s = \psi_{sd} + j\psi_{sq}$ and $\Psi_r = \psi_{rd} + j\psi_{rq}$; ω_e, ω_{slip} are the synchronous angular speed and slip angular speed respectively; R_s and R_r are the stator and rotor resistance; $L_{\sigma s}$ and $L_{\sigma r}$ are the stator leakage inductance and rotor leakage inductance; L_m is the magnetizing inductance which can be measured by using different approaches[41,42].

The stator flux vector and the rotor flux vector can be expressed as following.

$$\Psi_s = L_s I_s + L_m I_r \tag{3.3}$$

$$\Psi_r = L_r I_r + L_m I_s \tag{3.4}$$

, where $L_s = L_{\sigma s} + L_m$ and $L_r = L_{\sigma r} + L_m$.

Equations (3.1) - (3.4) are valid not only under the balanced operating conditions, but also the unbalanced operating conditions. Under the balanced condition, the wound rotor induction generator is being controlled in dq synchronous rotating frame, where the d-axis is along with the stator flux vector's position.

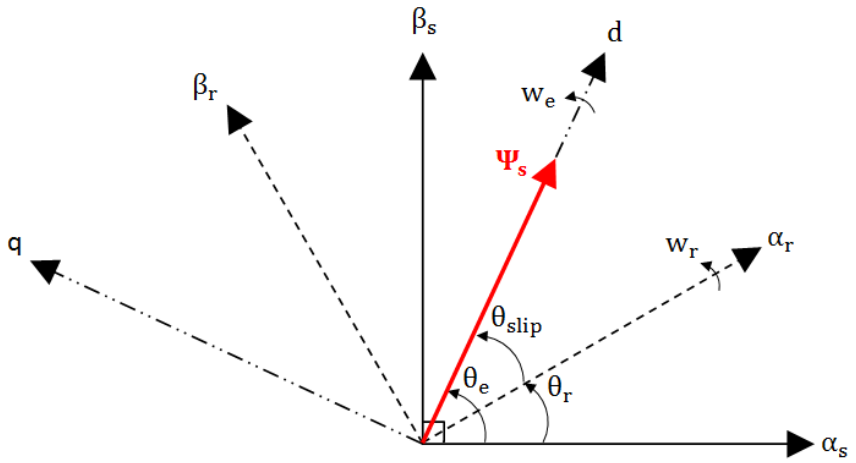

Figure 3.2: Vector diagram of stator flux oriented control method (SFOC) under the balanced conditions[24]

As displayed in Figure 3.2, the stator flux vector in dq-axis is obtained as following.

$$\psi_{sd} = \Psi_s = L_s i_{sd} + L_m i_{rd} \tag{3.5}$$

$$\psi_{sq} = 0 = L_s i_{sq} + L_m i_{rq} \tag{3.6}$$

Under the balanced operating conditions, the resistance of the stator windings is small and negligible, as well as the stator flux can be considered constant. With such consideration, Equation (3.1) can be substituted by Equations (3.5) and (3.6), where the dq components of the stator voltage vector can be approximately represented as below:

$$u_{sd} = -\omega_e \psi_{sq} = 0 \tag{3.7}$$

$$u_{sq} = \omega_e \psi_{sd} = U_s \tag{3.8}$$

The stator active power P_s and reactive power Q_s can be represented as below:

$$P_s = \frac{3}{2}\left(u_{sd} i_{sd} + u_{sq} i_{sq}\right) \tag{3.9}$$

$$Q_s = \frac{3}{2}\left(u_{sq} i_{sd} - u_{sd} i_{sq}\right) \tag{3.10}$$

From Equation (3.6) the following equation is obtained and given by:

$$i_{sq} = -\frac{L_m}{L_s} i_{rq} \tag{3.11}$$

By combining Equations (3.7), (3.8),(3.11) and (3.9) the following equation is obtained,

$$P_s = -\frac{3}{2}\frac{L_m}{L_s}U_s i_{rq} \tag{3.12}$$

By combining Equations (3.8) and (3.5) the following equation is obtained and given by,

$$\psi_{sd} = \frac{U_s}{\omega_e} = L_s i_{sd} + L_m i_{rd} \tag{3.13}$$

i_{sd} can be expressed as:

$$i_{sd} = \frac{U_s}{\omega_e L_s} - \frac{L_m}{L_s} i_{rd} \tag{3.14}$$

By substituting variables in Equations (3.7), (3.8) and (3.14) into Equations (3.10)the following equation is obtained and given by,

$$Q_s = \frac{3}{2}U_s\left(\frac{U_s}{\omega_e L_s} - \frac{L_m}{L_s} i_{rd}\right) \tag{3.15}$$

As expressed in Equations (3.12) and (3.15), the stator active power and the stator reactive power are controlled by i_{rq} and i_{rd} only. However, under the unbalanced operating conditions, the approximately linear characteristics as shown in these two equations are no longer valid. Under the unbalanced operating conditions, the active stator power will contain a second order harmonic. This will in turn generate pulsating power in the RSC and DC link capacitor. In addition, the grid currents will no longer be sinusoidal.

In such consideration, a generalized control method with both positive sequence controller and negative sequence controller is proposed and implemented in this chapter. The positive sequence controller is to regulate the average stator active power and the average stator reactive power at some certain levels, while the negative sequence controller is to eliminate the oscillation and pulsation of the stator active

power.

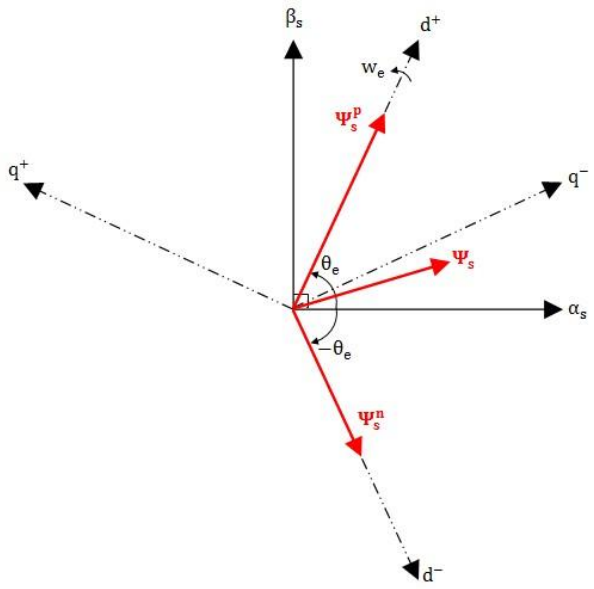

Figure 3.3: Vector diagram of stator flux oriented control method under the unbalanced operating conditions

As shown in Figure 3.3, under the unbalanced operating conditions, stator flux vector can be decomposed and extracted into two symmetrical components which are the positive sequence components and negative sequence components[43].

$$\Psi_s = \Psi_s^p e^{j(\omega_e t+\theta^p)} + \Psi_s^n e^{j(-\omega_e t+\theta^n)} = \left(\psi_{sd}^p + j\psi_{sq}^p\right)e^{j\omega_e t} + \left(\psi_{sd}^n + j\psi_{sq}^n\right)e^{-j\omega_e t} \quad (3.16)$$

, where ψ_{sd}^p and ψ_{sq}^p are the dq components of stator flux vector's positive sequence quantities, ψ_{sd}^n and ψ_{sq}^n are the dq components of stator flux vector's negative sequence quantities.

Similarly, stator current and stator voltage vectors can be represented in the following two equations.

$$I_s = \left(i_{sd}^p + ji_{sq}^p\right)e^{j\omega_e t} + \left(i_{sd}^n + ji_{sq}^n\right)e^{-j\omega_e t} \quad (3.17)$$

, where i_{sd}^{p} and i_{sq}^{p} are represented as the dq components of stator current vector's positive sequence quantities separately, i_{sd}^{n} and i_{sq}^{n} are defined as the dq components of stator current vector's negative sequence quantities respectively.

$$U_s = \left(u_{sd}^{p} + ju_{sq}^{p}\right)e^{j\omega_e t} + \left(u_{sd}^{n} + ju_{sq}^{n}\right)e^{-j\omega_e t} \tag{3.18}$$

, where u_{sd}^{p} and u_{sq}^{p} are the dq components of stator voltage vector's positive sequence quantities, u_{sd}^{n} and u_{sq}^{n} are the dq components of stator voltage vector's negative sequence quantities.

Under the unbalanced operating conditions, positive dq reference frame is chosen in which the positive d-axis is along the stator flux's position. Then the stator voltage and stator flux vector can also be expressed by following two equations[44]:

$$\Psi_s = \Psi_s^{p} + \Psi_s^{n}e^{-j2\omega_e t} \tag{3.19}$$

$$U_s = U_s^{p} + U_s^{n}e^{-j2\omega_e t} \tag{3.20}$$

Under the unbalanced operating conditions, the stator flux cannot be considered constant. By neglecting the stator resistance and substituting Equation (3.19) into (3.1) the following equation is obtained and given by,

$$U_s = \frac{d\left(\Psi_s^{p} + \Psi_s^{n}e^{-j2\omega_e t}\right)}{dt} + j\omega_e\left(\Psi_s^{p} + \Psi_s^{n}e^{-j2\omega_e t}\right) = j\omega_e\Psi_s^{p} - j\omega_e\Psi_s^{n}e^{-j2\omega_e t} \tag{3.21}$$

From Equations (3.20) and (3.21), the relationships between the positive sequence components of the stator voltage vector and stator flux vector, as well as the negative sequence components of the stator voltage and stator flux are obtained by,

$$U_s^{p} = j\omega_e\Psi_s^{p} = j\omega_e\left(\psi_{sd}^{p} + j\psi_{sq}^{p}\right) \tag{3.22}$$

$$U_s^{n} = -j\omega_e\Psi_s^{n} = -j\omega_e\left(\psi_{sd}^{n} + j\psi_{sq}^{n}\right) \tag{3.23}$$

Since the positive d-axis is along the stator flux's vector, it yields as below.

$$\psi_{sq}^{p} = 0 \tag{3.24}$$

Equations (3.22) and (3.23) can be simplified as,

$$u_{sd}^{p} = -\omega_e \psi_{sq}^{p} = 0 \tag{3.25}$$

$$u_{sq}^{p} = \omega_e \psi_{sd}^{p} \tag{3.26}$$

$$u_{sd}^{n} = \omega_e \psi_{sq}^{n} \tag{3.27}$$

$$u_{sq}^{n} = -\omega_e \psi_{sd}^{n} \tag{3.28}$$

Under the unbalanced operating conditions, the stator active power and stator reactive power at the point of common coupling (PCC) are expressed as [43].

$$P_s = P_{s\_avg} + P_{s\_sin} \sin(2\omega_e t) + P_{s\_cos} \cos(2\omega_e t) \tag{3.29}$$

$$Q_s = Q_{s\_avg} + Q_{s\_sin} \sin(2\omega_e t) + Q_{s\_cos} \cos(2\omega_e t) \tag{3.30}$$

As shown above, the stator active power has three terms: DC average active power P_{s_avg}, pulsating active power P_{s_sin} and P_{s_cos} at twice the input frequency; the stator reactive power also has three terms: DC average reactive power Q_{s_avg}, pulsating reactive power Q_{s_sin} and Q_{s_cos} at twice the input frequency. All these six variables are given by the following equation[45].

$$\begin{bmatrix} P_{s\_avg} \\ P_{s\_sin} \\ P_{s\_cos} \\ Q_{s\_avg} \\ Q_{s\_sin} \\ Q_{s\_cos} \end{bmatrix} = \frac{3}{2} \begin{bmatrix} u_{sd}^{p} & u_{sq}^{p} & u_{sd}^{n} & u_{sq}^{n} \\ u_{sq}^{n} & -u_{sd}^{n} & -u_{sq}^{p} & u_{sd}^{p} \\ u_{sd}^{n} & u_{sq}^{n} & u_{sd}^{p} & u_{sq}^{p} \\ u_{sq}^{p} & -u_{sd}^{p} & u_{sq}^{n} & -u_{sd}^{n} \\ -u_{sd}^{n} & -u_{sq}^{n} & u_{sd}^{p} & u_{sq}^{p} \\ u_{sq}^{n} & -u_{sd}^{n} & u_{sq}^{p} & -u_{sd}^{p} \end{bmatrix} \begin{bmatrix} i_{sd}^{p} \\ i_{sq}^{p} \\ i_{sd}^{n} \\ i_{sq}^{n} \end{bmatrix} \tag{3.31}$$

Under the unbalanced operating conditions, Equation (3.3) can be expressed as,

$$i_{sd}^{p} = \frac{1}{L_s}\left(\psi_{sd}^{p} - L_m i_{rd}^{p}\right) \tag{3.32}$$

$$i_{sq}^{p} = \frac{1}{L_s}\left(\psi_{sq}^{p} - L_m i_{rq}^{p}\right) \tag{3.33}$$

$$i_{sd}^{n} = \frac{1}{L_s}(\psi_{sd}^{n} - L_m i_{rd}^{n}) \tag{3.34}$$

$$i_{sq}^{n} = \frac{1}{L_s}\left(\psi_{sq}^{n} - L_m i_{rq}^{n}\right) \tag{3.35}$$

, where i_{rd}^{p} and i_{rq}^{p} are the dq components of the rotor current vector's positive sequence quantities, i_{rd}^{n} and i_{rq}^{n} are the dq components of the rotor current vector's negative sequence quantities.

By replacing Equations (3.32) -(3.35) into Equation (3.31) the following equation is obtained and given by,

$$\begin{bmatrix} P_{s\_avg} \\ P_{s\_sin} \\ P_{s\_cos} \\ Q_{s\_avg} \\ Q_{s\_sin} \\ Q_{s\_cos} \end{bmatrix} = \frac{3}{2L_s} \begin{bmatrix} u_{sd}^{p} & u_{sq}^{p} & u_{sd}^{n} & u_{sq}^{n} \\ u_{sq}^{n} & -u_{sd}^{n} & -u_{sq}^{p} & u_{sd}^{p} \\ u_{sd}^{n} & u_{sq}^{n} & u_{sd}^{p} & u_{sq}^{p} \\ u_{sq}^{p} & -u_{sd}^{p} & u_{sq}^{n} & -u_{sd}^{n} \\ -u_{sd}^{n} & -u_{sq}^{n} & u_{sd}^{p} & u_{sq}^{p} \\ u_{sq}^{n} & -u_{sd}^{n} & u_{sq}^{p} & -u_{sd}^{p} \end{bmatrix} \left(\begin{bmatrix} \psi_{sd}^{p} \\ \psi_{sq}^{p} \\ \psi_{sd}^{n} \\ \psi_{sq}^{n} \end{bmatrix} - L_m \begin{bmatrix} i_{rd}^{p} \\ i_{rq}^{p} \\ i_{rd}^{n} \\ i_{rq}^{n} \end{bmatrix} \right) \tag{3.36}$$

By substituting Equations (3.25) - (3.28) into Equation (3.36), the following equation is obtained and expressed as below:

$$\begin{bmatrix} P_{s\_avg} \\ P_{s\_sin} \\ P_{s\_cos} \\ Q_{s\_avg} \\ Q_{s\_sin} \\ Q_{s\_cos} \end{bmatrix} = \frac{3}{2L_s} \begin{bmatrix} u_{sd}^{p} & u_{sq}^{p} & u_{sd}^{n} & u_{sq}^{n} \\ u_{sq}^{n} & -u_{sd}^{n} & -u_{sq}^{p} & u_{sd}^{p} \\ u_{sd}^{n} & u_{sq}^{n} & u_{sd}^{p} & u_{sq}^{p} \\ u_{sq}^{p} & -u_{sd}^{p} & u_{sq}^{n} & -u_{sd}^{n} \\ -u_{sd}^{n} & -u_{sq}^{n} & u_{sd}^{p} & u_{sq}^{p} \\ u_{sq}^{n} & -u_{sd}^{n} & u_{sq}^{p} & -u_{sd}^{p} \end{bmatrix} \left(\frac{1}{\omega_e} \begin{bmatrix} u_{sq}^{p} \\ -u_{sd}^{p} \\ -u_{sq}^{n} \\ u_{sd}^{n} \end{bmatrix} - L_m \begin{bmatrix} i_{rd}^{p} \\ i_{rq}^{p} \\ i_{rd}^{n} \\ i_{rq}^{n} \end{bmatrix} \right) \tag{3.37}$$

Then Equation (3.37) can be simplified as:

$$\begin{bmatrix} P_{s\_avg} \\ P_{s\_sin} \\ P_{s\_cos} \\ Q_{s\_avg} \\ Q_{s\_sin} \\ Q_{s\_cos} \end{bmatrix} =$$

$$\frac{3}{2\omega_e L_s}\begin{bmatrix} 0 \\ 2u_{sd}^{p}u_{sd}^{n} \\ -2u_{sd}^{p}u_{sq}^{n} \\ \left(u_{sd}^{p}\right)^2+\left(u_{sq}^{p}\right)^2-(u_{sd}^{n})^2-\left(u_{sq}^{n}\right)^2 \\ 0 \\ 0 \end{bmatrix} - \frac{3L_m}{2L_s}\begin{bmatrix} u_{sd}^{p} & u_{sq}^{p} & u_{sd}^{n} & u_{sq}^{n} \\ u_{sq}^{n} & -u_{sd}^{n} & -u_{sq}^{p} & u_{sd}^{p} \\ u_{sd}^{n} & u_{sq}^{n} & u_{sd}^{p} & u_{sq}^{p} \\ u_{sq}^{p} & -u_{sd}^{p} & u_{sq}^{n} & -u_{sd}^{n} \\ -u_{sd}^{n} & -u_{sq}^{n} & u_{sd}^{p} & u_{sq}^{p} \\ u_{sq}^{n} & -u_{sd}^{n} & u_{sq}^{p} & -u_{sd}^{p} \end{bmatrix}\begin{bmatrix} i_{rd}^{p} \\ i_{rq}^{p} \\ i_{rd}^{n} \\ i_{rq}^{n} \end{bmatrix}$$

(3.38)

To eliminate the pulsating stator active power, the following condition should be satisfied:

$$P_{s\_sin} = P_{s\_cos} = 0 \tag{3.39}$$

From Equations (3.25), (3.38) and (3.39), the dq components of the rotor current vector negative sequence quantities have to satisfy the following conditions

$$i_{rd}^{n} = \frac{u_{sq}^{n} i_{rd}^{p} - u_{sd}^{n} i_{rq}^{p}}{u_{sq}^{p}} \tag{3.40}$$

$$i_{rq}^{n} = \frac{-u_{sd}^{n} i_{rd}^{p} - u_{sq}^{n} i_{rq}^{p}}{u_{sq}^{p}} \tag{3.41}$$

By replacing Equations (3.40) and (3.41) into (3.38), the stator average active power and reactive power can be represented as,

$$P_{s\_avg} = -\frac{3L_m}{2L_s}\frac{i_{rq}^{p}}{u_{sq}^{p}}\left[\left(u_{sq}^{p}\right)^2-(u_{sd}^{n})^2-\left(u_{sq}^{n}\right)^2\right] \tag{3.42}$$

$$Q_{s\_avg} = \frac{3}{2\omega_e L_s}\left[\left(u_{sq}^{p}\right)^2-(u_{sd}^{n})^2-\left(u_{sq}^{n}\right)^2\right] - \frac{3L_m}{2L_s}\frac{i_{rd}^{p}}{u_{sq}^{p}}\left[\left(u_{sq}^{p}\right)^2+(u_{sd}^{n})^2+\left(u_{sq}^{n}\right)^2\right]$$

(3.43)

As shown in Equations (3.42) and (3.43), the stator active power and stator reactive power are controlled by i_{rq}^{p} and i_{rd}^{p} respectively, after the proposed method is implemented.

3.3 Control strategy for the GSC of DFIG under the unbalanced operating conditions

In this section, the method for harmonic elimination of the line current and DC link voltage in the GSC under a generalized unbalanced operating condition is proposed. The adjustable power factor of the GSC is also achieved. This generalized control method in ABC frame can be applied to all kinds of the unbalanced operating conditions of a wind turbine driven DFIG, including unbalanced grid voltages and unbalanced line impedances.

Ana V. Stankovic and Thomos A. Lipo proposed and implemented a general method of completely harmonic elimination for PWM boost type rectifiers under severe unbalanced voltage disturbances in the power system [14, 17]. However, the power factor is not adjustable and the sequence component decoupling is required with this method. To overcome these disadvantages, A.V. Stankovic and Ke Chen developed and implemented a new control method in the ABC reference frame for completely input-output harmonic elimination of PWM boost-type rectifier under extremely unbalanced operating conditions, which includes the unbalanced input voltages and unbalanced line impedances[13]. Shuang Wu and Xiangpeng Zheng proposed a new control method for the grid side PWM inverter and implemented it on a permanent-magnet generator and a squirrel-cage induction generator[18-22].

In the GSC of a wind turbine driven DFIG, the power can flow bidirectionally depending on the rotating of the shaft. At a super-synchronous speed, the GSC operates as an inverter, while at a sub-synchronous speed, it operates as a rectifier. The power flow of the grid side converter is displayed in Figure 3.4. The grid side converter circuit of a DFIG is analyzed and investigated under the following assumptions[18]:

1) The three phase output voltages of the GSC are unbalanced.

2) The line impedances of the GSC are unbalanced.

3) The converter is lossless.

Figure 3.5 shows the steady state equivalent circuits of the GSC under the unbalanced operating conditions[18]. The line current flows into the grid at a super-synchronous speed, while it flows from the gird at a sub-synchronous speed.

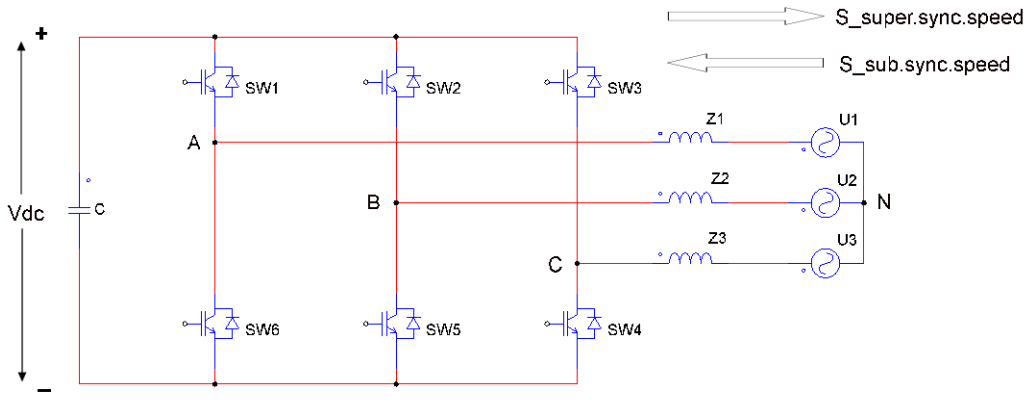

Figure 3.4: The GSC of a DFIG[18]

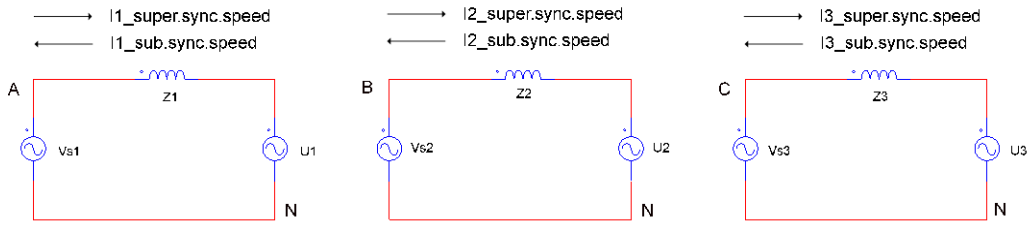

Figure 3.5: The GSC steady state equivalent circuits under unbalance operating conditions

According to Kirchhoff's voltage law, the following equations are obtained from Figure 3.5:

$$V_{s1} = U_1 + kZ_1I_1 \tag{3.44}$$

$$V_{s2} = U_2 + kZ_2I_2 \tag{3.45}$$

$$V_{s3} = U_3 + kZ_3I_3 \tag{3.46}$$

, where $U_1, U_2, U_3, I_1, I_2, I_3, Z_1, Z_2, Z_3, V_{s1}, V_{s2}$ and V_{s3} are three phase line voltages, line currents, line impedances and synthesized voltages of the GSC respectively, represented as phasors.

When k is equal to -1, the converter operates as an inverter, while it operates as a rectifier when k=1. Synthesized voltagesV_{s1}, V_{s2} and V_{s3} can be expressed as,

$$V_{s1} = SW_1 \frac{V_{dc}}{2\sqrt{2}} \tag{3.47}$$

$$V_{s2} = SW_2 \frac{V_{dc}}{2\sqrt{2}} \tag{3.48}$$

$$V_{s3} = SW_3 \frac{V_{dc}}{2\sqrt{2}} \tag{3.49}$$

, where V_{dc} is the DC link voltage.

On the basis of the Kirchhoff's current law, the following equation is obtained:

$$I_1 = -I_2 - I_3 \tag{3.50}$$

To eliminate the second order harmonics in line currents of the GSC, the following condition should be satisfied:

$$SW_1 I_1 + SW_2 I_2 + SW_3 I_3 = 0 \quad (3.51)$$

By replacing Equations (3.47) - (3.49) into Equations (3.44) - (3.46), the following set of equations is obtained:

$$U_1 = SW_1 \frac{V_{dc}}{2\sqrt{2}} + kZ_1 I_1 \quad (3.52)$$

$$U_2 = SW_2 \frac{V_{dc}}{2\sqrt{2}} + kZ_2 I_2 \quad (3.53)$$

$$U_3 = SW_3 \frac{V_{dc}}{2\sqrt{2}} + kZ_3 I_3 \quad (3.54)$$

By multiplying Equations (3.52) - (3.54) by I_1, I_2 and I_3 separately, and then adding them up, the following equation is satisfied:

$$U_1 I_1 + U_2 I_2 + U_3 I_3 = k(Z_1 I_1^2 - Z_2 I_2^2 - Z_3 I_3^2) + \frac{V_{dc}}{2\sqrt{2}}(SW_1 I_1 + SW_2 I_2 + SW_3 I_3) \quad (3.55)$$

By substituting Equation (3.51) into (3.55), the following equation is obtained:

$$U_1 I_1 + U_2 I_2 + U_3 I_3 = k(Z_1 I_1^2 - Z_2 I_2^2 - Z_3 I_3^2) \quad (3.56)$$

The complex conjugate value of the complex power can be represented as:

$$S^* = k(U_1^* I_1 + U_2^* I_2 + U_3^* I_3) \quad (3.57)$$

By substituting Equation (3.50) into Equations (3.56) and (3.57), the following equations are obtained:

$$U_1(-I_2 - I_3) + U_2 I_2 + \mathrm{U}_3 I_3 = kZ_1(-I_2 - I_3)^2 + kZ_2 I_2^2 + kZ_3 I_3^2 \quad (3.58)$$

$$S^* = k(-U_1^* I_2 - U_1^* I_3 + U_2^* I_2 + U_3^* I_3) \quad (3.59)$$

Then the above two equations can be simplified as below:

$$I_2(U_2 - U_1) + I_3(U_3 - U_1) = k(Z_1 + Z_2) I_2^2 + k(Z_1 + Z_3) I_3^2 + 2kZ_1 I_2 I_3 \quad (3.60)$$

$$I_2 = \frac{kS^* - I_3(U_3^* - U_1^*)}{U_2^* - U_1^*} \quad (3.61)$$

Finally by replacing Equation (3.61) into Equation (3.60), the following equation is satisfied:

$$\frac{kS^*-I_3(U_3^*-U_1^*)}{U_2^*-U_1^*}(U_2-U_1)+I_3(U_3-U_1)=k(Z_1+Z_2)\frac{S^{*2}-2kS^*I_3(U_3^*-U_1^*)+I_3^2(U_3^*-U_1^*)^2}{(U_2^*-U_1^*)^2}+$$

$$k(Z_1+Z_3)I_3^2+2kZ_1\frac{kS^*-I_3(U_3^*-U_1^*)}{U_2^*-U_1^*}I_3 \quad (3.62)$$

Equation (3.62) can be simplified as following:

$$\left[k\frac{2Z_1(U_3^*-U_1^*)}{U_2^*-U_1^*}-k\frac{(Z_1+Z_2)(U_3^*-U_1^*)^2}{(U_2^*-U_1^*)^2}-k(Z_1+Z_3)\right]I_3^2+\left[(U_3-U_1)-\frac{(U_3^*-U_1^*)(U_2-U_1)}{U_2^*-U_1^*}-\right.$$

$$\left.\frac{2Z_1S^*}{U_2^*-U_1^*}+\frac{2S^*(Z_1+Z_2)(U_3^*-U_1^*)}{(U_2^*-U_1^*)^2}\right]I_3+k\frac{S^*(U_2-U_1)}{U_2^*-U_1^*}-k\frac{(Z_1+Z_2)S^{*2}}{(U_2^*-U_1^*)^2}=0 \quad (3.63)$$

The quadratic equation as above in terms of the line currents I_3 can be resolved by using the quadratic general solution formula:

$$I_3=\frac{-b\pm\sqrt{b^2-4ac}}{2a} \quad (3.64)$$

, where the coefficients of the complex quadratic equation are given by:

$$a=k\left[(Z_1+Z_3)-\frac{2Z_1(U_3^*-U_1^*)}{U_2^*-U_1^*}+\frac{(Z_1+Z_2)(U_3^*-U_1^*)^2}{(U_2^*-U_1^*)^2}\right] \quad (3.65)$$

$$b=-(U_3-U_1)-\frac{(U_3^*-U_1^*)(U_2-U_1)}{U_1^*-U_2^*}-2(Z_1+Z_2)\frac{(U_3^*-U_1^*)S^*}{(U_1^*-U_2^*)^2}-2Z_1\frac{S^*}{U_1^*-U_2^*} \quad (3.66)$$

$$c=k\left[\frac{S^*(U_2-U_1)}{U_1^*-U_2^*}+\frac{(Z_1+Z_2)S^{*2}}{(U_1^*-U_2^*)^2}\right] \quad (3.67)$$

Equations (3.50), (3.61) and (3.64) represent the general solution at steady state for completely harmonic elimination in line currents under any kind of the unbalanced operating conditions. There is no solutions resolved by Equation (3.63) only if all the coefficients of the quadratic formula are set to zero.

By setting the reference value for the complex power in Equations (3.61) and (3.63), the adjustable power factor is then achieved as follows:

$$pf = \frac{P}{\sqrt{P^2+Q^2}} \tag{3.68}$$

, where P and Q are the GSC's active power and reactive power. The power factor can be set as unit only when the GSC's reactive power Q is set to zero in Equations (3.61) and (3.63).

CHAPTER IV

PROPOSED CONTROL STRATEGY AND SIMULATION RESULTS

Based on the analysis of the open loop as described in the previous chapter, the closed loop method for DFIG control under generalized unbalanced operating conditions is proposed. Under severe unbalanced operating conditions, DFIG power control is proposed and achieved with complete elimination of pulsating power and harmonics in grid currents. A wind turbine driven DFIG is simulated in PSIM. Five different cases of voltage unbalance are simulated to validate the theoretical analysis.

4.1 Control strategy for a wind turbine driven DFIG

The proposed generalized control scheme for DFIG under the balanced and unbalanced operating conditions is depicted in Figure 4.1. It can be noticed that a standard wound rotor induction machine is presented, where its stator windings is connected to the grid directly while its rotor windings is connected to the grid through a BTB PWM converter and a three phase transformer. The BTB converter consists of

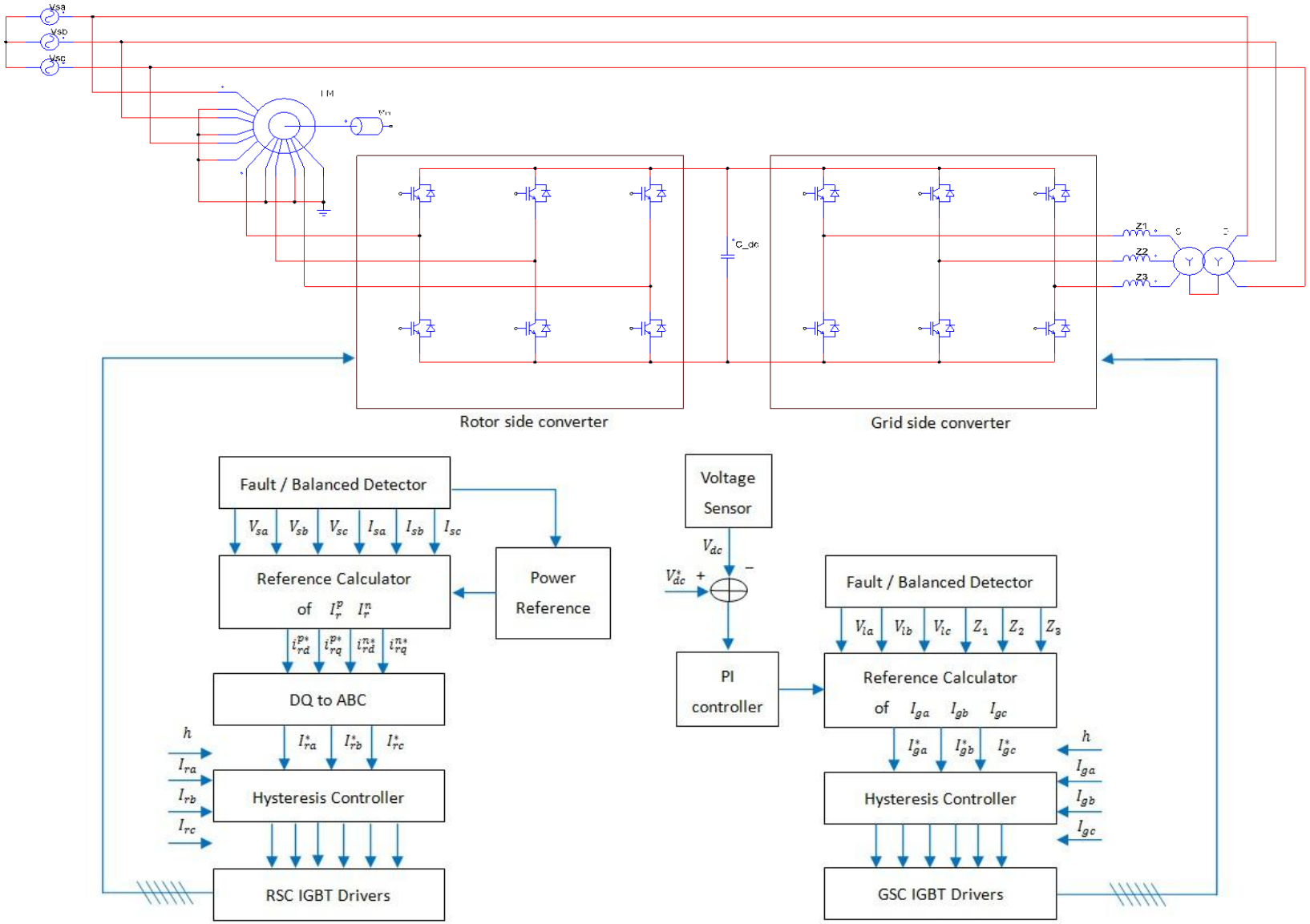

Figure 4.1: Generalized control scheme for DFIG under the balanced and unbalanced conditions

a RSC and a GSC. The RSC is connected between the DC link capacitor and the rotor windings of the wound rotor induction generator, while the GSC is connected between the DC link capacitor and through the transformer to the grid. In other word, the DC link capacitor is connected between the RSC and the GSC. The control strategy will be discussed in details in this chapter.

The operation of the proposed variable wind turbine power system for a wind turbine driven DFIG is simulated using PSIM. The overall systems circuit diagram is displayed in Figure 4.2. The RSC is displayed in Figure 4.3 and the GSC is depicted in Figure 4.4. Both of the RSC and GSC consist of six IGBTs and six anti-parallel diodes separately to form the three phase AC/DC or DC/AC bridges. The gating sequence signals for the IGBTs are generated by the control circuits.

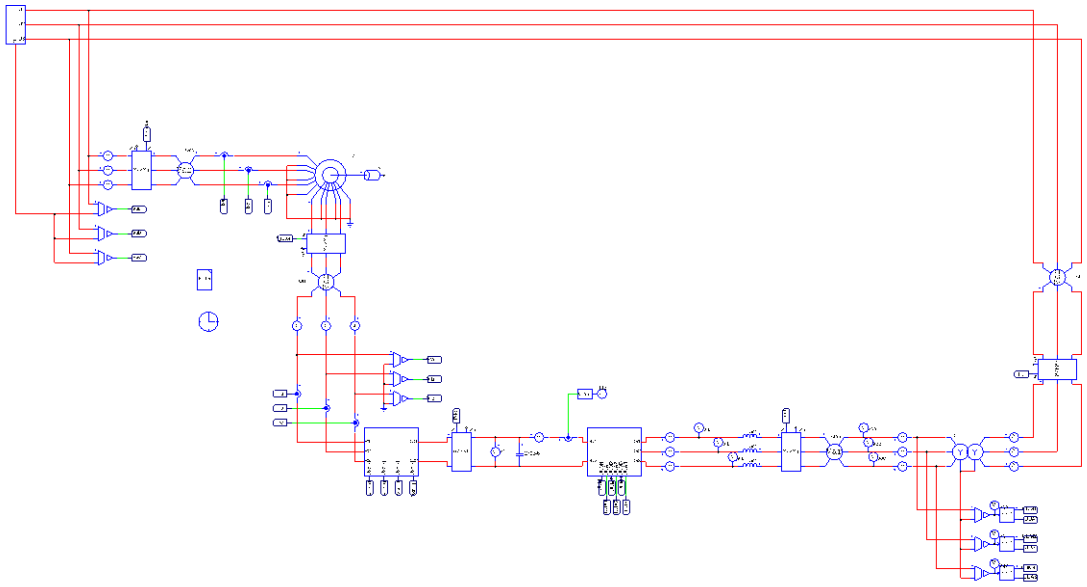

Figure 4.2: Diagram of a wind turbine driven DFIG simulated by PSIM

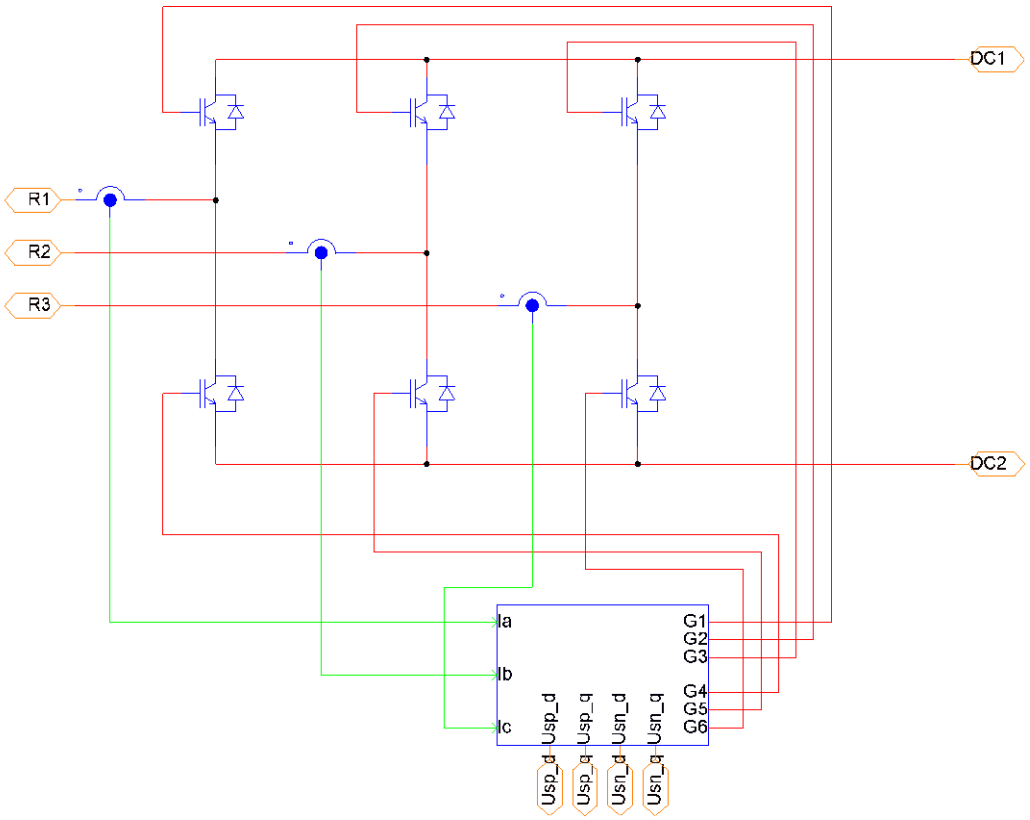

Figure 4.3: Diagram of the RSC of a wind turbine driven DFIG simulated by PSIM

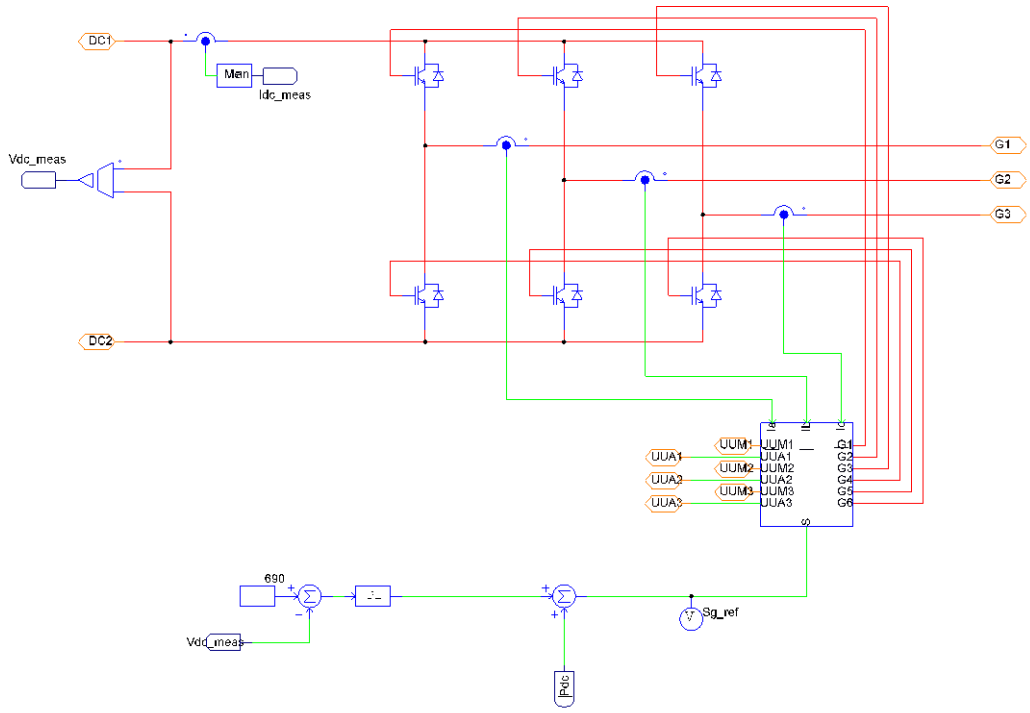

Figure 4.4: Diagram of the GSC of a wind turbine driven DFIG simulated by PSIM

4.2 Control strategy for the RSC of DFIG

Figure 4.5 presents the block diagram of the RSC's control system. As shown in this figure, stator voltage and stator current are measured during real time simulation.

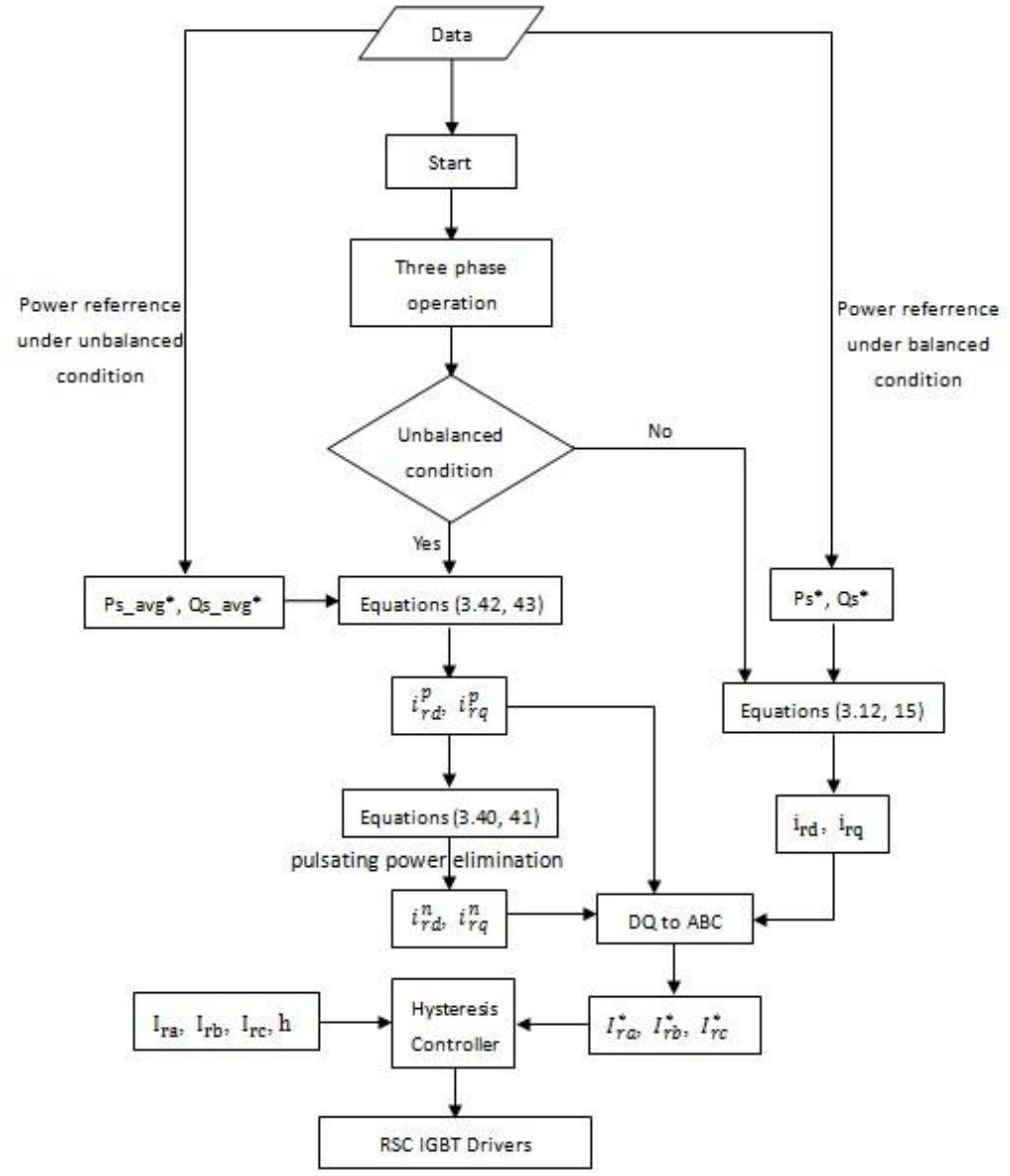

Figure 4.5: Block diagram of rotor side converter control system

Once the unbalanced operating conditions are detected, the average stator active power and average stator reactive power references are obtained to generate the

positive sequence components of the rotor current, which based on Equations (3.42, 43). The positive sequence controller is then activated to regulate the average stator power while the negative sequence controller is used to eliminate the oscillations and pulsations of the stator power based on Equations (3.40, 41). Under the balanced operating conditions, stator voltages and currents are without negative and zero components. In such a case, the negative sequence controller is inactive. Equations (3.42, 43) can be simplified as Equations (3.12, 15) to calculate the dq components of the rotor current in the RSC.

The desired rotor currents with both positive and negative dq components are then transformed to ABC coordinate through the entire simulation process. Hysteresis controller is used to generate six gating signals, making the rotor currents track the reference currents. The RSC communicates with the GSC by commanding the power reference signal to keep the power balance constant between each other.

4.3 Control strategy for the GSC of DFIG

As depicted in Figure 4.6, the closed loop operation of the GSC maintains the DC link voltage at a constant value. The actual DC link voltage is measured and fed back to the controller. The difference between the actual measured DC link voltage and the reference DC voltage is used to create an error signal. This error signal is updated along with the setting of the DC link power reference. The GSC communicates and talks with the RSC by receiving this power reference signal to keep the power balance constant between each other. In other word, the power flows through the GSC should be equal to the power flows through the DC-link bus, also the power flows through the DC-link bus should be equal to the power flows through the RSC.

The three phase reference of the GSC's line currents are generated based on Equations (3.50, 61, 64). Hysteresis controller is used to generate six gating signals, making the grid side currents track the reference currents all the time. The RSC communicates and talks with GSC by commanding the power reference signal to keep the power balance constant between each other. Variable power factor of the GSC including a unity power factor can be accomplished also.

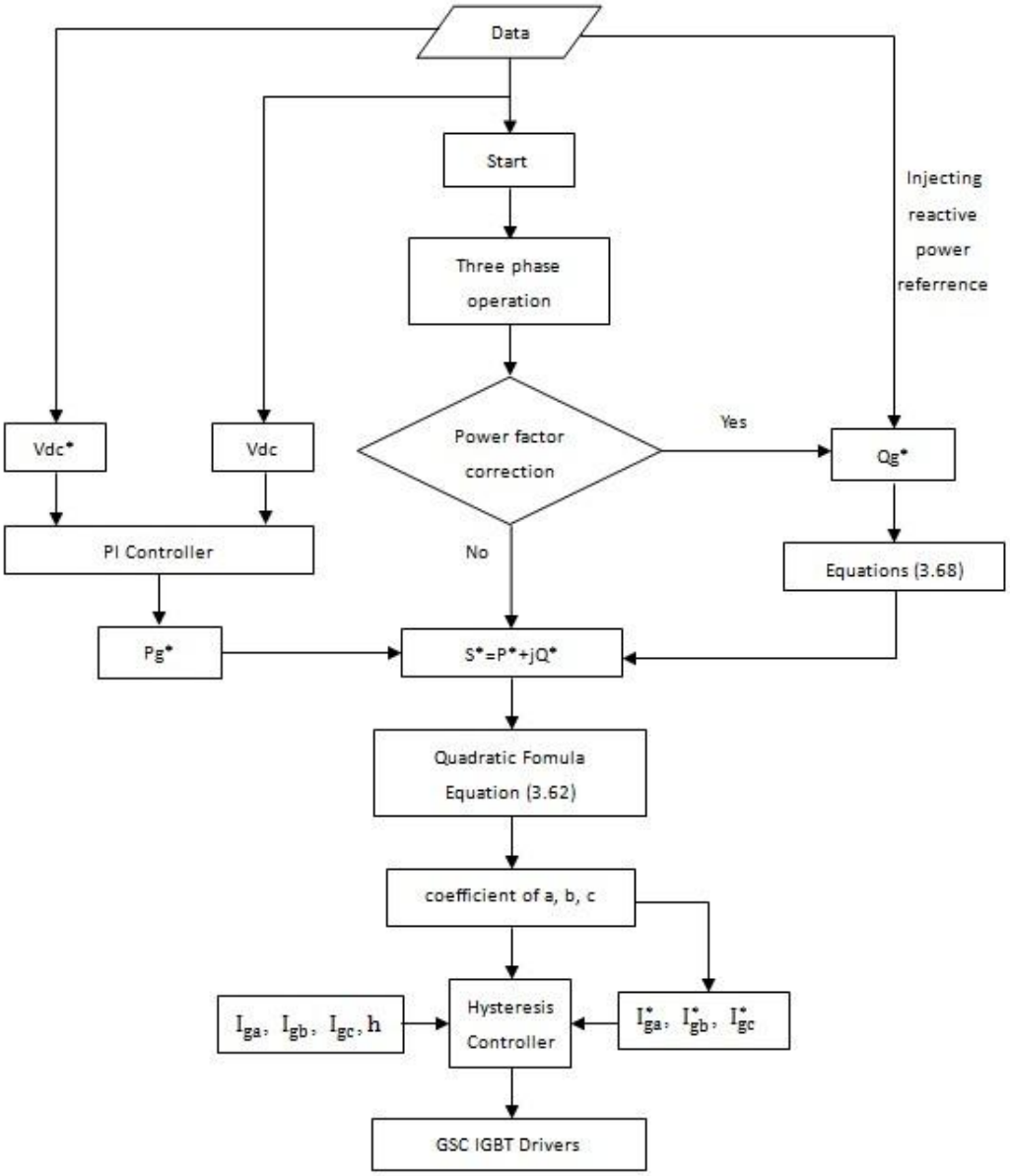

Figure 4.6: Block diagram of grid side converter control system

4.4 Simulation results of a wind turbine driven DFIG

Five simulation cases are selected to verify and demonstrate the proposed control method for a wind turbine driven DFIG. Table 4.1 lists all the parameters of a wind turbine driven DFIG used in the simulation program. Table 4.2 shows all of the five simulation cases.

Table 4.1: Parameters of the DFIG used in the PSIM simulation program

Stator resistance	1.115 Ohm	**Rated Speed**	1750 rpm
Stator inductance	0.005974 H	**Rated Voltage**	220 V
Rotor resistance	1.083 Ohm	**Grid frequency**	60 Hz
Rotor inductance	0.005974 H	**Hysteresis band**	0.02 A
Mutual inductance	0.2037 H	**DC link capacitor**	270 uF
Poles	4	**Sampling Time**	2e-6 s

Table 4.2: Five cases of different operating conditions used in the PSIM simulation program

Case	Grid voltage	Line impedance	Power factor
1	$V_{sa} = 220\angle 0, V_{sb} = 220\angle -120,$ $V_{sc} = 220\angle 120$	$L_1 = L_2 = L_3 = 5\ mL$	1
2	$V_{sa} = 110\angle 0, V_{sb} = 160\angle -120,$ $V_{sc} = 220\angle 120$	$L_1 = L_2 = L_3 = 5\ mL$	1
3	$V_{sa} = 110\angle 0, V_{sb} = 0\angle -120,$ $V_{sc} = 220\angle 120$	$L_1 = L_2 = L_3 = 5\ mL$	1
4	$V_{sa} = 110\angle 0, V_{sb} = 0\angle -120,$ $V_{sc} = 220\angle 120$	$L_1 = L_2 = 5mL;$ $L_3 = 2\ mL$	1
5	$V_{sa} = 110\angle 0, V_{sb} = 0\angle -120,$ $V_{sc} = 220\angle 120$	$L_1 = L_2 = 5mL;$ $L_3 = 2\ mL$	0.7laging

As depicted in Table 4.2, the operation of DFIG is simulated under the balanced condition, with balanced grid voltages and balanced line impedance in case 1. In case 2 and case 3, the grid voltages are unbalanced at different levels while the line impedances are balanced. In case 4, both the grid voltages and line impedances are unbalanced while the power factor is equal to unity as in the previous cases. In case 5, both the grid voltages and line impedances are unbalanced with its power factor set at 0.7 lagging. All these five cases are simulated at a constant rotating speed as 2100rpm. In case 2 to case 5, the system is changed from balanced condition to different unbalanced conditions at 1.0 second.

Figure 4.7, 4.19, 4.31, 4.43 and 4.55 show the three phase grid voltage for all the five cases separately. Figure 4.8, 4.20, 4.32, 4.44 and 4.56 show the DC link voltage for all the five cases separately. Figure 4.9, 4.21, 4.33, 4.45 and 4.57 show the electromagnetic torque for all the five cases separately. Figure 4.10, 4.22, 4.34, 4.46

and 4.58 show the stator active power and the stator reactive power for all the five cases separately. Figure 4.11, 4.23, 4.35, 4.47 and 4.59 show the RSC's active power and reactive power for all the five cases separately. Figure 4.12, 4.24, 4.36, 4.48 and 4.60 show the DC link active power for all the five cases separately. Figure 4.13, 4.25, 4.37, 4.49 and 4.61 show the GSC's active power and reactive power for all the five cases separately. Figure 4.14, 4.26, 4.38, 4.50 and 4.62 show the stator current for all the five cases separately. Figure 4.15, 4.27, 4.39, 4.51 and 4.63 show the rotor current for all the five cases separately. Figure 4.16, 4.28, 4.40, 4.52 and 4.64 show the line impedance current for all the five cases separately. Figure 4.17, 4.29, 4.41, 4.53 and 4.65 show the spectrum of the rotor current for all the five cases separately. Figure 4.18, 4.30, 4.42, 4.54 and 4.66 show the spectrum of the line impedance current for all the five cases separately.

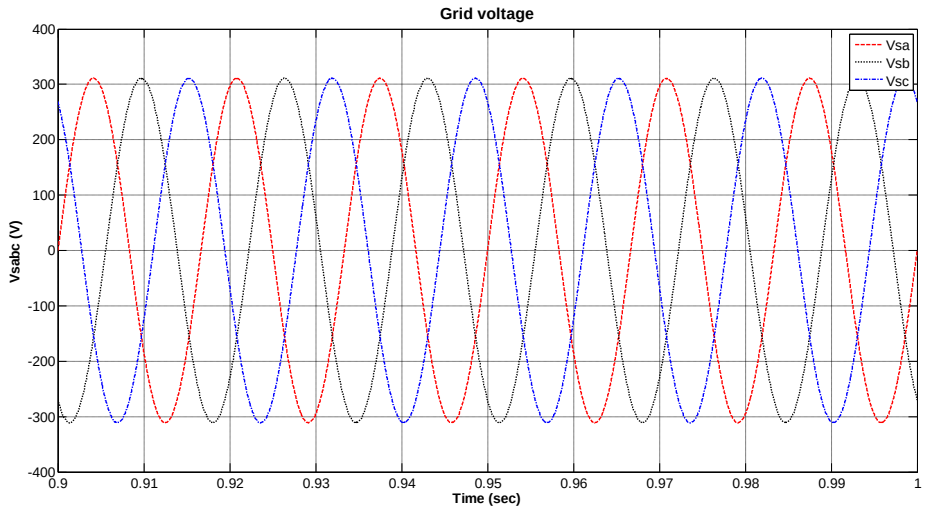

Figure 4.7: Three phase grid voltage (phase to neutral) for case 1

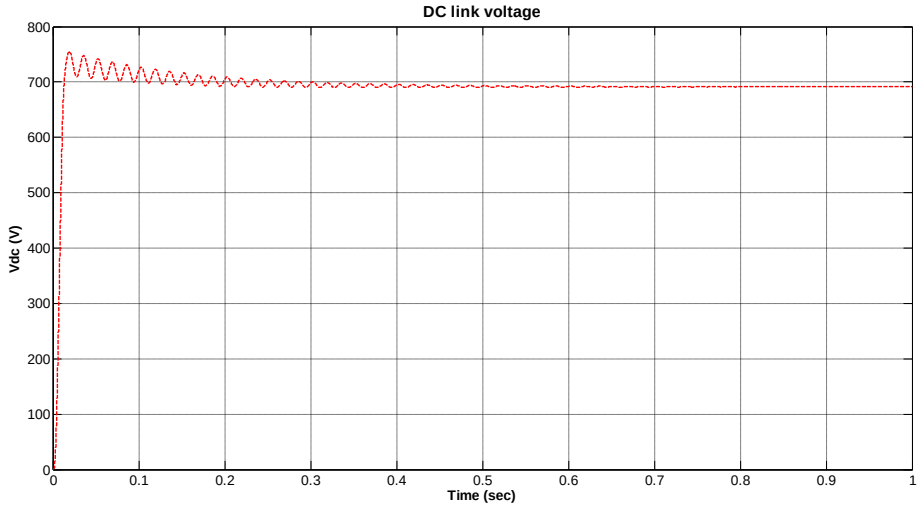

Figure 4.8: DC link voltage for case 1

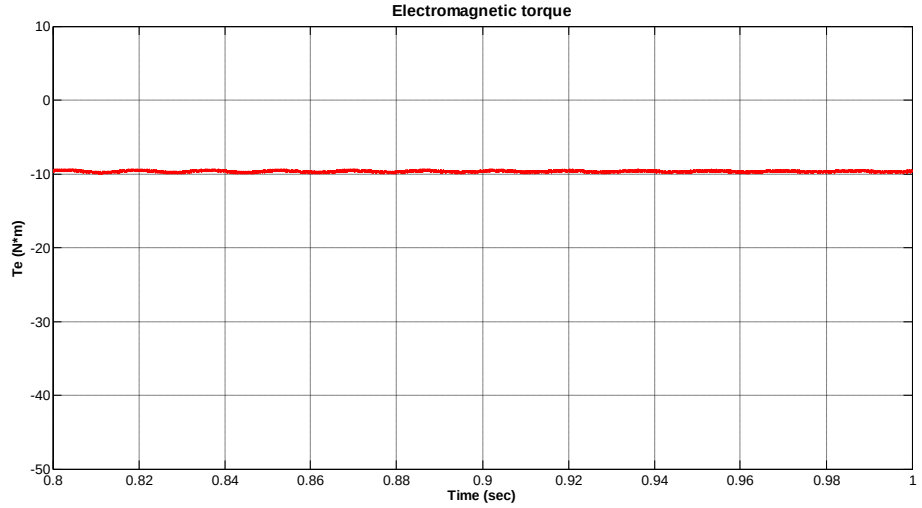

Figure 4.9: Electromagnetic torque for case 1

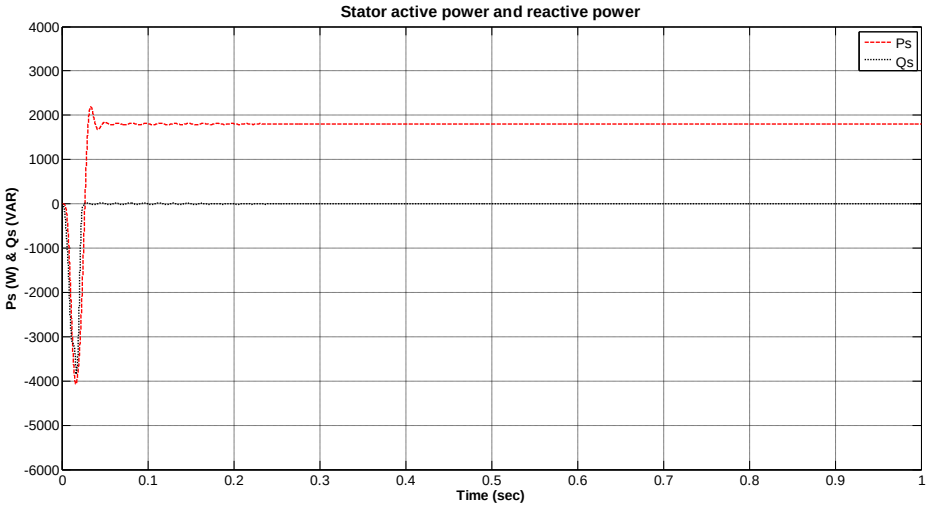

Figure 4.10: Stator active power and reactive power for case1

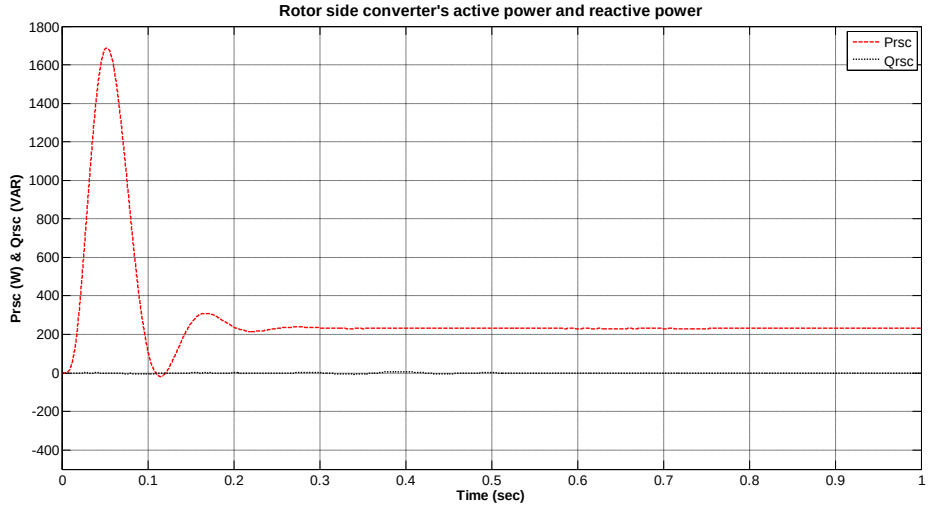

Figure 4.11: Rotor side converter's active power and reactive power for case 1

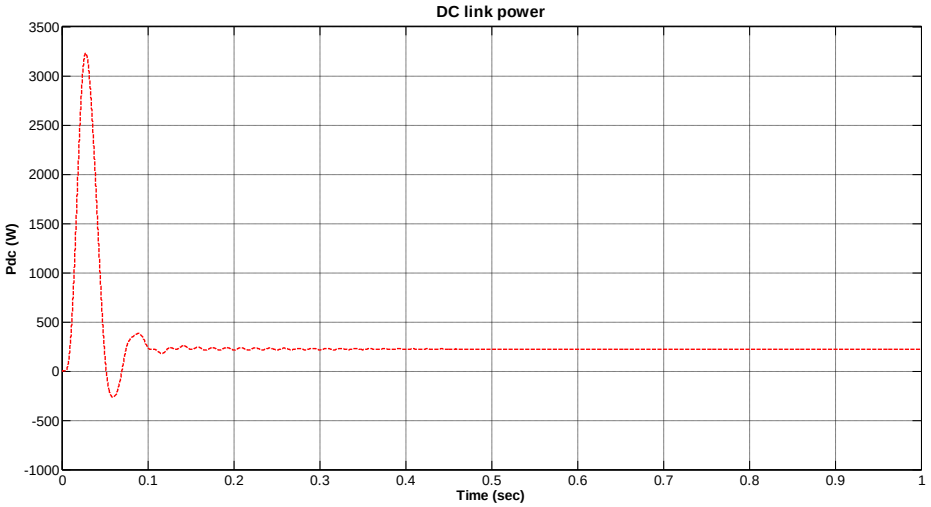

Figure 4.12: DC link active power for case 1

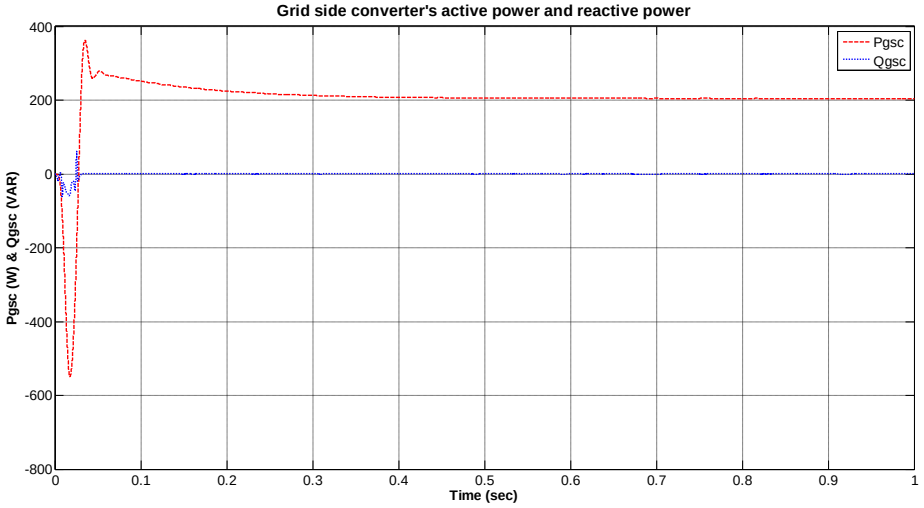

Figure 4.13: Grid side converter's active power and reactive power for case 1

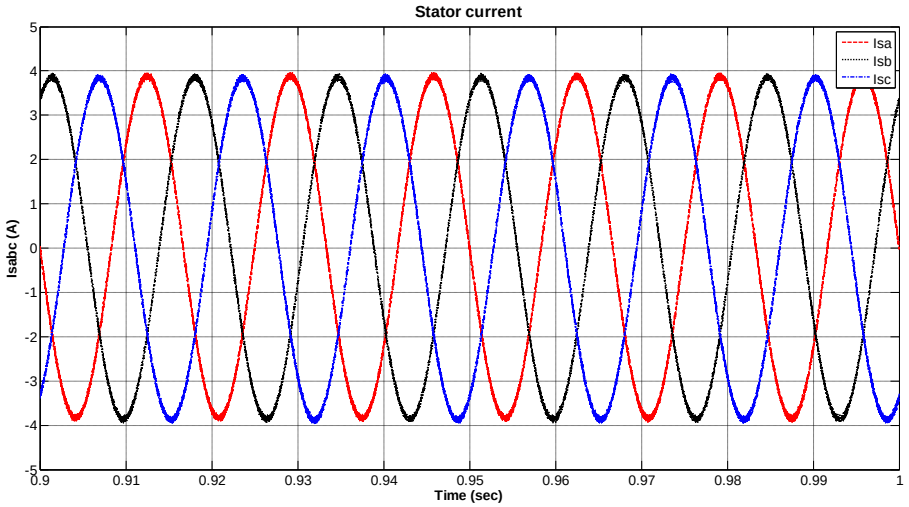

Figure 4.14: Stator current for case 1

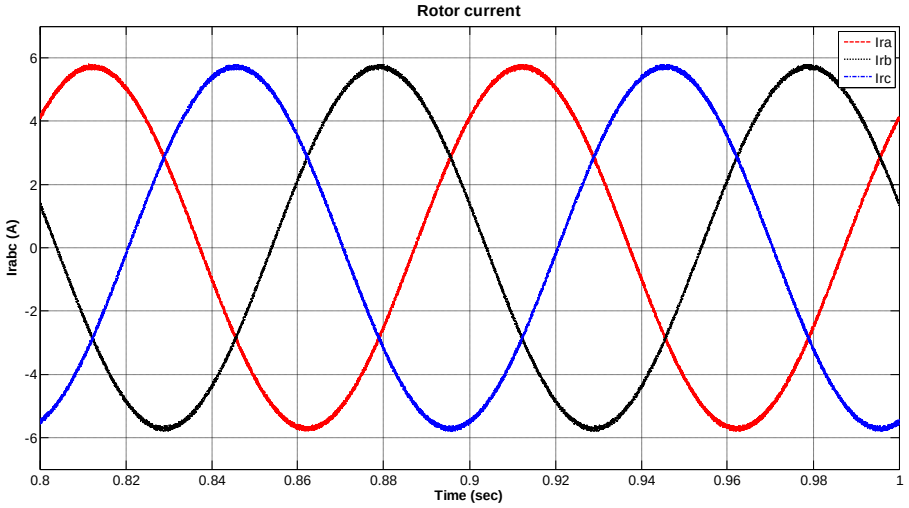

Figure 4.15: Rotor current for case 1

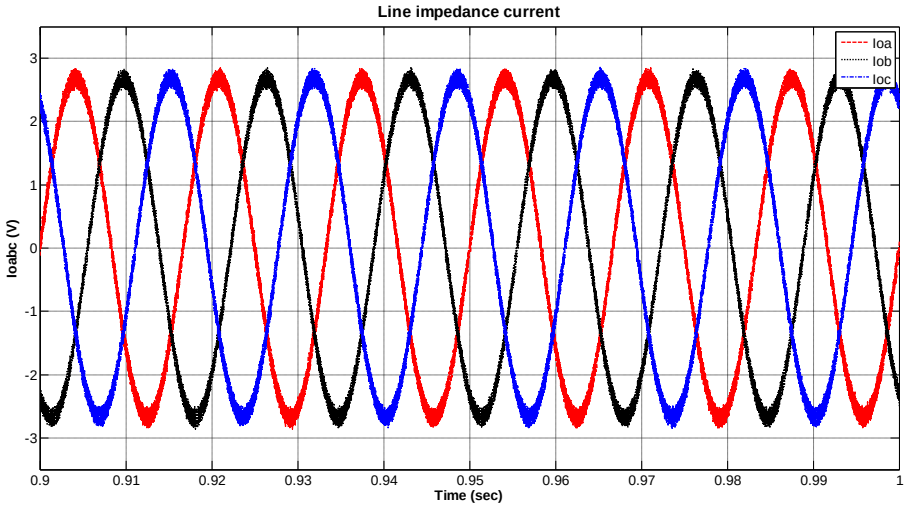

Figure 4.16: Line impedance current for case 1

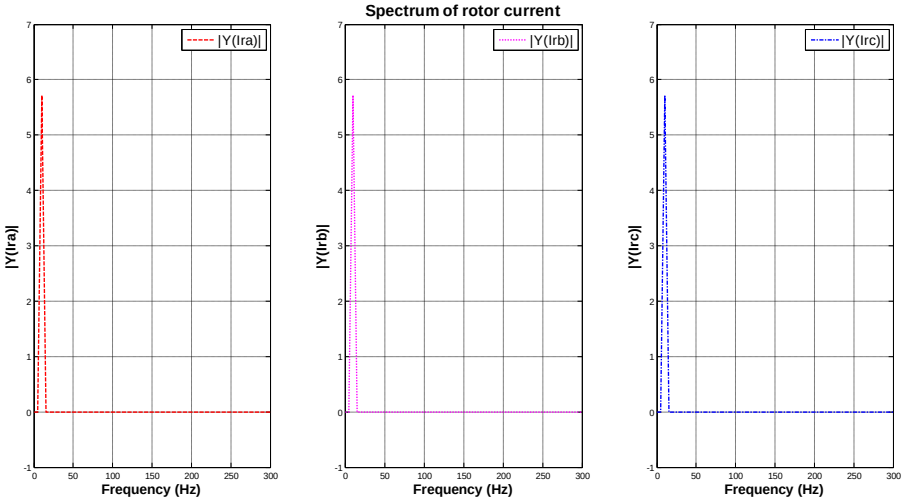

Figure 4.17: Spectrum of rotor current for case 1

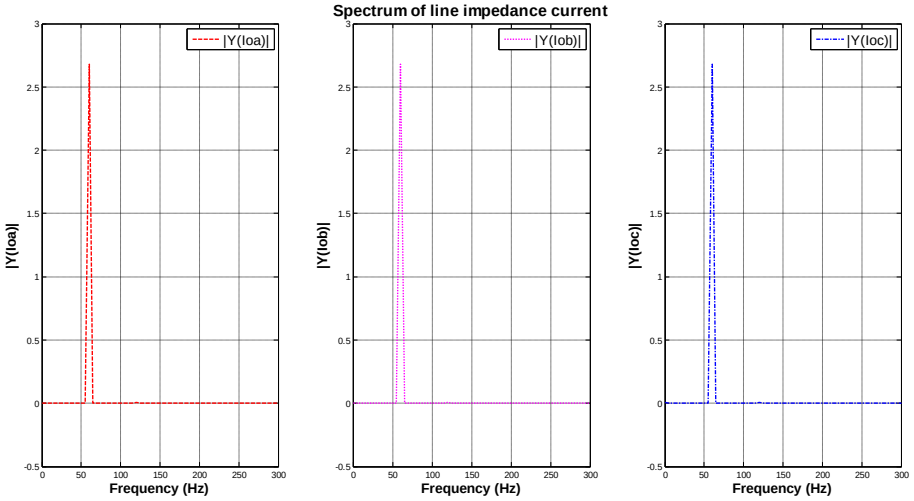

Figure 4.18: Spectrum of line impedance current for case 1

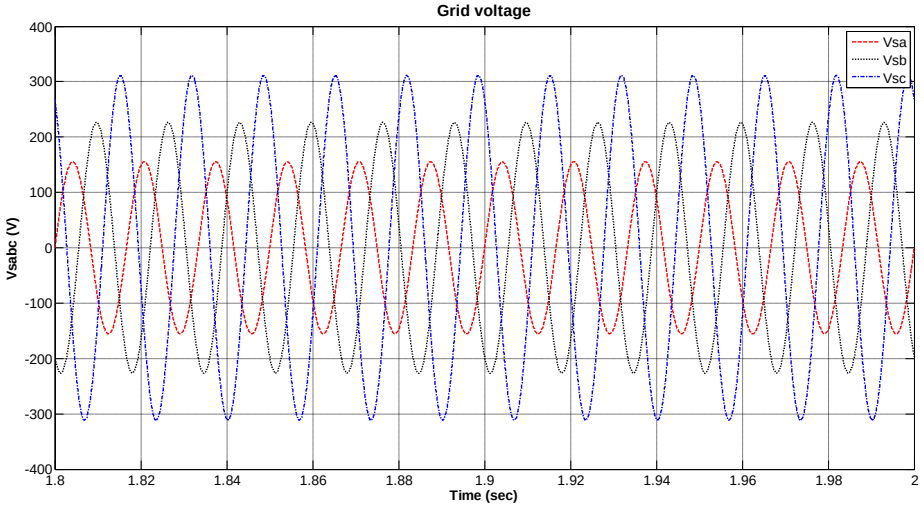

Figure 4.19: Three phase grid voltage (phase to neutral) for case 2

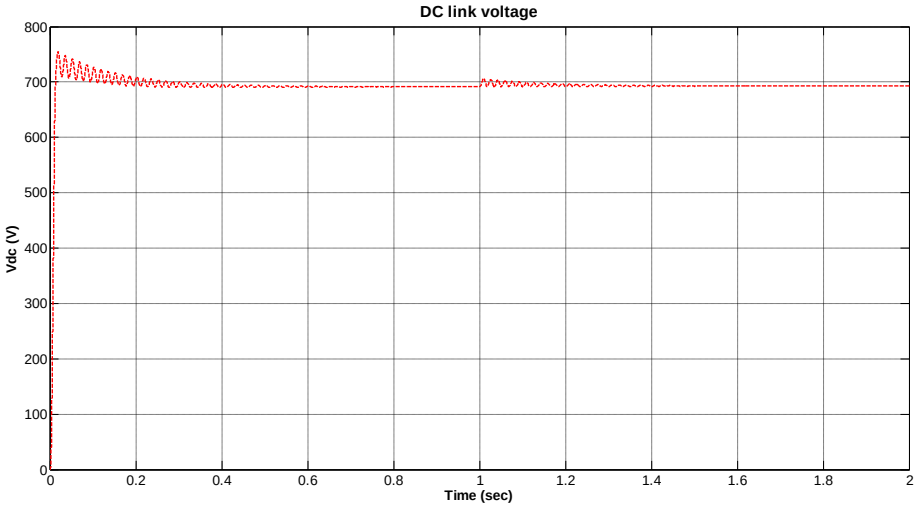

Figure 4.20: DC link voltage for case 2

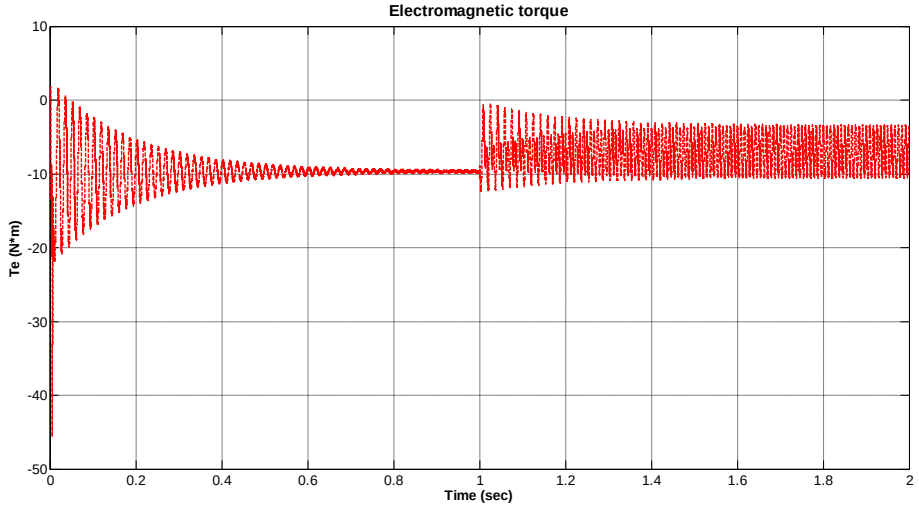

Figure 4.21: Electromagnetic torque for case 2

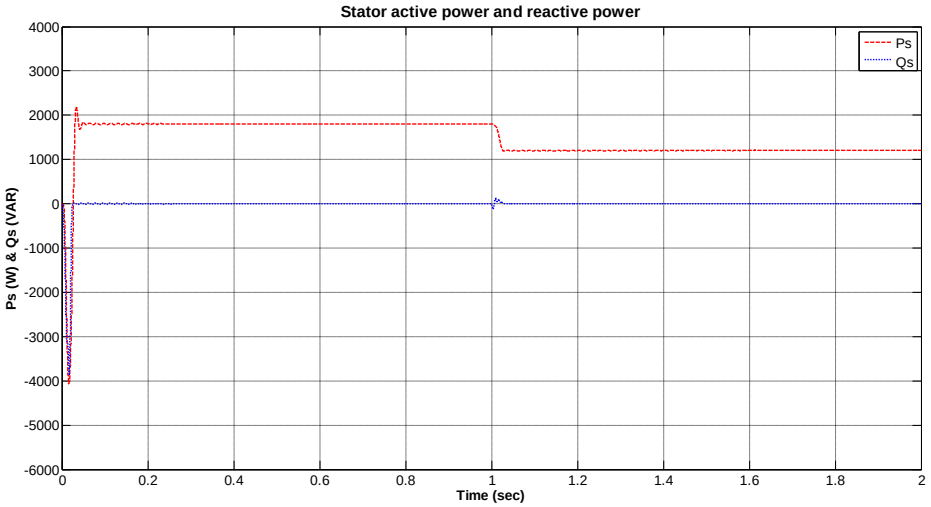

Figure 4.22: Stator active power and reactive power for case 2

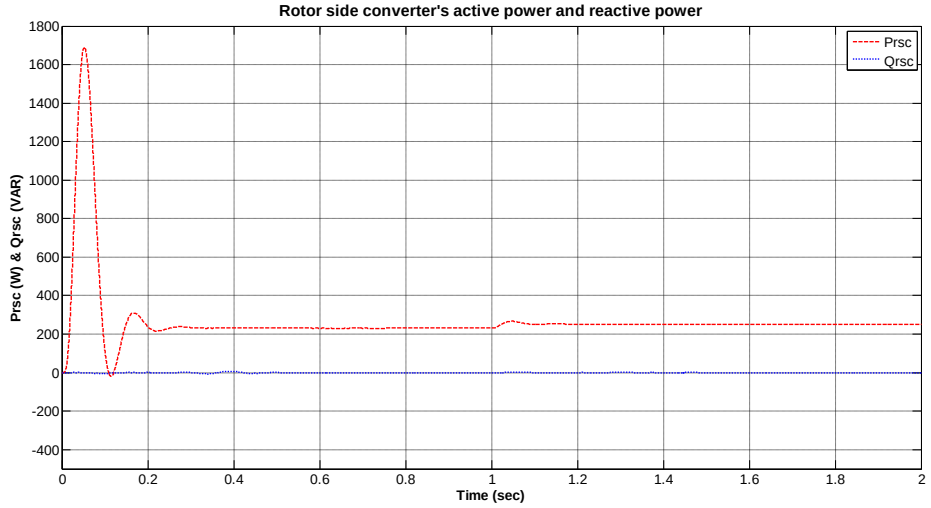

Figure 4.23: Rotor side converter's active power and reactive power for case 2

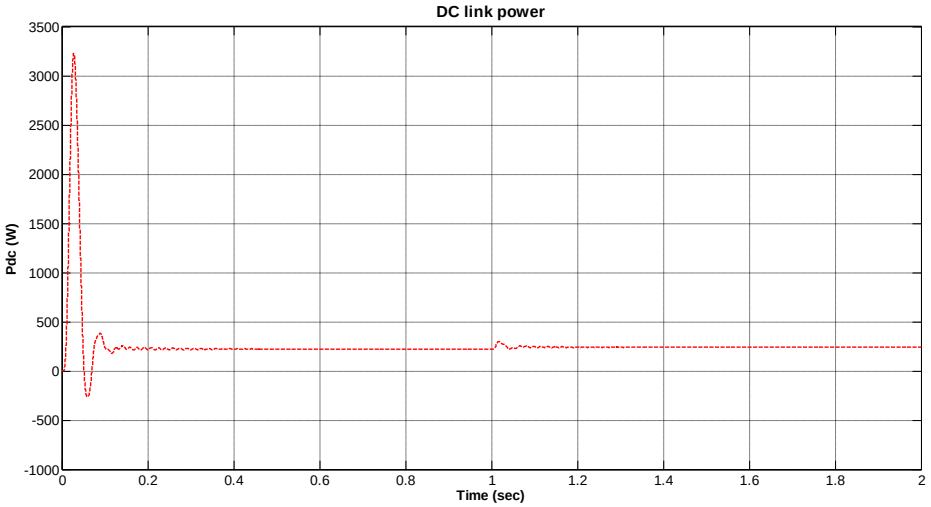

Figure 4.24: DC link active power for case 2

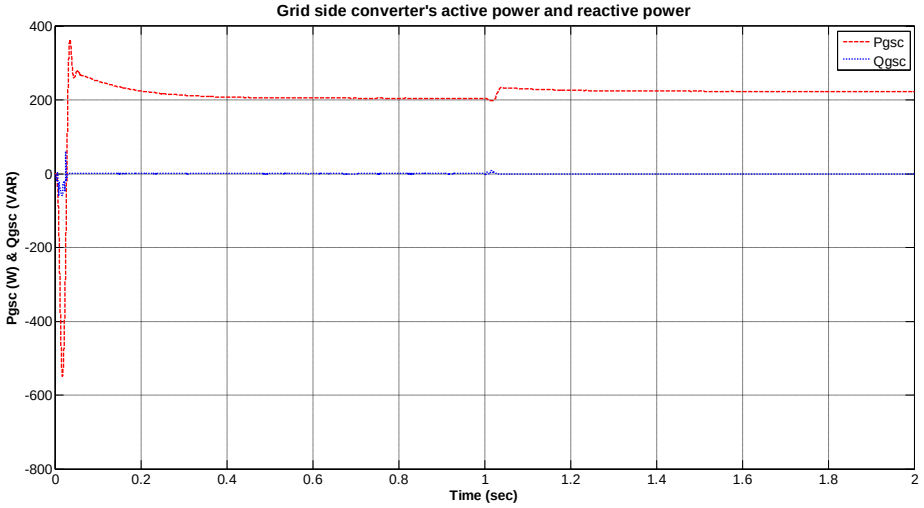

Figure 4.25: Grid side converter's active power and reactive power for case 2

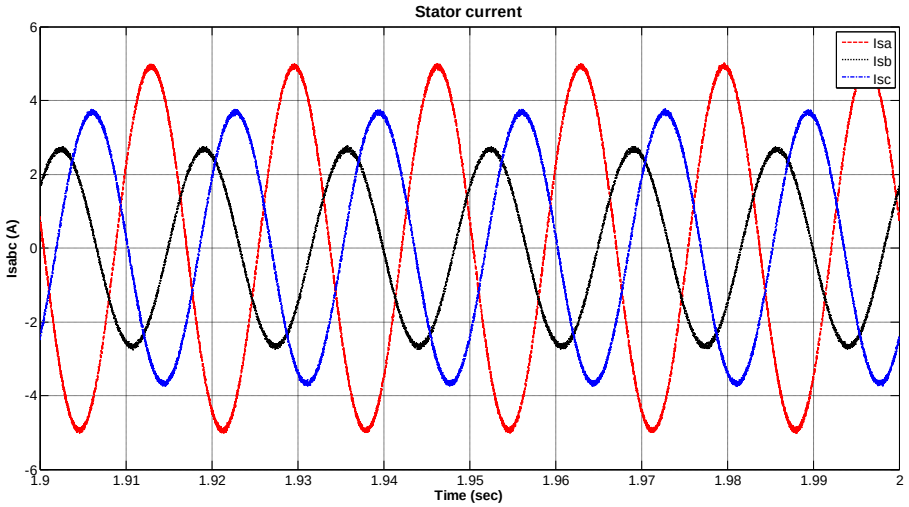

Figure 4.26: Stator current for case 2

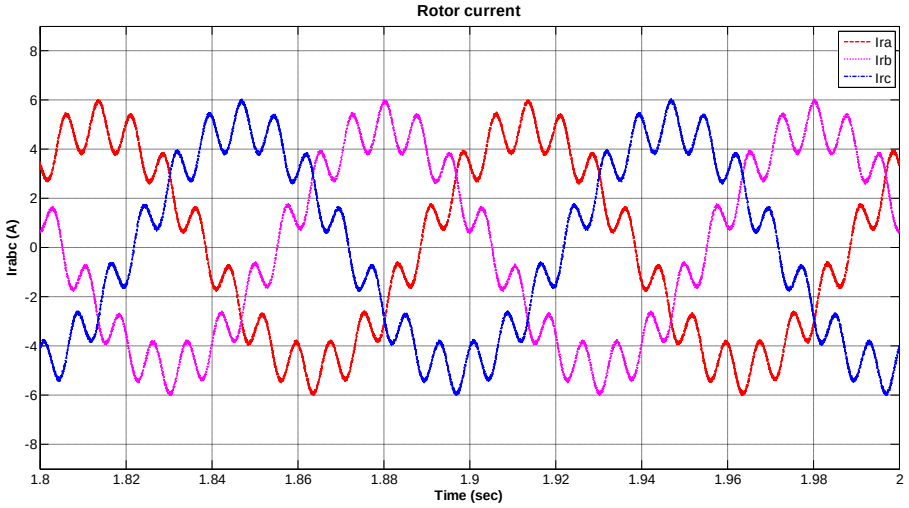

Figure 4.27: Rotor current for case 2

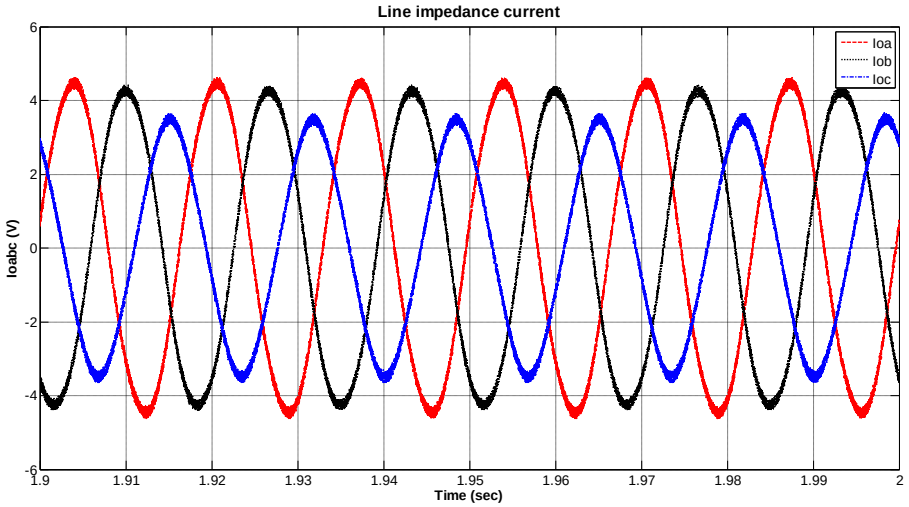

Figure 4.28: Line impedance current for case 2

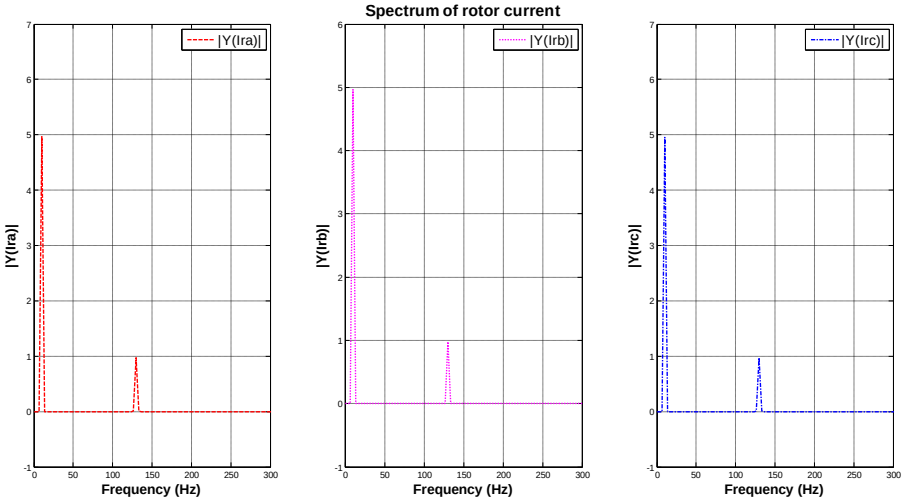

Figure 4.29: Spectrum of rotor current for case 2

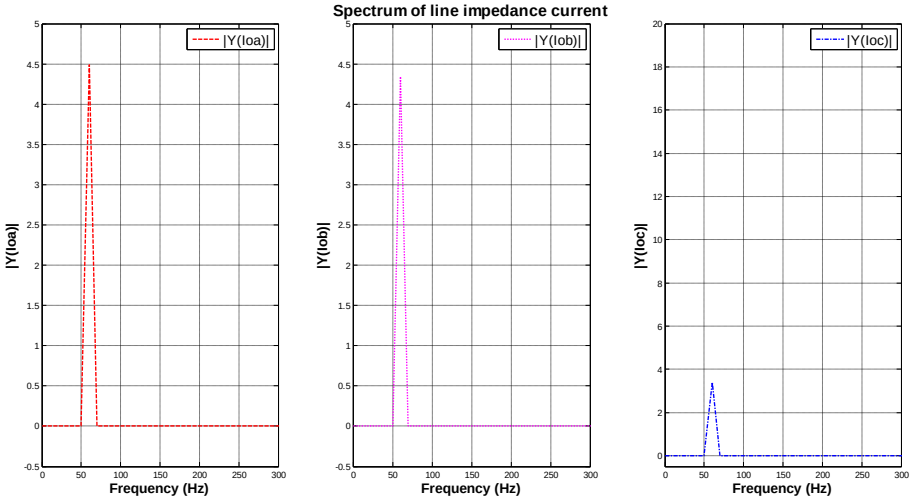

Figure 4.30: Spectrum of line impedance current for case 2

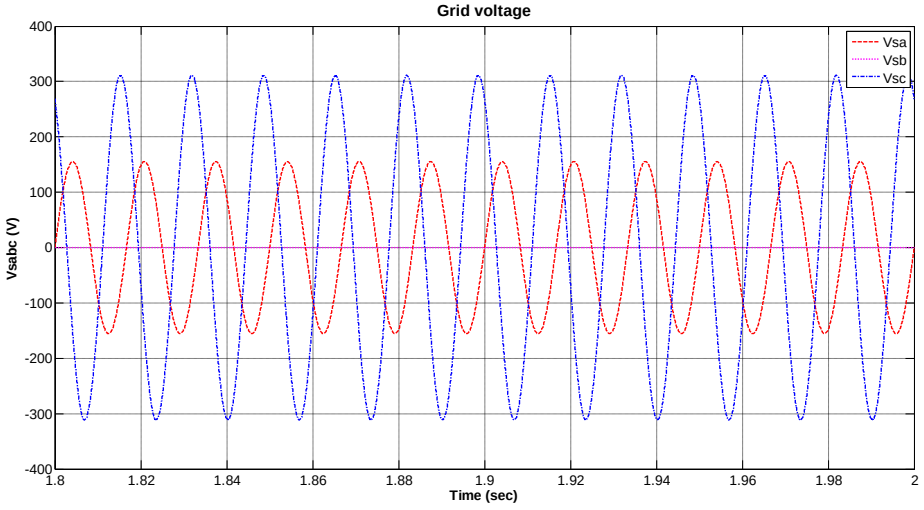

Figure 4.31: Three phase grid voltage (phase to neutral) for case 3

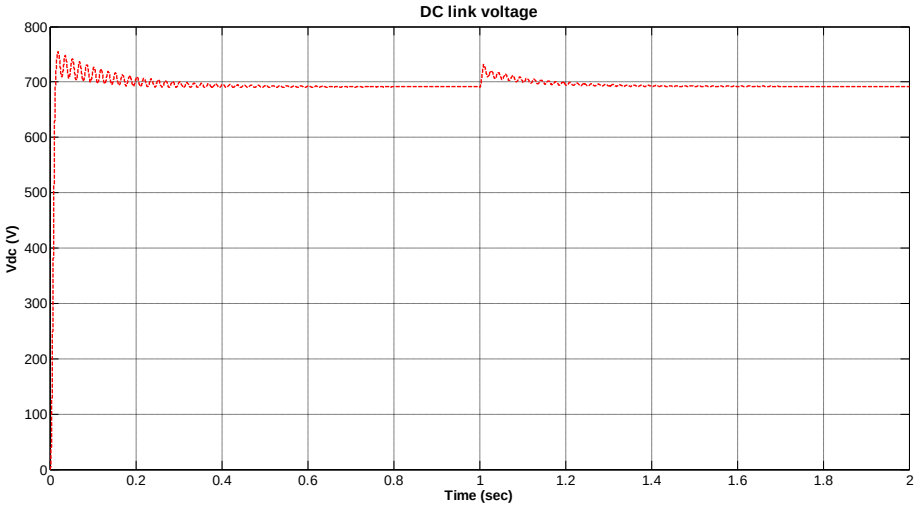

Figure 4.32: DC link voltage for case 3

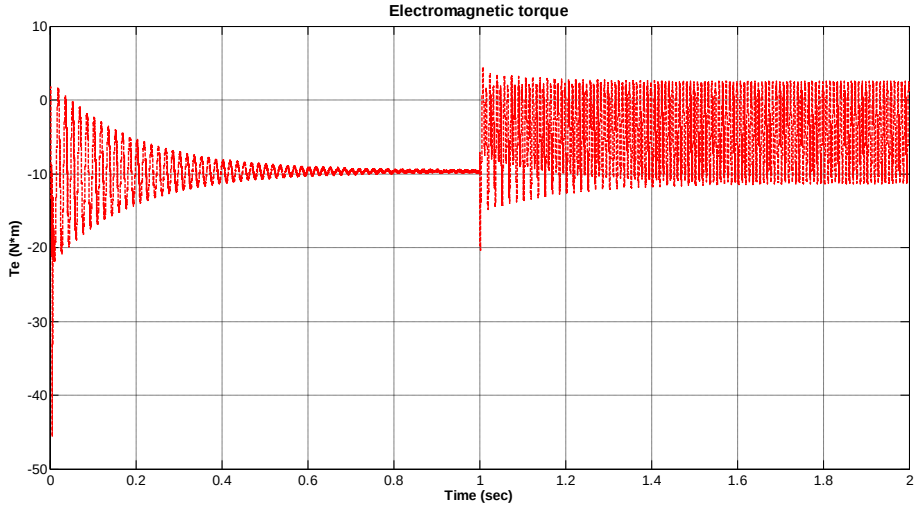

Figure 4.33: Electromagnetic torque for case 3

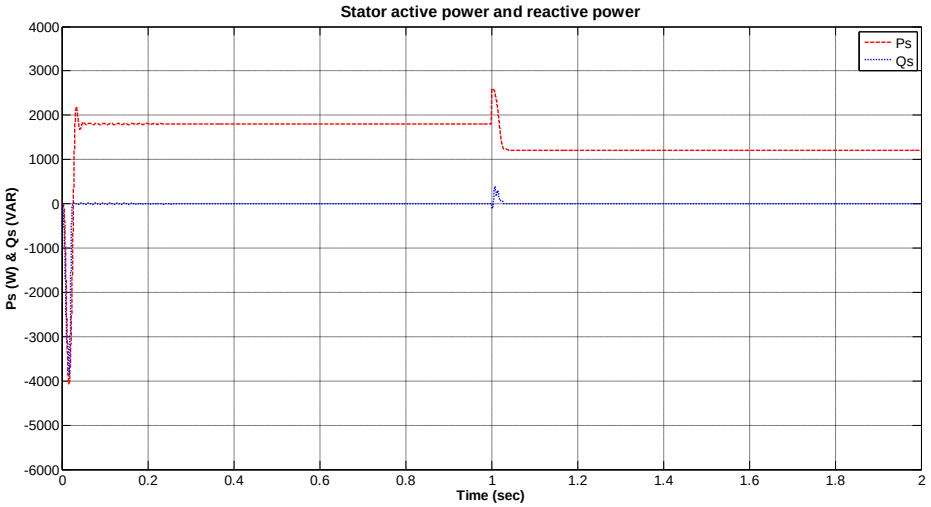

Figure 4.34: Stator active power and reactive power for case 3

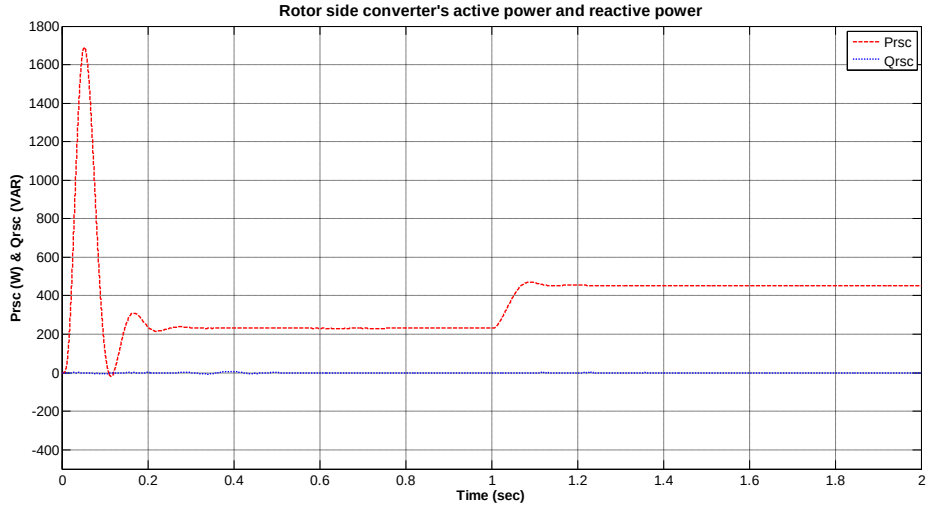

Figure 4.35: Rotor side converter's active power and reactive power for case 3

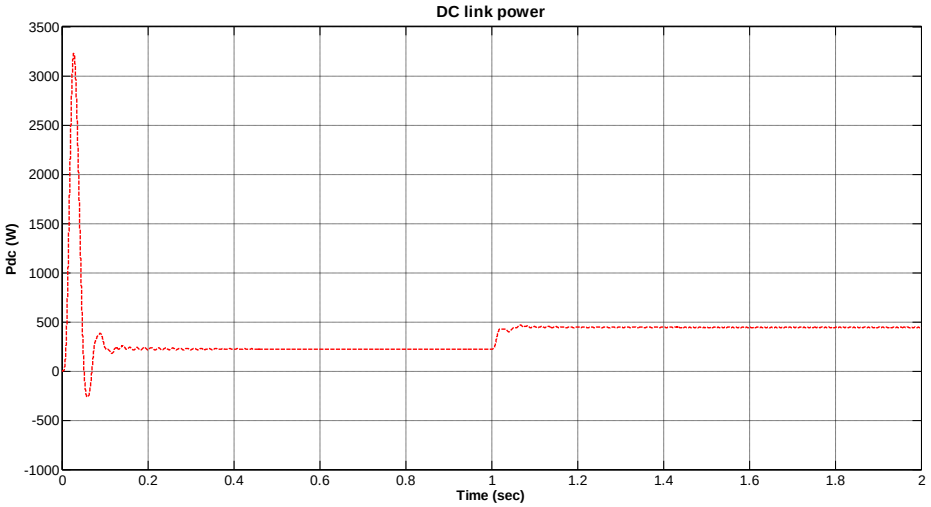

Figure 4.36: DC link active power for case 3

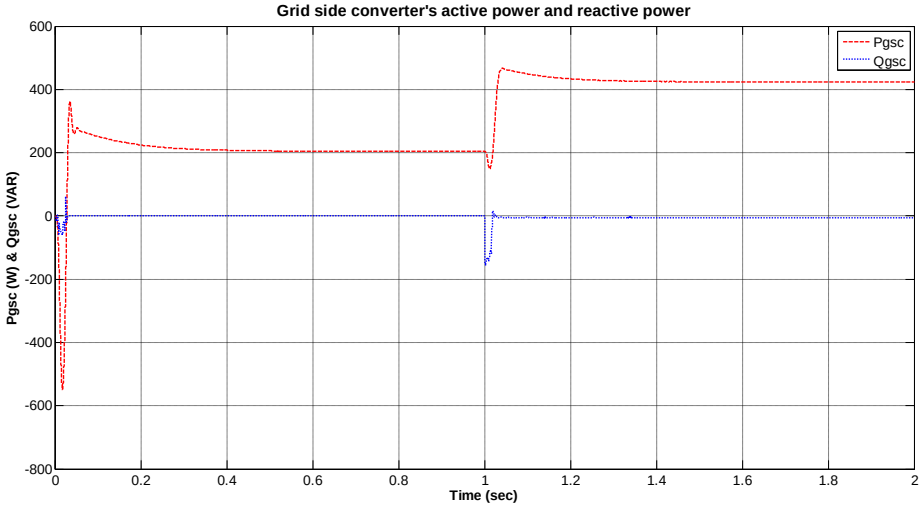

Figure 4.37: Grid side converter's active power and reactive power for case 3

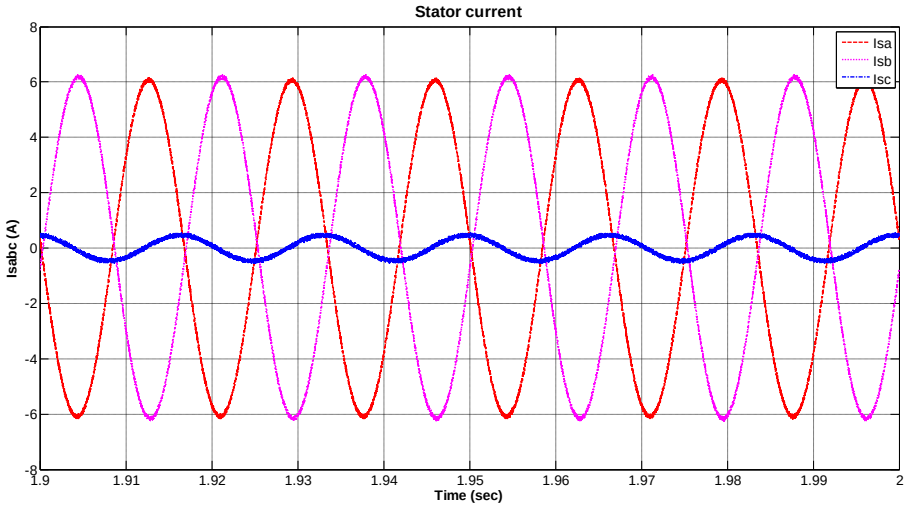

Figure 4.38: Stator current for case 3

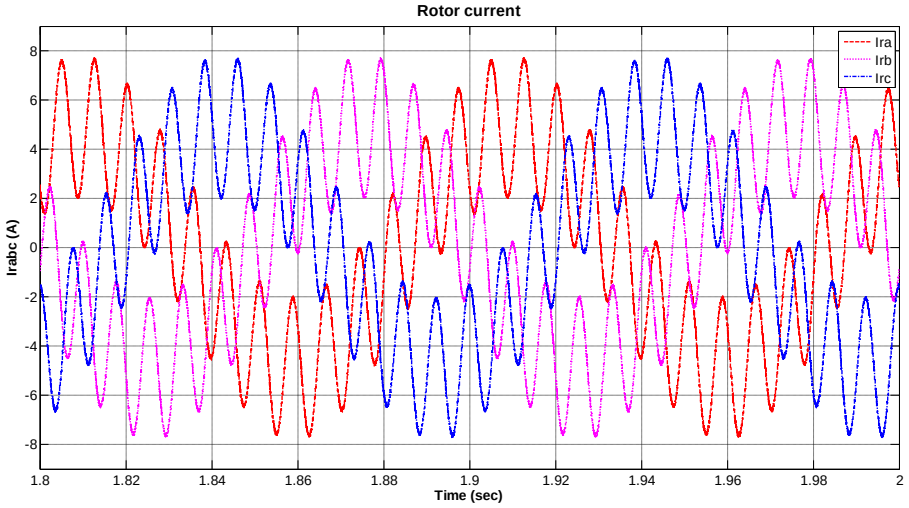

Figure 4.39: Rotor current for case 3

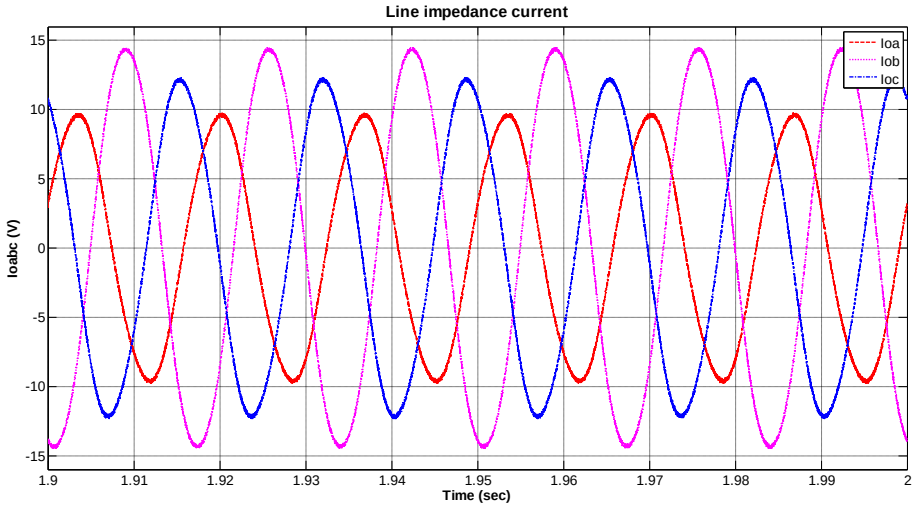

Figure 4.40: Line impedance current for case 3

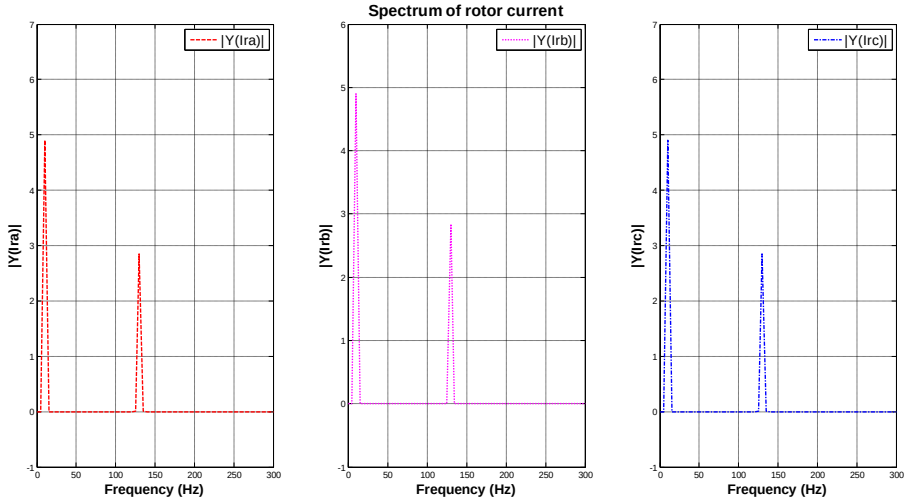

Figure 4.41: Spectrum of rotor current for case 3

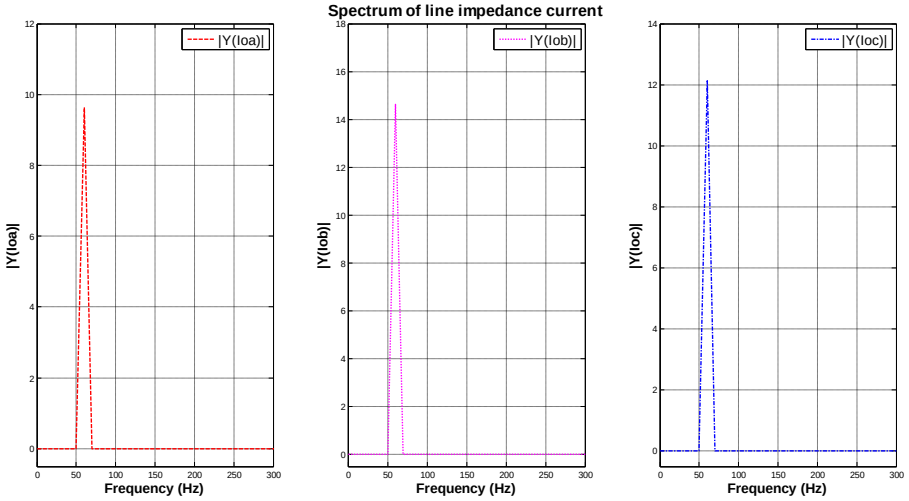

Figure 4.42: Spectrum of line impedance current for case 3

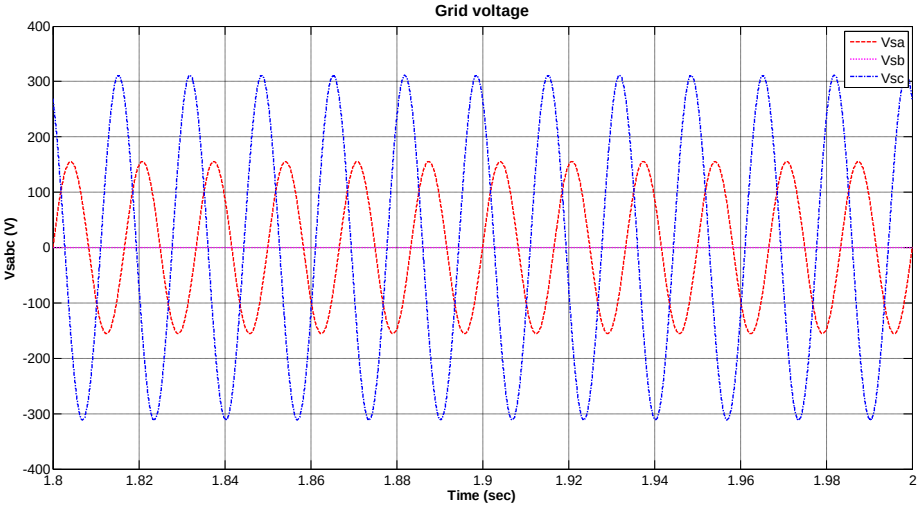

Figure 4.43: Three phase grid voltage (phase to neutral) for case 4

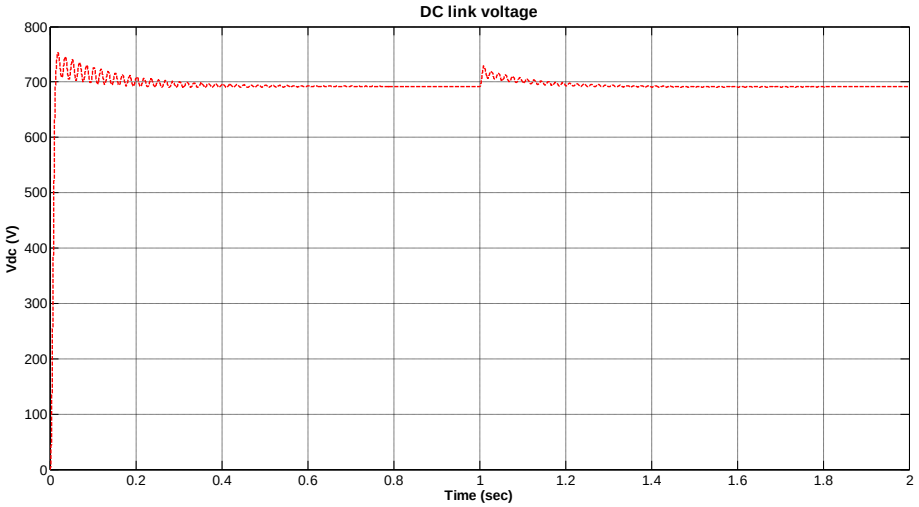

Figure 4.44: DC link voltage for case 4

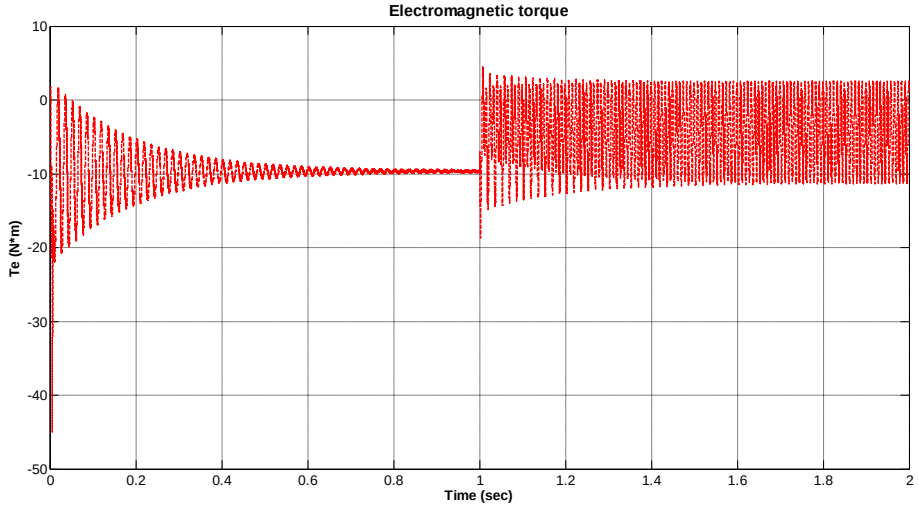

Figure 4.45: Electromagnetic torque for case 4

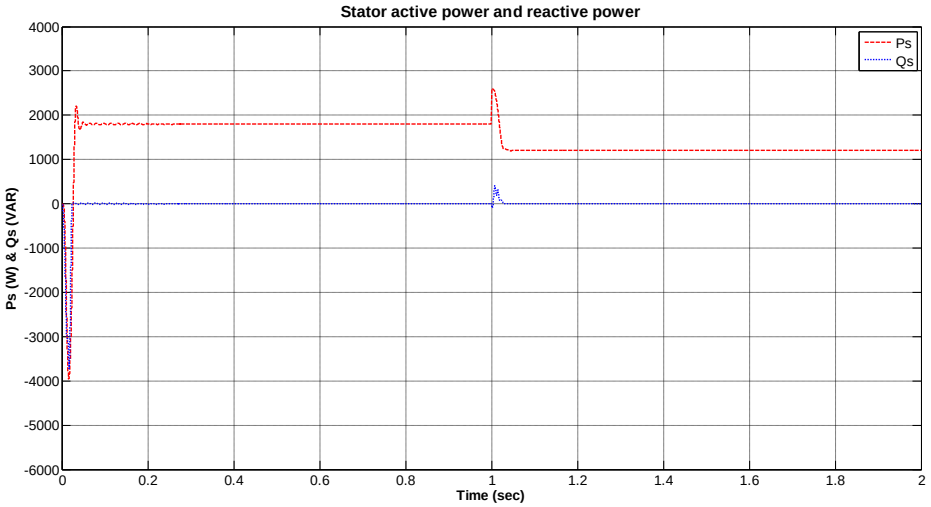

Figure 4.46: Stator active power and reactive power for case 4

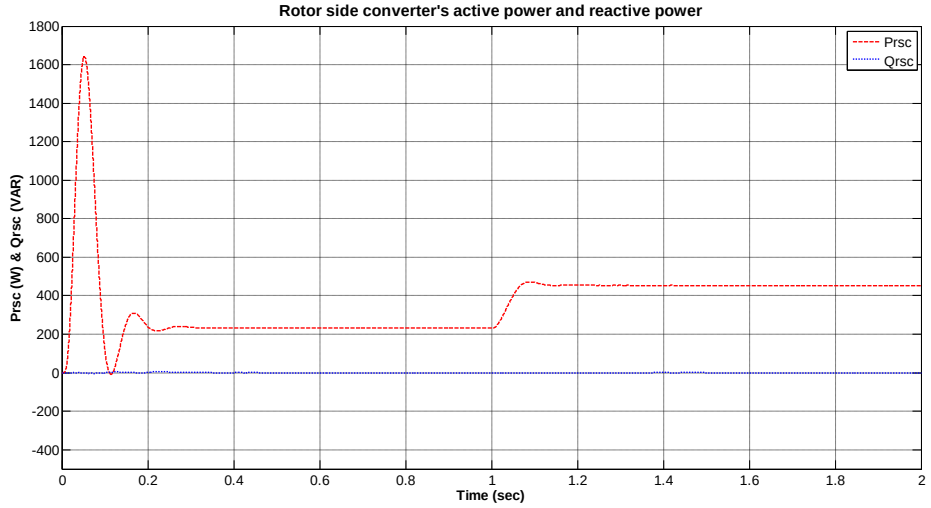

Figure 4.47: Rotor side converter's active power and reactive power for case 4

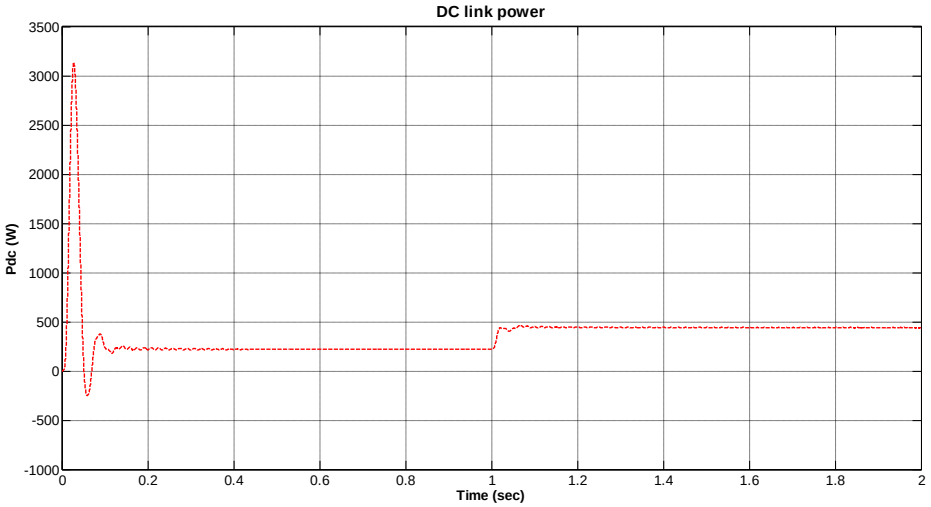

Figure 4.48: DC link active power for case 4

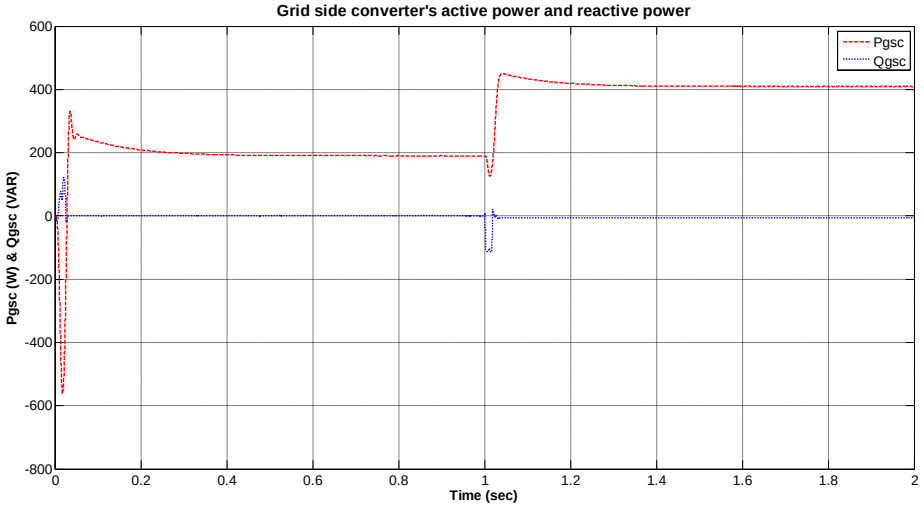

Figure 4.49: Grid side converter's active power and reactive power for case 4

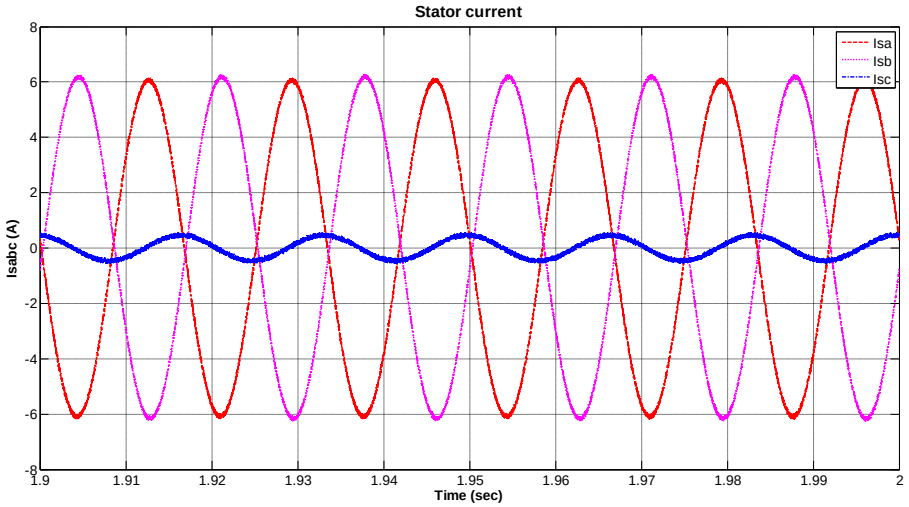

Figure 4.50: Stator current for case 4

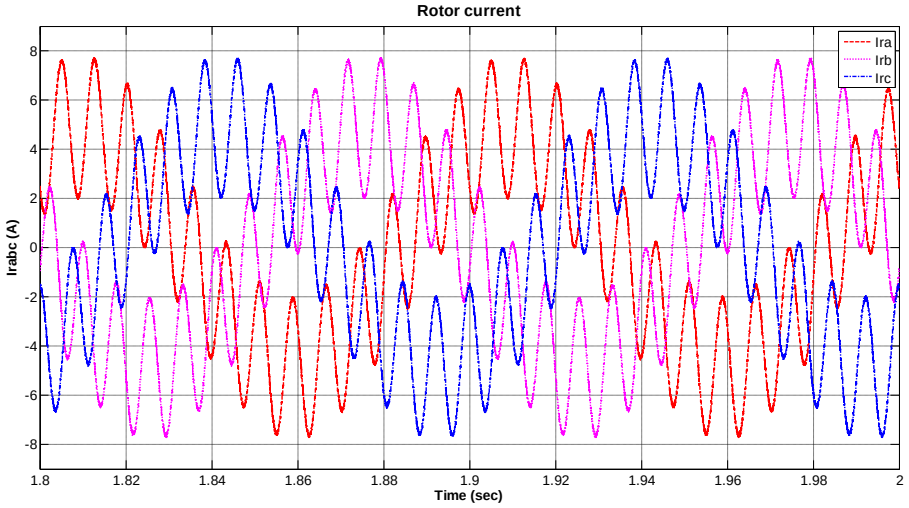

Figure 4.51: Rotor current for case 4

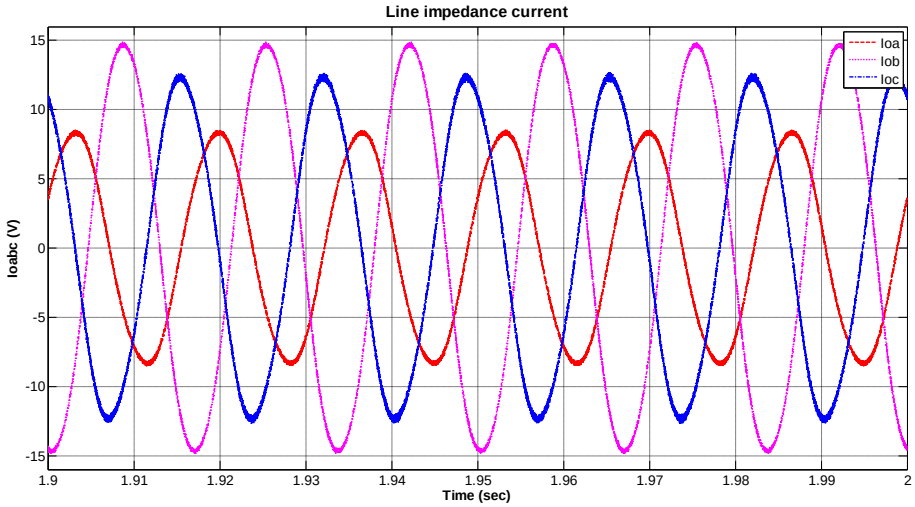

Figure 4.52: Line impedance current for case 4

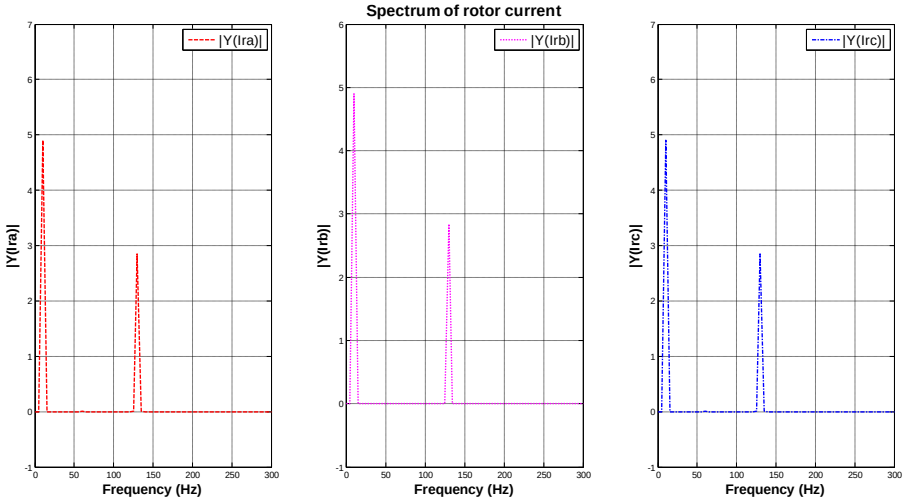

Figure 4.53: Spectrum of rotor current for case 4

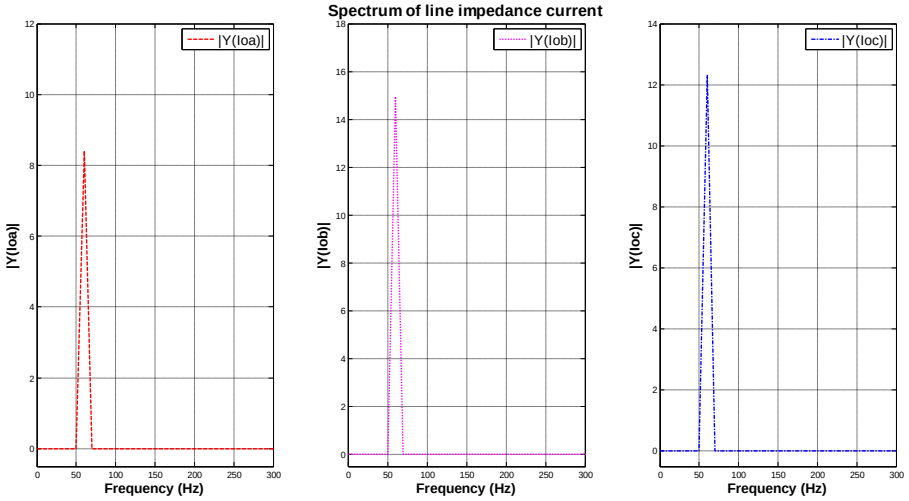

Figure 4.54: Spectrum of line impedance current for case 4

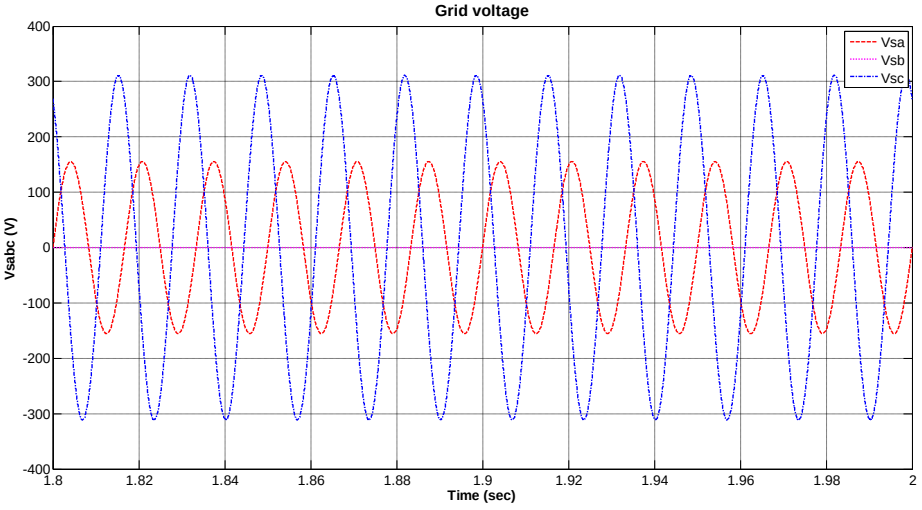

Figure 4.55: Three phase grid voltage (phase to neutral) for case 5

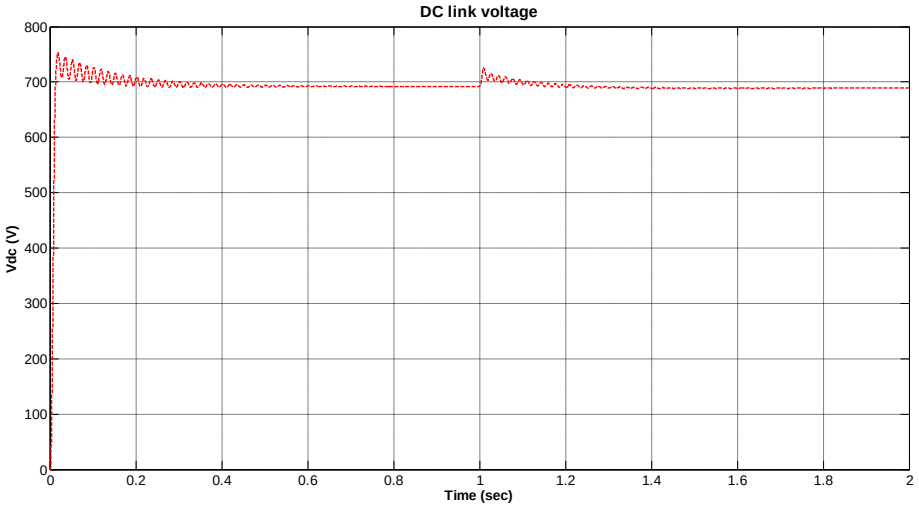

Figure 4.56: DC link voltage for case 5

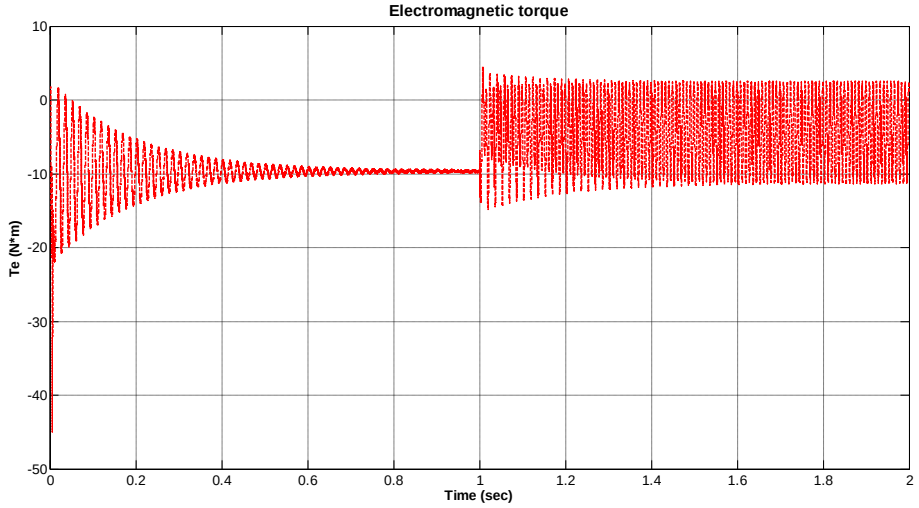

Figure 4.57: Electromagnetic torque for caser 5

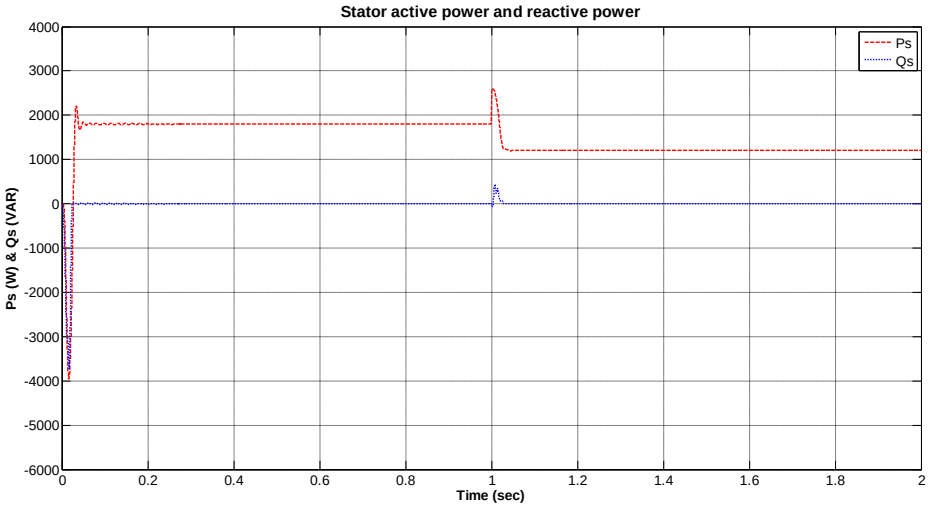

Figure 4.58: Stator active power and reactive power for case 5

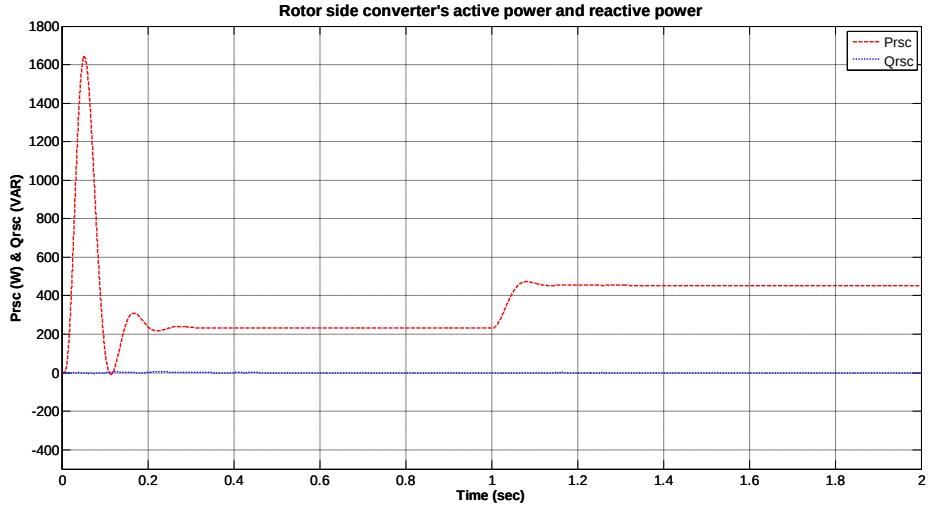

Figure 4.59: Rotor side converter's active power and reactive power for case 5

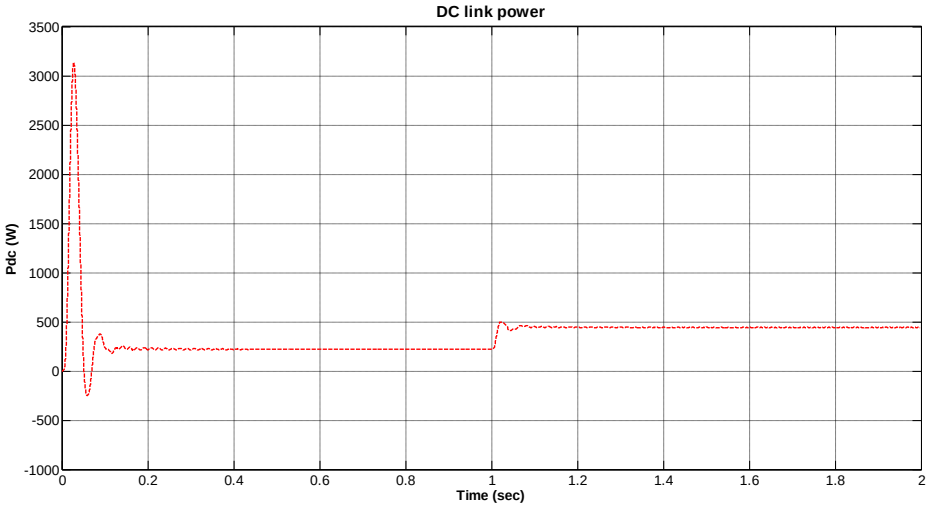

Figure 4.60: DC link active power for case 5

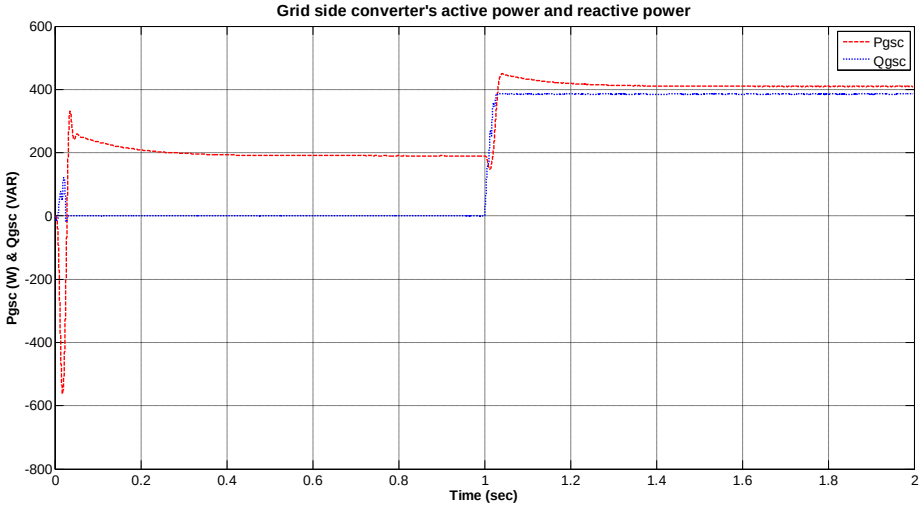

Figure 4.61: Grid side converter's active power and reactive power for case 5

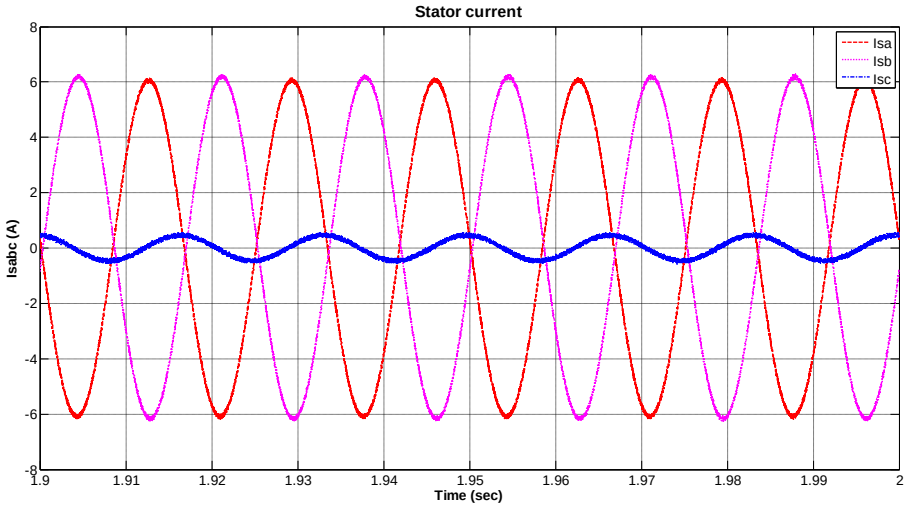

Figure 4.62: Stator current for case 5

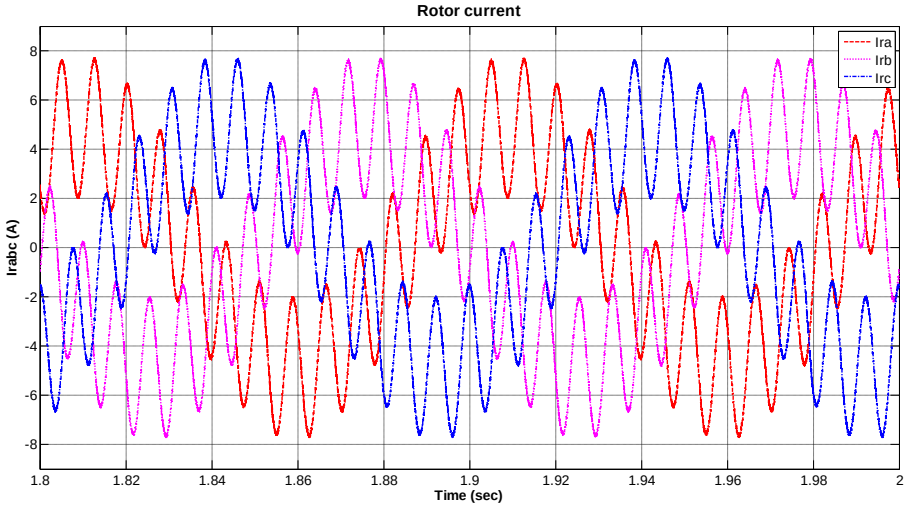

Figure 4.63: Rotor current for case 5

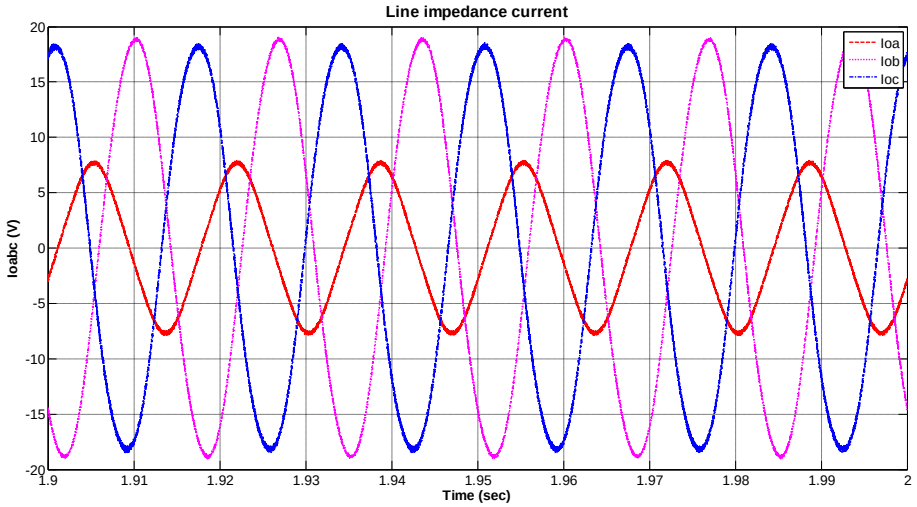

Figure 4.64: Line impedance current for case 5

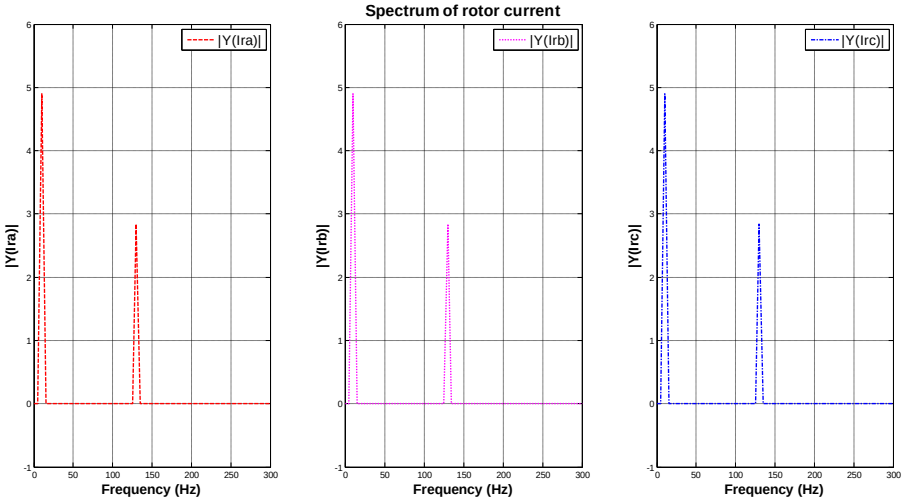

Figure 4.65: Spectrum of rotor current for case 5

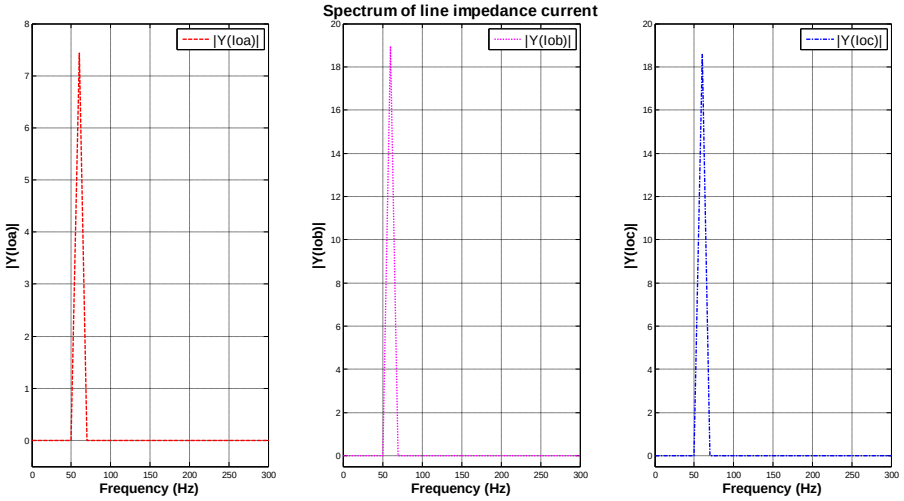

Figure 4.66: Spectrum of line impedance current for case 5

CHAPTER V

CONCLUSION AND FUTURE STUDY

5.1 Conclusion

This thesis presented and developed a generalized control method for pulsating power elimination and harmonic elimination in grid currents of a DFIG under the unbalanced operating conditions. It proposed and derived an analytical solution for complete pulsating power elimination as well as harmonic elimination in grid currents for a wind turbine driven DFIG under the unbalanced operating conditions. It achieved with adjustable power factor also. Based on this resolved open loop solution, the closed loop control method is verified and demonstrated by using the software Powersim. The simulation results demonstrate that stabilized stator power, rotor power, free harmonics of the line currents and constant DC link voltage are obtained when proposed method is used and implemented.

5.2 Future study

(1) A wind turbine driven DFIG under the balanced and unbalanced operating conditions is simulated by using PSIM program in this thesis. However, the experiment is not done to verify this proposed method.

(2) This thesis proposed a generalized pulsating power elimination and harmonic elimination control method. However, it inevitably sacrifices with the pulsating electromagnetic torque at the same time. In the future, different control target like the pulsating electromagnetic toque elimination while scarifying the stator pulsating power can be studied further.

REFERENCES

[1] H. Bindner, P. Lundsager, "Integration of Wind Power in the Power System," 28th Annual Conference of the Industrial Electronics Society, Vol. 4, pp. 3309-3316, Nov. 2002.

[2] Ryser, Jeffrey, "Wind power installation slowed in 2010, outlook for 2011 stronger: AWEA,". Platts. Retrieved, Feb. 2011.

[3] Reuters, "US wind power capacity up in '09, but jobs stalled," Jan. 2010.

[4] http://www.windpoweringamerica.gov/docs/installed_wind_capacity_by_state.xls

[5] U.S Department of Energy, 20% Wind Energy by 2030 Report, July 2008, http://www1.eere.energy.gov/windandhydro/pdfs/41869.pdf

[6] L. Soderlund and J-T. Eriksson, "A permanent-magnet generator for wind power applications," IEEE Trans. Magn., vol. 32, No. 4, pp. 2389-2392, July 1996.

[7] Chinchilla, M., Arnaltes, S., Burgos, J.C, "Control of permanent-magnet generator applied to variable-speed wind-energy systems connected to the grid," IEEE Transactions on Energy Conversion, vol. 21, no. 1, pp. 130-135, 2006.

[8] Wang, Q., Chang, L., "PWM control strategies for wind turbine inverters," Wind Engineering, vol.25, no.1, pp. 33-40(8), 2001.

[9] Dixon, J.W., Boon-TeckOoi, "Indirect Current control of a unity power factor sinusoidal current boost type three-phase rectifier," IEEE Transactions on Industrial Electronics, vol. 35, pp. 508-15, 1988.

[10] Zhang,Y., Gong, J., Xie, D. J., "Inverter control strategy for direct-drive permanent magnet wind generator under unbalance of three-phase source voltage," 11th International Conference on Electrical Machines and Systems, pp. 2497-501. Wuhan, China, 2008.

[11] Moran, L., Ziogas, P. D., Joos, G., "Design aspects of synchronous PWM rectifier-inverter systems under the unbalanced input voltage conditions," IEEE Transactions on Industry Applications, vol.28, no.6, pp.1286-93, 1992.

[12] Ng, C. H., Li, R., Bumby, J., "Unbalanced-grid-fault ride-through control for a wind turbine inverter," IEEE Transactions on Industry Applications, vol.44, no.3, pp. 845-56, 2008.

[13] Stankovic AV, Chen K, "A New Control Method for Input-Output Harmonic Elimination of the PWM Boost Type Rectifier Under Extreme Unbalanced Operating Conditions," IEEE Transactions on Industrial Electronics, vol. 56, pp. 2420-2430, 2009.

[14] A. V. Stankovic and T. A. Lipo, "A novel control method for input out-put harmonic elimination of the PWM boost type rectifier under the unbalanced operating conditions," IEEE Trans. Power Electron., vol. 16, no. 5, pp. 603–611, Sep. 2001.

[15] Ana Stankovic, "Three–Phase Pulse-Width-Modulated Boost-Type Rectifiers," THE POWER ELECTRONICS HANDBOOK (Edited by Tim Skvarenina), CRC Press, Chapter 4.3, pp. 4.33 - 4. 41. 2001.

[16] A. V. Stankovic, "Unbalanced Operation of Three-Phase Boost Type Rectifiers," HANDBOOK OF AUTOMOTIVE POWER ELECTRONICS MOTOR DRIVES (Edited by Ali Emadi), Taylor and Francis Group, LLC. Chapter 13.2005.

[17] A. V. Stankovic and T. A. Lipo, "A Novel Control Method for Input Output Harmonic Elimination of the PWM Boost Type Rectifiers Under the unbalanced Operating Conditions," IEEE APEC 2000, vol.1, pp.413-419, 2000.

[18] Xiangpeng Zheng and A. V. Stankovic, "Ride-Through Fault Generalized Control Method for a Wind Turbine Inverter," Conference Proceedings of IEEE Energy Tech, Cleveland, Ohio, pp. 1-6, May 2011.
[19] Ana Vladan Stankovic, Dejan Schreiber and Xiangpeng Zheng, "Grid-Fault-Ride Through Control Method for a Wind Turbine Inverter," Chapter 17 in SMART POWER GRIDS (Edited by Ali Keyhani and Muhammad Marwali), Springer, 2012.
[20] Shuang Wu and Ana Stankovic, "A Generalized Method for Wind Inverter Control under the unbalanced Operating Conditions," Conference Proceedings of IEEE ECCE, pp.865-870. Phoenix, Arizona, 2011.
[21] Ana Vladan Stankovic and Dejan Schreiber, Line side Converters in Wind Power Applications, HANDBOOK ON RENEWABLE ENERGY TECHNOLOGY (Edited by Ahmed Zobaa and Ramesh Bansal), Chapter 6, pp 119-146, World Scientific Publishing Company PTE LTD, 2011.
[22] Ana Vladan Stankovic, Dejan Schreiber and Shuang Wu, "Control Methods for Grid Side Converters under the unbalanced Operating Conditions in Wind Power Applications," MODELING AND CONTROL OF POWER SYSTEMS: TOWARDS SMARTER AND GREENER ELECTRIC GRIDS (Edited by Lingfeng Wang), Springer pp.127-153, 2012.
[23] Peterss, A., Lundberg, S., Thiringer, T., "Comparison between stator-flux and grid-flux-oriented rotor current control of doubly-fed induction generators," 35th Annual IEEE Power Electronics Specialists Conference, Aachen, Germany, pp. 482-486, 2004.
[24] Pena R., Clare J. C., Asher, G. M., "Doubly fed induction generator using BTB PWM converters and its application to variable speed wind energy generation," IEEE Proceeding on Electric Power Applications,vol.143, no.3, pp. 231-241, 1996.
[25] Jiabing Hu., Yikang, He, "Dynamic modeling and robust current control of wind-turbine driven DFIG during external AC voltage dip," Journal of Zhejiang University SCIENCE A, vol. 7, pp. 1757-1764, 2006.
[26] Chinchilla, M., Arnaltes, S., Burgos, J.C, "Control of permanent-magnet generator applied to variable-speed wind-energy systems connected to the grid," IEEE Transactions on Energy Conversion, vol. 21, no. 1, pp. 130-135, 2006.
[27] Wang, Q., Chang, L., "PWM control strategies for wind turbine inverters," Wind Engineering, vol.25, no.1, pp. 33-40(8), 2001.
[28] Dixon, J.W., Boon-Teck Ooi, "Indirect Current control of a unity power factor sinusoidal current boost type three-phase rectifier," IEEE Transactions on Industrial Electronics, vol. 35, pp. 508-15, 1988.
[29] Eltamaly, A.M., Alolah, A.I., Abdel-Rahman, M.H., "Modified DFIG control strategy for wind energy applications," IEEE International Symposium on Power Electronics Electrical Drives Automation and Motion (SPEEDAM) : 653 - 658 2010.
[30] Ganti, V.C., Singh, B., "Quantitative Analysis and Rating Considerations of a Doubly Fed Induction Generator for Wind Energy Conversion Systems," IEEE conference on Industry Applications Society Annual Meeting (IAS), pp. 1-7, Oct. 2010.
[31] Verma, V. and Pant, P. et al, "Decoupled indirect current control of DFIG for wind energy applications," India International Conference on Power Electronics (IICPE), pp. 1-6, Jan. 2011.

[32] Gomis-Bellmunt, O. and Junyent-Ferre, A. et. al., "Ride-Through Control of a Doubly Fed Induction Generator Under the unbalanced Voltage Sags," IEEE Transactions on Energy Conversion, vol. 23, no. 4, pp. 1036-1045, Dec. 2008.
[33] Flannery, P. and Venkataramanan, G., "Unbalanced Voltage Sag Ride-Through of a Doubly Fed Induction Generator Wind Turbine with Series Grid Side Converter," IEEE Industry Applications Society Annual Meeting, pp. 1-8, Oct. 2008.
[34] Castilla, M. and Miret, J. et al, "Direct Rotor Current-Mode Control Improves the Transient Response of Doubly Fed Induction Generator-Based Wind Turbines," IEEE Transactions on Energy Conversion, vol. 25, no. 3, pp. 722-731, Sept. 2010.
[35] Luna, A. et al, "Control of DFIG-WT under the unbalanced grid voltage conditions," 2009 IEEE Conference of Energy Conversion Congress and Exposition, pp. 370-377, Sep. 2009.
[36] Abad, G. and Rodriguez, M.A. et al, "Direct Power Control of Doubly-Fed-Induction-Generator-Based Wind Turbines Under the unbalanced Grid Voltage," IEEE Transactions on Power Electronics, vol. 25, no. 2, pp. 442-452, Feb. 2010.
[37] Jun Yao and Hui Li et al, "An Improved Control Strategy of Limiting the DC-Link Voltage Fluctuation for a Doubly Fed Induction Wind Generator," IEEE Transactions on Power Electronic, vol. 23, no. 3, pp. 1205-1213, May 2008.
[38] Dawei Xiang and Li Ran, "Control of a doubly fed induction generator in a wind turbine during grid fault ride-through," IEEE Transactions on Energy Conversion, vol. 21, no. 3, pp. 652-662, Sep. 2006.
[39] Santos-Martin, D.,Rodriguez-Amenedo, J.L.and Arnaltes, S., "Providing Ride-Through Capability to a Doubly Fed Induction Generator Under the unbalanced Voltage Dips," IEEE Transactions on Power Electronics, vol. 24, no. 7, pp. 1747-1757,July 2009.
[40] D. Santos-Martin et al, "Direct Power Control Applied to Doubly Fed Induction Generator Under the unbalanced Grid Voltage Conditions," IEEE Transaction on Power Electronics, vol. 23, no. 5, pp. 2328-2336, Sep. 2008.
[41] A.V. Stankovic, E. Benedict, V. John and T. A. Lipo, "A Novel Method for Measuring Induction Machine Magnetizing Inductance," IEEE Transactions on Industry Applications, vol. 39. No.5, pp. 1257-1263, Sep/Oct, 2003.
[42] A. Stankovic, E. Benedict, V. John and T. A. Lipo, "A Novel Method for Measuring Induction Machine Magnetizing Inductance," IEEE Industry Applications Society Annual Meeting, New Orleans, Louisiana. Conference Record of the 1997 IEEE Industry Applications Conference Thirty-Second IAS Annual Meeting, vol.1, pp.234-8, 1997.
[43] L. Xu, B. R. Andersen, P. Cartwright, "VSC transmission operating under the unbalanced AC conditions - analysis and control design," IEEE Transaction on Power Delivery, vol. 20, pp. 427-434, January 2005.
[44] Lie Xu and Yi Wang, "Dynamic Modeling and Control of DFIG-Based Wind Turbines Under the unbalanced Network Conditions," IEEE Transaction on Power Systems, vol. 22, pp. 314-323, Feb. 2007.
[45] D. Roiu and R. Bojoi, et al, " New Stationary Frame Control Scheme for Three Phase PWM Rectifiers under the unbalanced Voltage Dips Conditions," 2008 IEEE Industry Applications Society Annual Meeting, pp. 1-7, Oct. 2008.